Seepage Measured During May and June 2017 at 18 Locations in Newtown Creek, New York

U.S. Geological Survey Administrative Report to U.S. Environmental Protection Agency, Special Projects Branch, New York, New York

Donald Rosenberry, U.S. Geological Survey, Lakewood, Colorado
rosenber@usgs.gov

Data collected May 18, 2017–June 23, 2017

Flow across the sediment-water interface, herein termed "seepage," was measured with electromagnetic seepage meters (ESMs) at 18 locations in Newtown Creek, New York, from May 18, 2017, to June 23, 2017. Seepage (q) was measured once every 5 seconds, and a digital datalogger calculated average values once every minute. Seepage was measured for three or more tidal cycles at each location to determine the direction and magnitude of seepage in response to tides. Vertical hydraulic gradient (i) and tide also were measured at each location and related to measured seepage. Ebullition from the portion of the sediment bed covered by each seepage meter was measured and corrections to measured seepage were made where ebullition was large. This summary report presents (1) a general overview of seepage, hydraulic gradients, and ebullition as they responded to tides at Newtown Creek; (2) summary statistics for each measurement location; and (3) a detailed description of these variables at each measurement location.

U.S. Department of the Interior
U.S. Geological Survey

D.O Rosenberry

Photo of electromagnetic seepage meter on boat deck.

Contents

Figures

Tables

Overview of Seepage Measured at Newtown Creek During May and June 2017

Seepage, hydraulic-gradient, and ebullition data were collected in support of the Remedial Investigation/Feasibility Study for the Newtown Creek Study Area. During May and June 2017, average seepage was upward, indicating net flow from groundwater to surface water, at 15 of 18 locations at Newtown Creek, New York. Average values from 1-minute output collected during 2 or more tidal cycles measured at 18 locations ranged from −0.3 to 8.6 centimeters per day (cm/d), with negative values indicating net downward seepage and positive values indicating net upward seepage (fig. 1).

Average upward seepage was typically less than 2 cm/d. Fastest average upward seepage of 6.0 cm/d or more was measured at locations NC338 and NC273. Upward seepage at EK013 during a second deployment in June also was fast, averaging 8.6 cm/d. However, diurnal variability of seepage at EK013 during June was nearly perfectly out of phase with measured hydraulic gradient, which is difficult to explain, and average seepage measured at this same location, but during May, was less than 1 cm/d.

Seepage was influenced by tidal cycles at most locations. Smallest tidal ranges occurred during neap tides on May 18 and June 17, during which the minimum range over two sequential tidal cycles was still 1.01 and 1.11 meters (m), respectively (National Oceanic and Atmospheric Administration, 2017). However, there was no indication of tidal influence in seepage measurements at four locations (NC168, NC320, NC337, and NC362), weak influence at NC008, and very weak influence at NC266, where much larger influence of waves from East River boat traffic overwhelmed any tidal signal that might otherwise have been evident. Tidal signals were present in the seepage data at NC273 and NC336, and to variable extents during two deployments at NC340, but were weaker than at the other 10 locations where seepage clearly was influenced by tides.

Occasional brief departures from typical seepage rates (“spikes”) were recorded at several measurement locations. In some cases, these departures can be attributed to passing watercraft. At other locations, filtering animals, either on the bed or in or adjacent to the electromagnetic flowmeter, created measurable flow that was not related to gradient-driven seepage.

Seepage was analyzed as consistently as possible to allow unbiased comparisons between locations. During each deployment, basic analysis periods of two complete tidal cycles were selected, ideally beginning and ending at low tide. Two separate analysis periods, each beginning and ending with low tide, were determined for every deployment except at NC273 (table 1). In most instances, values in figure 1 are averages of the two average values presented for each location in table 1. The first analysis period at NC273 began and ended at high tide to exclude unusual and noisy data collected during the early part of the deployment. An additional analysis period was selected for NC320 to exclude questionable data during early and late portions of that deployment. Data summaries (table 1) include the number of 1-minute values; median, average, maximum, and minimum seepage values during each analysis period; 0.75 and 0.25 quartiles; the difference between the 0.75 and 0.25 quartiles; approximate time to head equilibration following installation of sensors in the sediment; and average vertical hydraulic gradient. Average seepage from the two analysis periods for each measurement location are presented in figure 1. Values in figure 1 were subsequently corrected for the effects of ebullition, discussed later, and those ebullition-corrected values are presented in the “Ebullition Results” section.

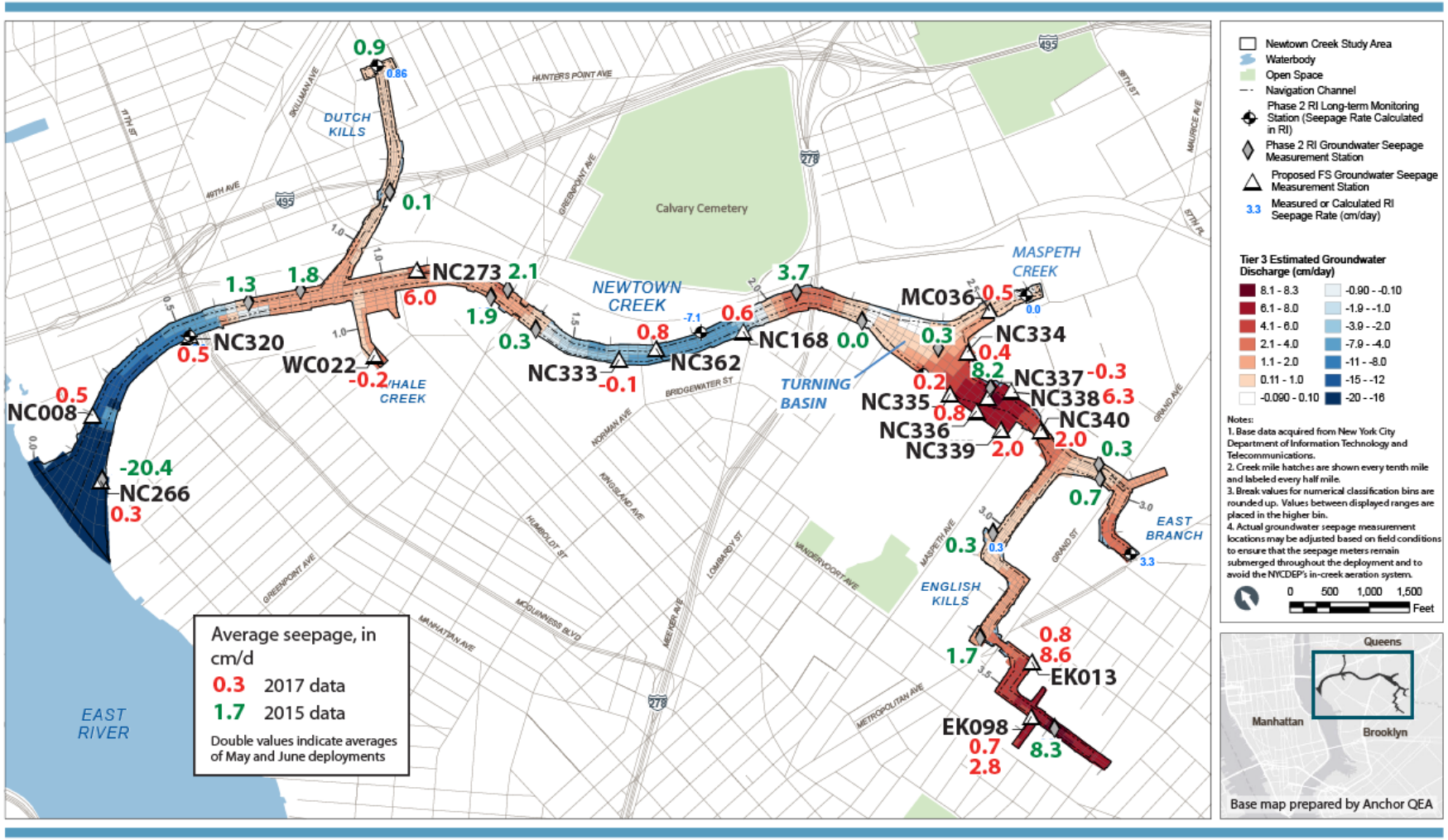

Figure 1. Seepage-measurement locations at Newtown Creek, New York. Values in red are best determinations of average seepage during 2017 sensor deployments. Values in green are average seepage during 2015 sensor deployments (Rosenberry, 2016). Positive values indicate upward flow and negative values indicate downward flow. (cm/d, centimeter per day; RI, remedial investigation; NYCDEP, New York City Department of Environmental Protection)

Table 1. Summary of Newtown Creek seepage and vertical hydraulic gradient (*i*) data. Data for five tidal-cycle period types were summarized: (1) "lo hi early" indicates two complete tidal cycles during the early portion of the deployment beginning and ending with low tide, (2) "lo hi late" indicates two complete tidal cycles during the later portion of the deployment beginning and ending with low tide, (3) "hi lo" indicates two complete tidal cycles beginning and ending with high tide, (4) "lo hi" indicates two complete tidal cycles beginning and ending with low tide, and (5) "Stable" indicates a period of relatively stable data collection at NC320. All values except "n" (number of 1-minute values), "Equil." (approximate time of head equilibration following sensor installation, in hours) and "*i*" (period-average vertical hydraulic gradient) in centimeters per day. Positive values indicate upward flow and negative values indicate downward flow. [Med, median of n values; Ave, average of n values (red text indicates either seepage flow in the opposite direction of that indicated by *i*, or an *i* that is too large because the head had not yet equilibrated following sensor installation); Max, maximum of n values; Min, minimum of n values; 0.75 quart, 75th quartile; 0.25 quart, 25th quartile; 0.75–0.25, difference between the 75th and 25th quartiles (representing the range of half of the data)]

Location	Cycle type	n	Med	Ave	Max	Min	0.75 quart	0.25 quart	0.75–0.25	Equil., h	*i*
EK098	lo hi early lo	1,412	0.7	0.7	20.3	-14.2	2.7	-1.5	4.2	3	0.072
	hi late	1,479	0.6	0.6	22.8	-31.7	3.6	-2.4	6.0		0.073
EK098-2	lo hi early lo	1,429	3.4	3.8	15.3	-6.1	6.3	0.9	5.5	3	0.041
	hi late	1,459	1.6	1.9	11.8	-6.2	3.6	0.2	3.4		0.046
EK013	lo hi early lo	1,379	0.7	0.8	31.7	-34.2	3.1	-1.0	4.1	1	0.008
	hi late	1,496	-0.4	0.7	17.6	-21.2	5.9	-5.3	11.2		0.020
EK013-2	lo hi early lo	1,456	3.5	7.3	42.7	-32.4	24.4	-5.8	30.2	1	0.010
	hi late	1,452	5.7	9.9	44.7	-25.7	21.4	-0.9	22.3		0.019
NC337	lo hi early lo	1,171	-0.3	-0.3	1.1	-1.9	-0.1	-0.6	0.5	10	0.121
	hi late	1,210	-0.2	-0.3	1.1	-1.9	0.0	-0.5	0.5		0.122
NC338	lo hi early lo	1,496	4.9	7.8	53.8	-9.6	13.7	1.3	12.3	1	0.116
	hi late	1,437	1.9	4.8	57.5	-9.1	8.7	-0.2	8.9		0.078
NC336	lo hi early lo	1,386	1.5	1.3	36.9	-22.3	2.7	0.1	2.6	12	0.066
	hi late	1,390	0.2	0.2	7.6	-4.4	0.9	-0.5	1.4		0.042
NC334	lo hi early lo	1,412	-11.8	-12.3	5.2	-27.1	-7.5	-16.6	9.1	12	0.132
	hi late	1,432	-7.5	-6.4	16.4	-22.4	0.4	-11.1	11.5		0.108
NC334-3	lo hi early lo	1,454	0.6	0.5	7.5	-6.2	2.0	-1.0	3.0	16	0.107
	hi late	1,464	0.2	0.3	9.5	-6.0	1.7	-1.3	3.0		0.080
NC335	lo hi early lo	1,430	0.2	0.2	1.5	-1.5	0.4	0.0	0.3	5	0.014
	hi late	1,476	0.2	0.2	1.5	-1.5	0.4	0.0	0.4		0.009

Location	Cycle type	n	Med	Ave	Max	Min	0.75 quart	0.25 quart	0.75–0.25	Equil., h	*i*
NC339	lo hi early lo	1,474	0.8	1.0	5.8	-7.3	1.9	0.2	1.7	26	0.010
	hi late	1,441	0.6	0.5	4.7	-7.3	1.5	-0.3	1.9		0.006
NC340-2	lo hi early lo	1,478	2.2	2.0	5.1	-3.2	2.8	1.3	1.4	5	0.065
	hi late	1,482	2.0	2.0	4.9	-2.0	2.8	1.2	1.5		0.059
NC168	lo hi early lo	1,466	0.5	0.6	2.7	-0.9	0.8	0.3	0.5	1	-0.084
	hi late	1,491	0.5	0.6	2.1	-0.9	0.8	0.3	0.5		-0.088
MC036	lo hi early	1,478	0.1	0.4	47.2	-43.1	3.9	-3.0	6.9	13	[a]---
	lo hi late	1,450	0.4	0.6	31.3	-28.0	4.3	-2.7	7.0		[a]---
NC273	hi lo	1,441	6.3	5.6	15.7	-7.2	7.9	3.6	4.3	18	0.002
	lo hi	1,427	6.7	6.4	15.7	-2.3	8.0	5.0	2.9		-0.005
NC333	lo hi early	1,433	-0.1	-0.1	0.4	-0.9	0.1	-0.4	0.5	20	-0.375
	lo hi late	1,459	-0.2	-0.2	0.4	-0.9	0.0	-0.5	0.4		-0.400
NC320	lo hi early	1,354	1.1	2.8	87.0	-19.2	3.4	-0.4	3.8	26	0.040
	lo hi late	1,455	0.5	-0.1	87.0	-32.9	1.6	-0.6	2.2		0.024
	Stable	1,063	0.4	0.5	18.8	-19.2	1.3	-0.5	1.8		0.019
WC022	lo hi early	1,445	-0.5	-0.7	8.5	-18.5	0.9	-2.3	3.2	24	0.081
	lo hi late	1,461	0.6	0.5	7.5	-7.0	1.7	-0.6	2.3		0.047
NC362	lo hi early	1,481	0.6	0.7	3.1	-0.8	0.9	0.4	0.6	12	-0.003
	lo hi late	1,506	1.0	0.9	4.6	-2.5	1.2	0.7	0.6		-0.010
NC266	lo hi early	1,453	0.4	0.3	64.1	-48.5	2.6	-2.3	5.0	10	0.058
	lo hi late	1,492	0.4	0.2	53.2	-46.5	2.0	-1.2	3.2		0.038
NC008	lo hi early	1,481	0.3	0.4	53.2	-34.8	1.1	-0.4	1.5	20	0.062
	lo hi late	1,496	0.6	0.6	8.6	-8.8	1.4	-0.1	1.5		0.025

[a] Locally determined gradients could not be determined due to a failed upper vertical hydraulic gradient pressure transducer.

Methods

Seepage

The following is a brief description of the procedure that was used to measure seepage at Newtown Creek. More details about electromagnetic seepage meter (ESM) systems are presented in the standard operating procedure SOP NC-34 (Anchor QEA, 2015) and Rosenberry (2016). Data used in the study are stored in USGS project files, Lakewood, Colorado.

The same ESMs that were used to collect seepage data at Newtown Creek in 2015 (Rosenberry and Morin, 2004; Swarzenski and others, 2004; Waldrop and Swarzenski, 2006) were deployed at 18 measurement locations within the Newtown Creek area during May and June 2017. Three complete ESM systems were used at Newtown Creek along with two spare electromagnetic (EM) flowmeters that could be exchanged if needed. Each ESM (fig. 2) consisted of an electromagnetic flowmeter mounted in a horizontal position to an approximately 1.1-m-diameter seepage cylinder. The submerged flowmeter received power from a signal-processing unit deployed in a boat anchored at least 10 m lateral to the seepage cylinder. Two or more deep-cycle marine batteries wired in parallel supplied power to the ESM. The flowmeter transmitted an analog signal through a shielded data cable to the signal-processing unit and voltage from the signal processing unit was sent through stranded, shielded wires to a digital Campbell Scientific[1] datalogger. The datalogger recorded output in millivolts (mV) from the ESM every 5 seconds and was programmed to calculate average values and standard deviations once every minute.

Three ESM systems were used at Newtown Creek, two that included an aluminum cylinder that covered 9,260 square centimeters (cm^2) of the sediment bed and one that included a plastic cylinder that covered 8,938 cm^2 of the bed. Neither the slight difference in diameter nor the composition of the seepage cylinder should have any effect on measured seepage. Given the substantial ebullition observed during the 2015 deployments, ESMs were modified prior to the 2017 field work to collect gas released from the sediment during each deployment. A 15.2-centimeter- (cm) diameter section of polyvinyl chloride (PVC) pipe was added to the top of each meter so that any released gas would collect inside the gas-collection chamber (fig 2*A* inset). Approximately 3 liters of gas could be stored in the chamber; any additional gas released from the sediment would accumulate in the upper portion of the horizontal pipe just below the chamber and eventually exhaust through the flowmeter. A valve and connector were mounted at the top of the gas-collection chamber so a diver could release the trapped gas into a collection bottle during calibration visits. Similar to the 2015 field campaign, a hard-hat diver facilitated each installation and ensured that the bottom edge of the seepage cylinder was inserted at least 5 cm but no more than 20 cm into the sediment bed along the entire cylinder perimeter. Seepage cylinders were secured to 1.5-m lengths of PVC pipe pushed vertically into the sediment until refusal. Each of the three pipes was then pinned to the seepage cylinder with a set screw to eliminate the possibility of any movement of the seepage cylinder in the soft sediment. When installation was complete, the diver closed the valve at the top of the gas-collection chamber and ensured that the flowmeter exhaust-port valve was open, enabling the system to begin measuring seepage. Initial values commonly were very large due to sediment disturbance and compression during meter installation. The logging period for each location did not start until seepage stabilized after installation.

[1] Any use of trade, firm, or product names is for descriptive purposes only and does not imply endorsement by the U.S. Government.

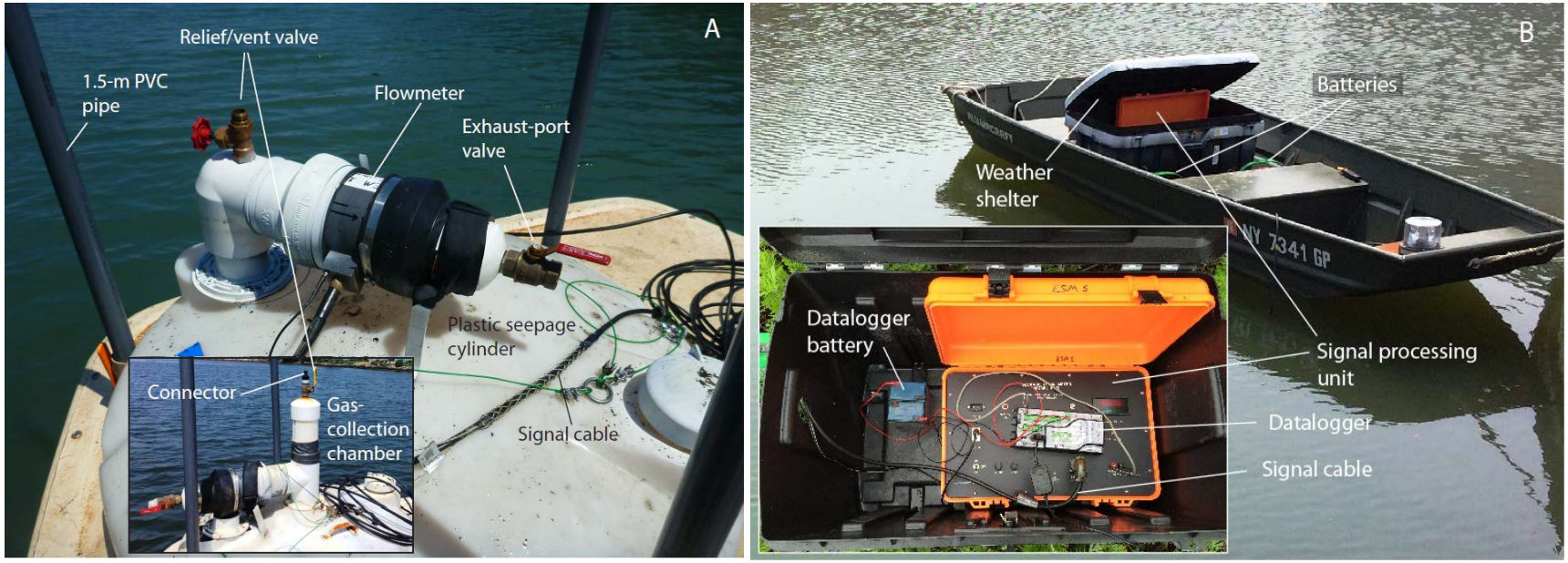

Figure 2. Photos of an electromagnetic seepage meter deployed at Newton Creek, New York. *A*, Seepage cylinder and an electromagnetic flowmeter prior to being lowered onto the sediment bed in 2015; photograph also shows the three polyvinyl chloride (PVC) pipes that will be pushed into the sediment by a diver. Inset photo shows an electromagnetic flowmeter that was modified for 2017 deployments by adding a gas-collection chamber. *B*, Signal-processing unit in an anchored boat. Inset photo of the weather-shelter interior shows the signal-processing unit, attached datalogger, and battery that supplies power to the datalogger.

Each ESM was revisited at least twice during each deployment to collect data during zero-flow periods, which are designed to allow data adjustments that correct for system drift. During each zero-flow period, the diver opened the relief valve at the top of the gas-collection chamber and then closed the flowmeter exhaust-port valve to begin the zero-flow period. The relief (top) valve was opened first to allow any seepage across the bed to continue during the zero-flow period. Zero-flow periods lasted a minimum of 15 minutes, after which the diver opened the flowmeter valve and closed the top valve so that normal measurements resumed. Averages were calculated for each zero-flow period using eleven 1-minute values and excluding data that indicated output had not yet stabilized to zero flow. Standard deviations were determined for those eleven 1-minute values. Linear interpolation was used during data analysis to determine zero-flow values for every minute increment between actual zero-flow periods. Measured or interpolated zero-flow values were then subtracted from the raw ESM output. Zero-flow adjusted values were converted to output in milliliters per minute by multiplying the adjusted value by a regression coefficient, which was determined for each sensor system at the Anchor QEA dock, located on the north side of Newtown Creek about half way between NC008 and NC320 (fig. 1). Onsite calibrations were conducted once during the May 2017 deployment and once during the June 2017 deployment. Output in milliliters per minute was then converted

to output in centimeters per day by dividing milliliters per minute by the area covered by the seepage cylinder (9,260 cm^2 for the aluminum cylinders or 8,938 cm^2 for the plastic cylinder) and multiplying by 1,440 minutes in each day.

Vertical Hydraulic Gradient

A vertical hydraulic gradient device (VHG rod) was deployed 1 m from each ESM installation. The device consisted of two submersible pressure transducers placed inside two screened intervals of a PVC pipe. The PVC pipe was filled with solid material between the screened intervals so no water could flow vertically through the pipe (fig. 3). The two transducers were placed 1.5 m apart and were designed to measure the difference in head, relative to hydrostatic head, between the sediment-water interface and 1.5-m beneath the sediment-water interface. The hydrostatic head difference was determined by positioning the VHG rod in a vertical orientation in the open-water column for at least 5 minutes so the dataloggers in each of the submersible pressure transducers could log five values collected at 1-minute intervals. Any drift of the sensors was corrected using linear interpolation based on water-column calibration periods before and immediately following sensor deployment. Local sediment compression caused by sediment displacement during VHG-rod installation resulted in over-pressuring and an artificially increased pressure was recorded at the deeper piezometer. Pressure dissipation following installation commonly took 2–12 hours. The largest overpressure occurred during early deployment, so data from early deployment are not included in analyses that relate vertical hydraulic gradient with other variables. The upper pressure transducer also served as a local tide gage with 1-minute resolution. For this report, “stage” refers to a specific value for surface-water level at a specific time, whereas “tide” (also referred to as “relative tide”) indicates the cyclical change in surface-water stage. However, “high tide” or “low tide” indicates the specific stage of the highest or lowest point of an individual tidal cycle.

Four Solinst LTC Levelogger Edge 10-m full scale submersible pressure transducers were used for two of the VHG rods. Two Schlumberger CTD Diver submersible pressure transducers with a 10-m pressure range were used in the third VHG rod. All six transducers were programmed to log temperature, pressure, and conductivity each minute. Stated accuracies were +/−0.05 °C, +/−5 millimeters (mm) of water head, and +/−300 microsiemens per centimeter (µS/cm) for temperature, pressure, and conductivity, respectively, for the Solinst loggers (https://www.solinst.com/products/data/3001-ltc-edge.pdf). Stated accuracies were +/−0.1 °C, +/−5 mm of water head, and 300 µS/cm for temperature, pressure, and conductivity, respectively, for the Schlumberger loggers (https://diver-water-level-logger.com/en/diver-water-level-loggers/ctd-diver.html). All loggers were calibrated for conductivity against a 30.1 millisiemens per centimeter conductivity standard at the Anchor QEA Newtown Creek facility. Submersible sensors measure total head, so a Solinst barometer was deployed at the Anchor QEA facility and output from the barometer was subtracted from output from each submerged pressure sensor to remove the effects of atmospheric pressure during each deployment.

In addition to atmospheric-pressure adjustments, adjustments were made to (1) determine water density based on measured temperature (McCutcheon and others, 1993), (2) convert conductivity to specific conductance at 25 °C., (3) convert specific conductance to total dissolved solids (TDS) (Clesceri and others, 1999), and (4) use the TDS value in an equation from McCutcheon and others (1993) to determine total water density. For the deeper transducer installed in the sediment, an arithmetic mean was determined based on the density of the water column and the density of the water in the 1.5-m thickness of sediment. This assumes that the sediment column has the same water density throughout, which implies net upward flow of groundwater that negates any influence from surface water of a different density. Plots of the density-adjusted VHG

data indicate that tidally generated pressure changes were readily transmitted to the deeper pressure transducer (fig. 4), usually with very little lag. Density adjustments to measured head differences were on the order of 1–9 mm.

The hydrostatic head difference was then subtracted from the difference between density-adjusted pressures of the deeper and shallower pressure transducers to determine the vertical hydraulic head difference. That difference was divided by the depth below the sediment-water interface of the deeper pressure transducer to determine the vertical hydraulic gradient. At some installations, the diver was not able to press the rod all the way to the red line, in which case the distance between the red line and the sediment surface was measured and subtracted from 1.5 m to determine the depth of installation of the lower transducer.

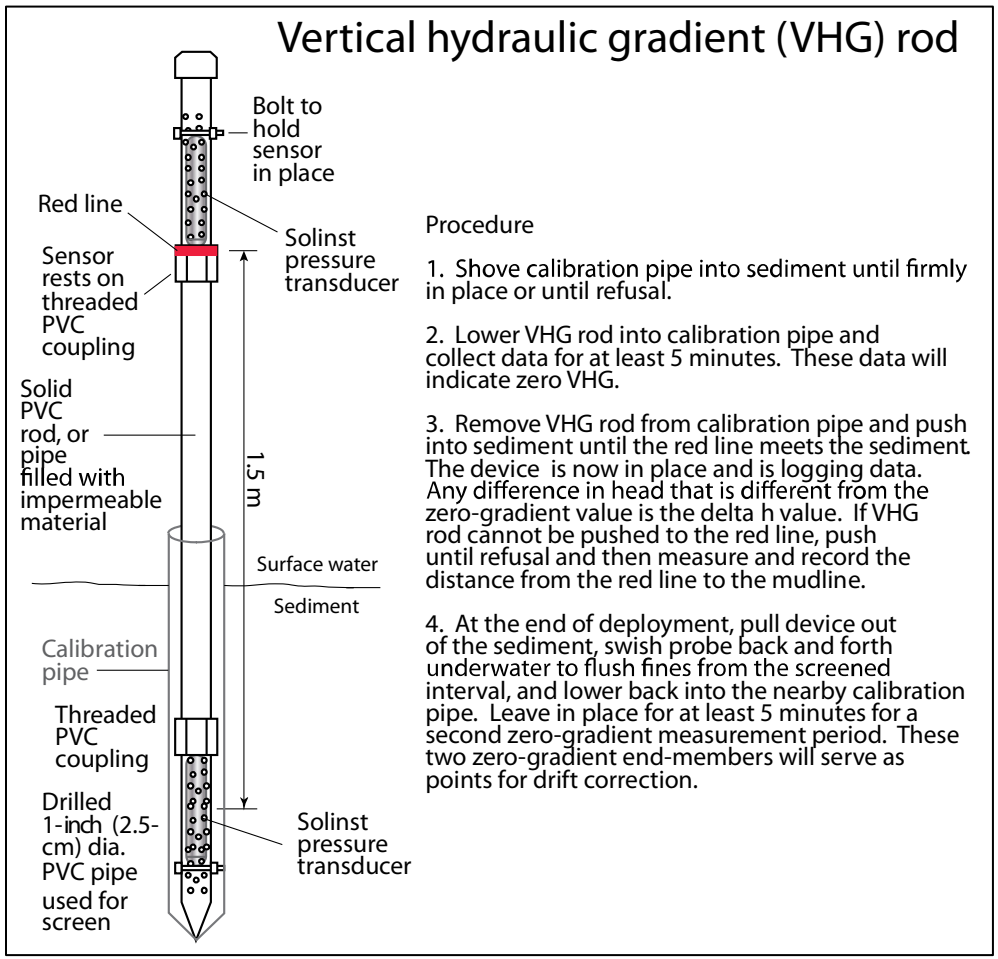

Figure 3. Components of a vertical hydraulic gradient rod designed to measure vertical hydraulic gradient in soft sediments over a 1.5-meter (m) vertical interval. The installation and deployment process is described in the figure. (PVC, polyvinyl chloride; cm, centimeter; dia., diameter]

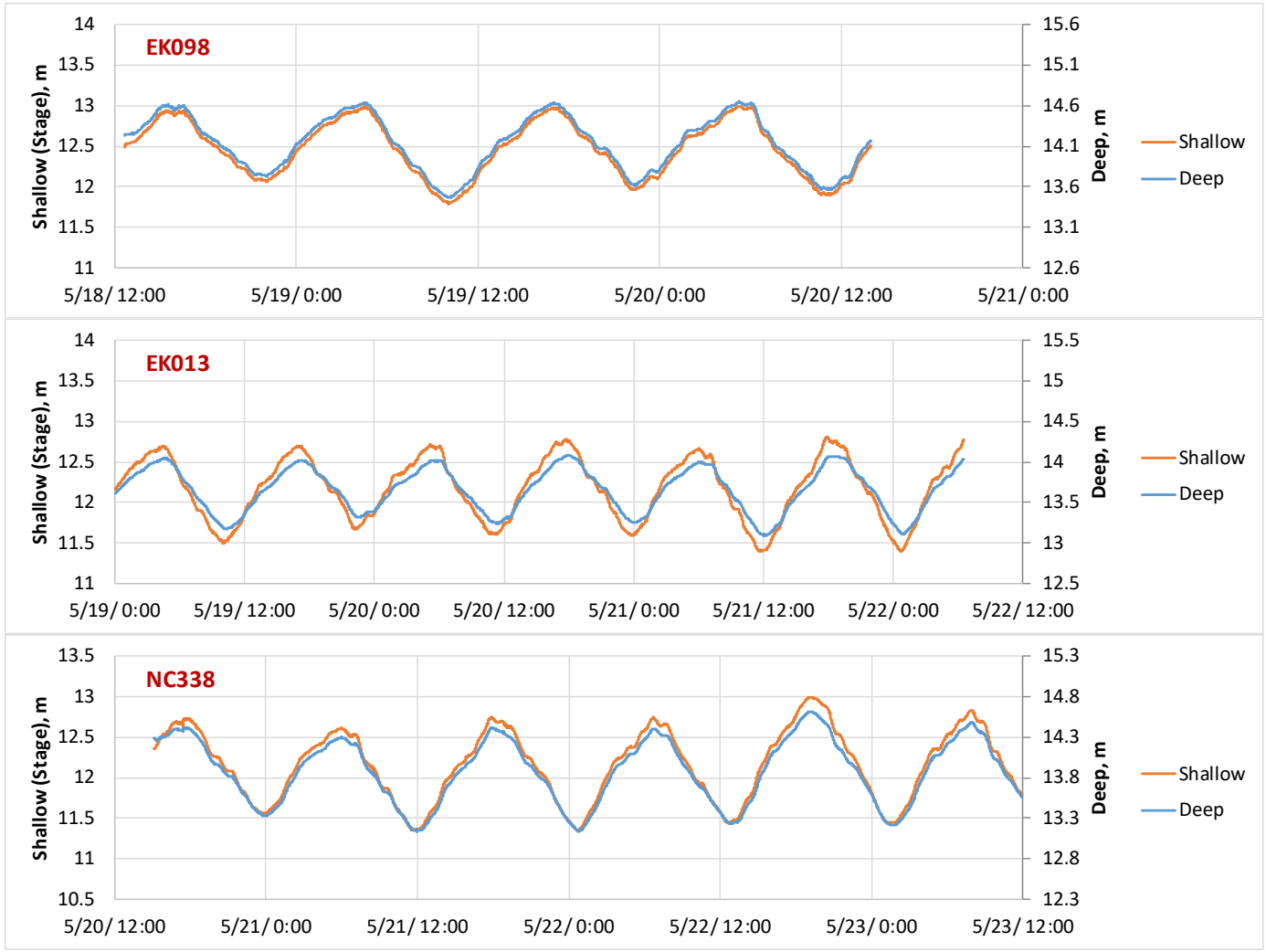

Figure 4. Density-corrected relative stage (shallow pressure transducer) and head (deep pressure transducer), in meters (m), for nine locations distributed approximately uniformly across the Newtown Creek study area. Different y-axis scales are used for the shallow and deep pressure transducers for each location to better show similarities in the stage variations.

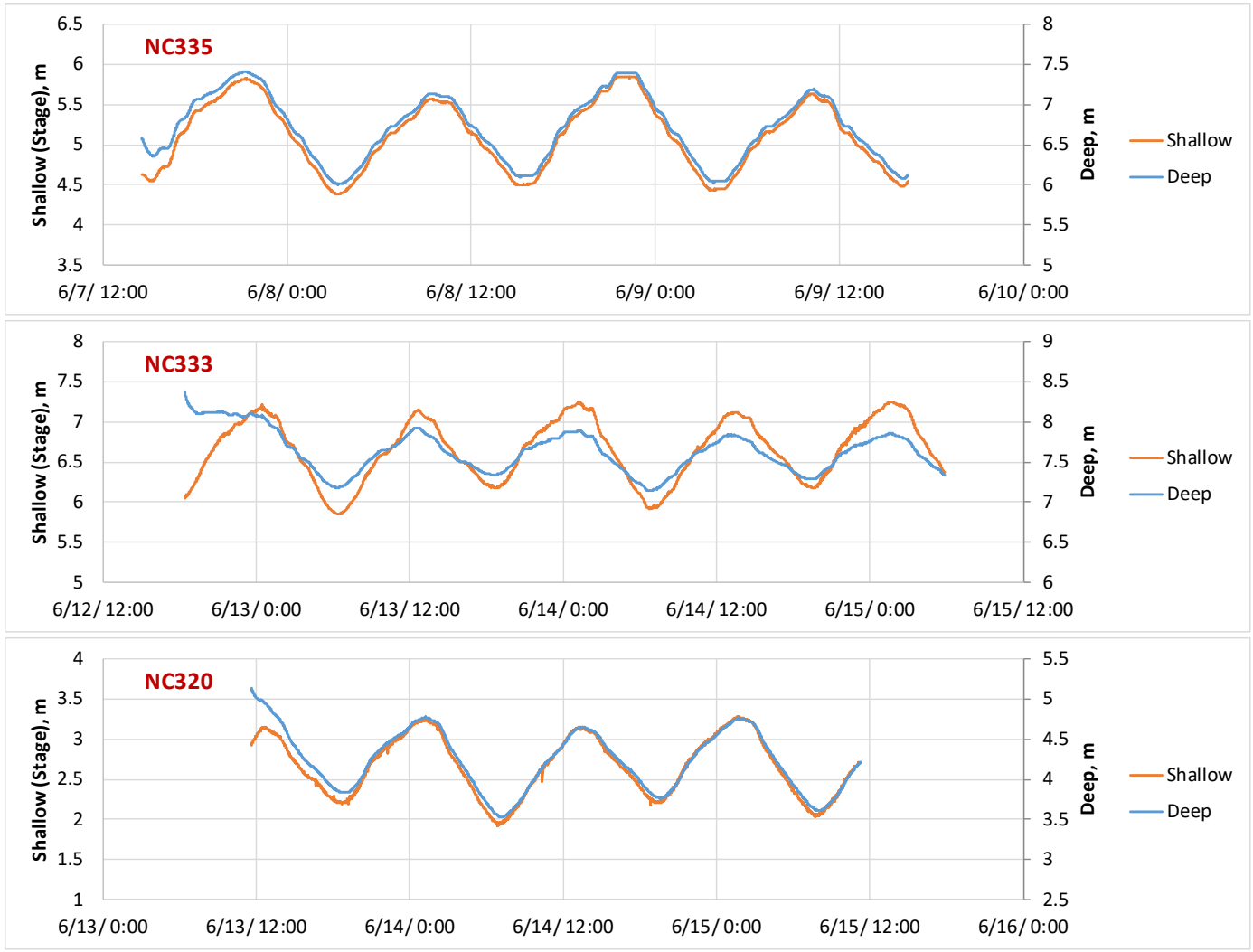

Figure 4 – Continued.

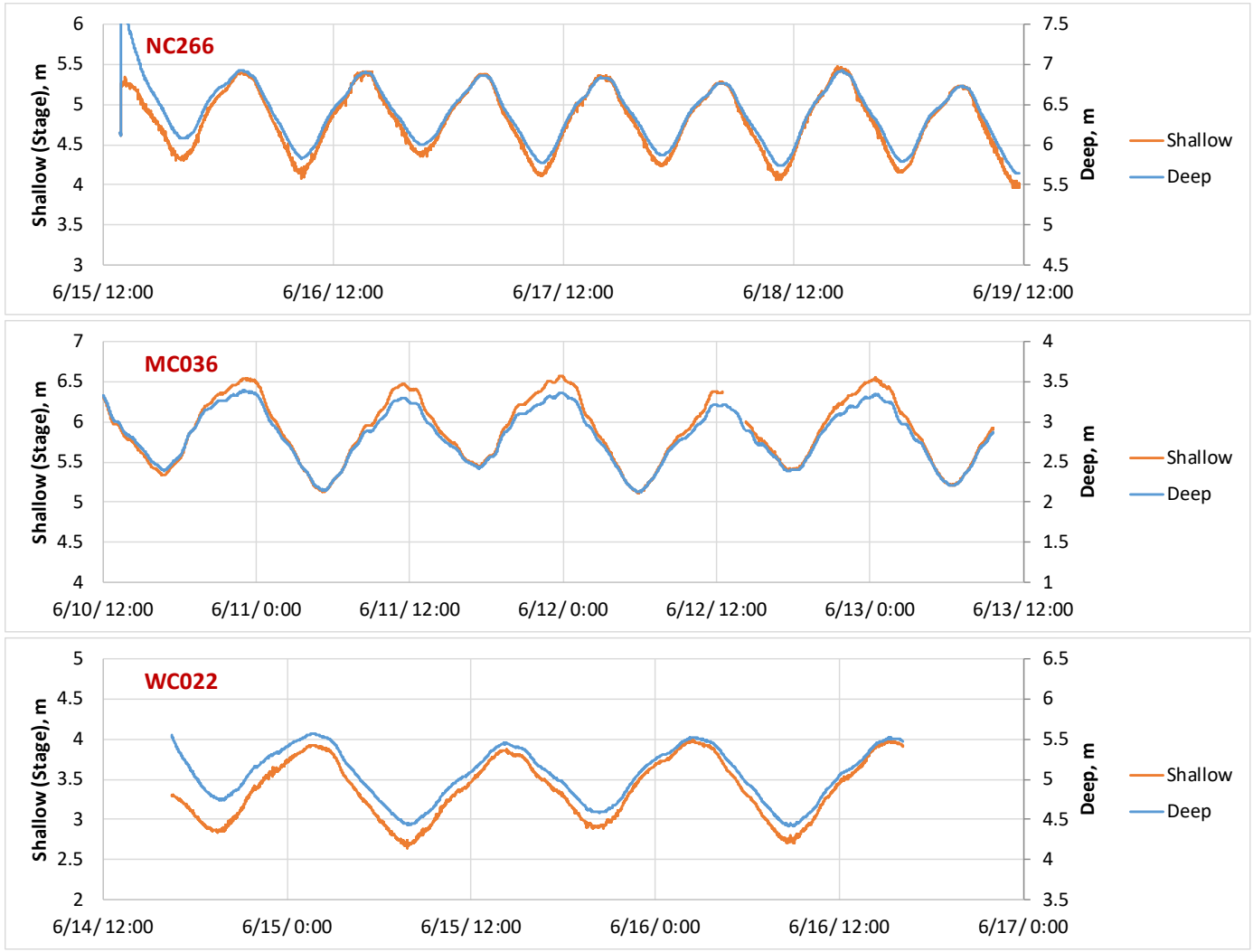

Figure 4 -- Continued.

Ebullition

Gas released from the sediment covered by each ESM was collected in the 3-liter gas-collection chamber during intervals bounded by zero-flow calibration periods. Prior to initiation of all but the first zero-flow calibration period, the hard-hat diver connected a 1-liter inverted collection bottle filled with water to the top of the gas-collection chamber. After connection, valves on the bottle and at the top of the ESM gas-collection chamber were opened, allowing trapped gas to rise into the collection bottle. The diver waited until bubbles, visible through the translucent plastic, stopped rising into the collection bottle. The diver then closed the valve, removed the bottle from the connector, and brought the bottle to the surface. Any remaining water in the bottle was poured into and measured with a graduated cylinder and the measured volume was subtracted from the known volume for a completely full bottle. The difference in volumes was equivalent to the volume of gas released into the collection bottle. During gas collection, if the diver observed that the collection bottle was becoming nearly full of gas, the chamber and bottle valves were closed, the bottle was brought to the surface for measurement, and the process was repeated until no additional gas was released from the ESM. The total gas collected was then divided by the time interval between zero-flow calibration periods, and gas release in units of milliliters per minute and milliliters per day were calculated.

This method of determining ebullition volume is appropriate for making corrections to measured seepage fluxes because the volume of gas accumulated inside the cylinder displaced an equal volume of water that was exhausted from the ESM through the flowmeter. However, the actual volume of gas released at the sediment-water interface was less than the calculated volume. Based on the pressure-depth relation assuming a seawater density of 1,025 kilograms per cubic meter, and assuming the gas-collection bottle was 0.5 m above the sediment bed, actual gas released at the sediment bed would be reduced by 50 to 13 percent for water depths ranging from 1 to 4 m.

Accuracy

The ESM output is approximately 1 mV for each milliliter per minute of flow through the flowmeter over a range from +/−1 to 2,000 mV. Sensors typically operate near the low end of their designed input range. Sensitivity to salinity is small, but to achieve greater accuracy, sensors were calibrated at the Anchor QEA dock at Newtown Creek, once at the beginning of the field campaign in May and once after measurements were completed in June. Flowmeter EM5 was replaced with EM4 when excessively noisy data was collected at NC336 and EM5 was calibrated at the end of the May field campaign. Calibrations were made by connecting each flowmeter to ESM2, placing the cylinder on the sediment bed at the edge of the dock, connecting flexible tubing to the exhaust port of the flowmeter, and pumping water from or to the flowmeter with a peristaltic pump that pushed water into or pulled water out of a graduated cylinder, depending on whether upward or downward seepage was simulated. Flow rates were generated to span the normal range of flow rates, not including data spikes caused by external factors, based on field data collected in 2015 (Rosenberry, 2016). The time-averaged output from the ESM was related to change in volume in the graduated cylinder during each measurement period. Measurements began and ended precisely at the beginning of each minute as determined by the datalogger clock. Each constant-flow-rate period typically lasted for 7–10 minutes. Data were interpreted using simple linear regression with average output from each ESM plotted on the x-axis and change in volume in the graduated cylinder plotted on the y-axis. Calibration results are summarized in table 2.

Accuracy, the difference between measured and true values, can be viewed as a combination of precision and bias. System precision was determined from short-term variability in sensor output during periods of constant input. When no water flows through an immersed flowmeter, variability in sensor output, also referred to as "noise," is an indication of instrument precision. Precision was determined from standard deviations that were calculated during zero-flow periods when the flowmeter valve was closed. Sensor bias was addressed in two steps. First, sensor output was adjusted with instrument-specific multipliers that were determined using regression analysis against "known" values (table 2). Second, to correct for sensor drift, flow through the flowmeters was zeroed three to eight times during each sensor deployment at Newtown Creek. Standard deviations during zero-flow periods are presented in table 3 and summary values are presented in table 4. Whether the average or maximum values are used, standard deviations are suitable error bars for measurements made during each seepage-meter deployment.

Table 2. Onsite calibrations of electromagnetic (EM) flowmeters. [All EM calibrations were conducted using signal-processing unit no. 2. R^2, coefficient of determination; n, number of generated constant flow rates]

Date	Meter	Multiplier	R^2	n
5/17/17	EM1	1.1647	0.9998	12
5/17/17	EM3	0.8554	0.99998	10
5/26/17	EM4	1.1011	0.9999	10
5/17/17	EM5	1.1697	0.9998	9
6/23/17	EM1	1.0942	0.9989	10
6/24/17	EM4	1.2539	0.9997	10
6/23/17	EM5	1.1048	0.9999	10

Table 3. Averages of sensor output (in both millivolts [mV] and centimeters per day [cm/d]) during zero-flow drift-correction periods. The range in zero-flow average values during each sensor deployment, standard deviation (StDev), and average (Ave.) standard deviation during each zero-flow period are also shown. Values highlighted in yellow indicate a failed sensor component and were not used in determinations of the deployment-averaged zero-period standard deviation. Positive values indicate upward flow and negative values indicate downward flow. [Dates are given in M/DD/YYYY format; time is given in HH:MM format on a 24-hour clock. no., number; ESM, electromagnetic seepage meter; EM., electromagnetic]

Meter no. (ESM/EM)	Location	Date and time	Ave. zero (mV)	Ave. zero (cm/d)	Zero range (cm/d)	Zero StDev (cm/d)	Ave. Zero StDev (cm/d)
4/1	EK098	5/19/2017 9:28	11.7	2.13	0.94	0.56	2.24
4/1	EK098	5/19/2017 15:13	10.0	1.81		3.18	
4/1	EK098	5/20/2017 10:10	11.7	2.11		2.18	
4/1	EK098	5/20/2017 14:09	6.6	1.19		3.02	
2/1	EK098-2	6/20/2017 9:58	−0.1	−0.01	0.33	0.05	0.04
2/1	EK098-2	6/20/2017 14:35	1.0	0.17		0.04	
2/1	EK098-2	6/21/2017 11:15	0.6	0.10		0.03	
2/1	EK098-2	6/21/2017 15:30	0.3	0.05		0.04	
2/1	EK098-2	6/22/2017 8:19	−0.6	−0.10		0.03	
2/1	EK098-2	6/22/2017 10:40	−0.9	−0.16		0.06	
5/5	EK013	5/18/2017 13:43	−112.0	−21.11	5.95	0.73	2.67
5/5	EK013	5/19/2017 10:10	−111.5	−21.03		5.24	
5/5	EK013	5/19/2017 14:44	−108.7	−20.49		2.53	
5/5	EK013	5/20/2017 9:43	−80.4	−15.16		3.59	
5/5	EK013	5/22/2017 11:28	−97.2	−18.31		1.24	
4/4	EK013-2	6/19/2017 16:27	−65.4	−12.75	3.32	0.46	0.83
4/4	EK013-2	6/20/2017 10:25	−60.8	−11.85		0.61	
4/4	EK013-2	6/20/2017 15:02	−60.2	−11.75		1.54	
4/4	EK013-2	6/21/2017 10:48	−48.4	−9.43		0.35	
4/4	EK013-2	6/21/2017 15:57	−48.5	−9.46		1.21	
2/3	NC337	5/20/2017 15:51	0.6	0.08	0.31	0.09	0.18
2/3	NC337	5/22/2017 14:25	2.9	0.39		0.27	
2/3	NC337	5/23/2017 10:21	−5.9			4.14	
4/1	NC338	5/20/2017 15:27	10.7	1.93	2.81	3.77	1.99
4/1	NC338	5/22/2017 13:58	1.1	0.19		0.94	
4/1	NC338	5/23/2017 8:54	5.8	1.05		0.68	
4/1	NC338	5/23/2017 14:47	14.3	2.58		2.01	
4/1	NC338	5/24/2017 9:44	−1.2	−0.22		1.32	

Meter no. (ESM/EM)	Location	Date and time	Ave. zero (mV)	Ave. zero (cm/d)	Zero range (cm/d)	Zero StDev (cm/d)	Ave. Zero StDev (cm/d)
4/1	NC338	5/24/2017 14:10	4.9	0.89		3.14	
4/1	NC338	5/25/2017 8:53	7.3	1.32		2.57	
4/1	NC338	5/25/2017 13:19	6.0	1.09		1.47	
5/4	NC336	5/22/2017 14:54	5.7			7.75	
5/4	NC336	5/23/2017 9:32	−49.1	−8.71	7.43	1.43	0.88
5/4	NC336	5/23/2017 10:44	−52.7	−9.35		0.53	
5/4	NC336	5/23/2017 14:19	−79.4	−14.08		0.59	
5/4	NC336	5/24/2017 9:17	−41.1	−7.30		1.15	
5/4	NC336	5/24/2017 14:43	−40.9	−7.25		0.84	
5/4	NC336	5/25/2017 9:18	−37.5	−6.65		0.59	
5/4	NC336	5/25/2017 13:47	−39.9	−7.08		0.99	
4/4	NC334	6/7/2017 13:39	−89.7	−17.49	11.96	0.87	2.57
4/4	NC334	6/8/2017 10:56	−102.6	−20.02		3.98	
4/4	NC334	6/8/2017 14:59	−119.3	−23.26		2.54	
4/4	NC334	6/9/2017 10:04	−151.0	−29.45		4.69	
4/4	NC334	6/9/2017 14:20	−122.1	−23.82		0.74	
4/4	NC334-3	6/21/2017 17:14	-45.5	−8.87	1.35	1.22	0.65
4/4	NC334-3	6/22/2017 7:47	-49.6	−9.68		0.68	
4/4	NC334-3	6/22/2017 14:30	-44.3	−8.63		0.59	
4/4	NC334-3	6/23/2017 10:49	-44.0	−8.58		0.39	
4/4	NC334-3	6/23/2017 16:58	-42.7	−8.33		0.35	
2/1	NC335	6/7/2017 14:46	−2.6	−0.44	0.59	0.14	0.06
2/1	NC335	6/8/2017 10:31	−0.6	−0.11		0.05	
2/1	NC335	6/8/2017 14:31	−0.4	−0.06		0.03	
2/1	NC335	6/9/2017 10:33	0.5	0.09		0.02	
2/1	NC335	6/9/2017 16:41	0.9	0.15		0.04	
5/5	NC339	6/8/2017 10:00	−105.1	−18.71	0.66	0.30	0.28
5/5	NC339	6/8/2017 14:05	−106.0	−18.88		0.33	
5/5	NC339	6/9/2017 10:59	−107.4	−19.12		0.15	
5/5	NC339	6/9/2017 16:16	−108.8	−19.38		0.30	
5/5	NC339	6/10/2017 8:37	−105.6	−18.80		0.32	
4/4	NC340-2	6/9/2017 15:52	−120.6	−23.53	13.35	2.19	1.30
4/4	NC340-2	6/10/2017 8:10	−135.5	−26.42		1.40	
4/4	NC340-2	6/12/2017 12:14	−67.0	−13.07		0.31	

Meter no. (ESM/EM)	Location	Date and time	Ave. zero (mV)	Ave. zero (cm/d)	Zero range (cm/d)	Zero StDev (cm/d)	Ave. Zero StDev (cm/d)
2/1	NC168	6/9/2017 17:53	1.9	0.32	0.12	0.06	0.05
2/1	NC168	6/10/2017 7:37	2.1	0.35		0.03	
2/1	NC168	6/12/2017 15:45	1.4	0.23		0.05	
5/5	MC036	6/10/2017 10:03	−105.9	−18.86	0.26	0.42	0.40
5/5	MC036	6/12/2017 11:38	−106.0	−18.87		0.56	
5/5	MC036	6/13/2017 9:51	−104.5	−18.61		0.23	
4/4	NC273	6/12/2017 15:12	−103.2	−20.12	7.61	0.78	0.75
4/4	NC273	6/13/2017 8:46	−102.1	−19.91		0.82	
4/4	NC273	6/13/2017 14:44	−92.5	−18.05		0.65	
4/4	NC273	6/14/2017 10:17	−65.6	−12.79		0.78	
4/4	NC273	6/14/2017 14:56	−64.2	−12.52		0.68	
2/1	NC333	6/12/2017 17:10	1.7	0.28	0.19	0.03	0.04
2/1	NC333	6/13/2017 9:13	1.6	0.28		0.01	
2/1	NC333	6/13/2017 14:14	1.2	0.20		0.11	
2/1	NC333	6/14/2017 9:51	2.2	0.37		0.02	
2/1	NC333	6/14/2017 14:22	1.0	0.18		0.04	
2/1	NC333	6/15/2017 6:06	2.0	0.34		0.02	
5/5	NC320	6/13/2017 11:37	−104.6	−18.63	0.79	1.41	0.54
5/5	NC320	6/13/2017 15:13	−107.7	−19.17		0.52	
5/5	NC320	6/14/2017 10:44	−103.2	−18.38		0.26	
5/5	NC320	6/14/2017 13:52	−105.4	−18.76		0.53	
5/5	NC320	6/15/2017 8:23	−103.4	−18.40		0.25	
5/5	NC320	6/15/2017 12:25	−105.4	−18.76		0.28	
4/4	WC022	6/14/2017 16:25	−99.5	−19.41	9.04	2.27	0.95
4/4	WC022	6/15/2017 7:56	−96.2	−18.75		1.15	
4/4	WC022	6/15/2017 11:52	−84.3	−16.43		0.65	
4/4	WC022	6/16/2017 11:01	−58.0	−11.31		0.37	
4/4	WC022	6/16/2017 16:30	−53.2	−10.37		0.31	
2/1	NC362	6/15/2017 7:22	2.1	0.35	0.50	0.03	0.03
2/1	NC362	6/15/2017 11:23	0.8	0.14		0.03	
2/1	NC362	6/16/2017 11:34	1.5	0.26		0.04	
2/1	NC362	6/16/2017 15:53	1.2	0.21		0.04	
2/1	NC362	6/17/2017 7:52	−0.9	−0.15		0.02	
5/5	NC266	6/15/2017 14:02	−107.1	−19.07	0.38	0.36	0.23

Meter no. (ESM/EM)	Location	Date and time	Ave. zero (mV)	Ave. zero (cm/d)	Zero range (cm/d)	Zero StDev (cm/d)	Ave. Zero StDev (cm/d)
5/5	NC266	6/16/2017 10:30	−105.0	−18.69		0.19	
5/5	NC266	6/16/2017 15:23	−105.8	−18.84		0.22	
5/5	NC266	6/17/2017 7:05	−105.8	−18.83		0.24	
5/5	NC266	6/19/2017 11:57	−106.8	−19.01		0.13	
4/4	NC008	6/16/2017 17:46	−53.8	−10.49	1.42	1.30	0.79
4/4	NC008	6/17/2017 6:43	−52.2	−10.18		0.53	
4/4	NC008	6/19/2017 11:20	−49.5	−9.65		0.51	
4/4	NC008	6/19/2017 14:37	−46.5	−9.07		0.82	

Table 4. Average and maximum of the two to eight zero-flow standard deviations (from table 3) determined at each measurement location, in centimeters per day. [ESM, electromagnetic seepage meter; EM, electromagnetic flowmeter; Ave., average; SD, standard deviation; Max., maximum; n, number of zero-flow measurement periods]

ESM/EM	Location	Ave. SD	Max. SD	n
ESM2/1	EK098-2	0.04	0.06	6
ESM2/1	NC335	0.06	0.14	5
ESM2/1	NC168	0.05	0.06	3
ESM2/1	NC333	0.04	0.11	6
ESM2/1	NC362	0.03	0.04	5
ESM4/1	EK098	2.24	3.20	4
ESM4/1	NC338	1.99	3.80	8
ESM2/3	NC337	0.18	0.27	2
ESM4/4	EK013-2	0.83	1.54	5
ESM4/4	NC334	2.57	4.69	5
ESM4/4	NC334-3	0.65	1.22	5
ESM4/4	NC340-2	1.30	2.19	3
ESM4/4	NC273	0.75	0.82	5
ESM4/4	WC022	0.95	2.27	5
ESM4/4	NC008	0.79	1.30	4
ESM5/4	NC336	0.88	1.43	7
ESM5/5	EK013	2.67	5.24	5
ESM5/5	NC339	0.28	0.33	9
ESM5/5	MC036	0.40	0.56	3
ESM5/5	NC320	0.54	1.41	6
ESM5/5	NC266	0.23	0.36	5

Accuracy Concerns Where Standard Deviation was Greater Than 1

Some of the standard deviations in table 4 are unusually large, which was a concern when determining period-averaged values where seepage was very slow. Several of the larger values can be discounted. For example, the large average standard deviations of 2.24, 2.57, and 2.67 cm/d at EK098, NC334, and EK013, respectively, were greatly diminished when those three locations were revisited in June. Other large standard deviations may be due to filtering animals creating microcurrents during zero-flow periods. Although measurement errors can overwhelm the input signal when seepage rates are particularly slow, random errors during periods of seconds to minutes can be substantially reduced by averaging output during periods of hours to days. If errors are random, the standard deviation is halved every time the sample size increases by four times. Furthermore, seepage often was substantially faster than the time-averaged values due to tidally driven perturbations, so that seepage at any given moment likely was faster than the standard deviation, even where the standard deviations were larger than expected. After further investigation, larger standard deviations likely were due to data cables that allowed excessive passage of electromagnetic noise, perhaps due to failing signal shielding.

Accuracy can be determined on the basis of (1) differences between measured and regression-modeled values, (2) variability in sensor output during periods of zero flow due to sensor drift, and (3) the standard deviation of average values during zero-flow periods.

1. Differences in modeled values
   Differences between measured and modeled values is a commonly used measure of accuracy. Regression-based calibrations for each ESM all have very large R^2 values (table 2) but because of the relatively large range over which field-based calibrations were made (to represent the range of 1-minute values typically measured during the 2015 field campaign [Rosenberry, 2016]), even small offsets from the regression line can cause substantial inaccuracy when flows are slow. However, comparisons between modeled and measured seepage during onsite calibrations were remarkably good, with 40 of 41 differences of 0.5 cm/d or less during May calibration measurements and 27 of 30 differences of 0.5 cm/d or less during June calibration measurements.

2. Sensor drift
   Adjustments made for sensor drift inherently assume that the drift is linear between periods when flow is shut off. If drift is indeed linear, and several periods of zero-flow measurements are generated during each sensor deployment, sensor drift can be eliminated. One indicator of the degree of potential error that would occur if this assumption were not true is to compare the range in average values of zero-flow periods during each sensor deployment, as given in the sixth column in table 3. The range in zero-flow values for each deployment was less than 1 cm/d for 11 of the 20 deployments (table 3). Two deployments (NC334, NC340-2) had a range in zero-flow-value output greater than 10 cm/d. It is likely that biological activity was responsible for the larger range in zero-flow values at NC334, which is why that location was revisited later in the data-collection period (NC334-3), during which the range in zero values was only 1.35 cm/d. However, no explanation is readily available for the larger range in zero-output values at NC340-2. This does not imply that drift corrections were not successful at eliminating drift-associated error, only that the potential for an uncorrected error is greater when larger drift corrections are required.

3. Standard deviations (Inherent system noise)
   Standard deviations of the eleven 1-minute values analyzed during each zero-flow period generally were small during zero-flow periods; maximum values ranged from 0.04 cm/d to generally less than 1 cm/d (table 4). The largest standard deviations were associated with output from ESM4/4 (or ESM5/4 during a later deployment), with maximum standard deviations exceeding 1 cm/d at seven of the eight locations where ESM4/4 or 5/4 was deployed (table 4). Averages of standard deviations during zero-flow periods were greater than 1 cm/d at only two of those eight locations and at one of those locations, NC334, the larger standard deviation may have been biologically induced. Several of these larger values likely were caused or exacerbated by a noisy data cable; others may have been caused by electromagnetic noise in the area during zero-flow periods. Two other locations, both where ESM4/1 was deployed, also had larger standard deviations during zero-flow periods. At EK098, noise increased substantially about half way through the deployment period and that location was revisited a month later. The increased noise may have been due to filtering animals or nearby industrial processes. At NC338, seepage commonly was quite fast; therefore, larger-than-normal standard deviations had little if any effect on interpretation of the data. One other location, EK013, had unusually large standard deviations during zero-flow periods and, fortunately, that location also had large diurnal fluctuations in seepage such that this larger-than-normal standard deviation had no effect on interpretation of the data.

Collectively, these three measures of ESM accuracy indicate that, unless special circumstances were noted, accuracy was approximately 0.5 cm/d and sensor drift or standard deviation was the largest source of error.

Interpretations for Specific Measurement Locations

Two charts are presented at the beginning of the description for each measurement location. Descriptions are presented in the same order as data collection (table 1). Commonly, the three ESMs were deployed during overlapping periods (fig. 5). For each measurement location, the upper chart displays seepage data plotted on the left axis that have been smoothed. Each smoothed value on the plot is an average of seven 1-minute values centered in time around each time-averaged value. Relative tide (the height of the water column above the pressure transducer) in units of meters, measured at the upper pressure transducer of the VHG rod installed adjacent to each seepage cylinder, is plotted on the right axis. Green rectangles indicate periods for which data were summarized. For all deployments, two periods were analyzed; therefore, two green rectangles indicate the durations of those data-analysis periods. For consistency of interpretation, analysis periods began and ended at low tide unless otherwise indicated. Tidal ranges varied during the study and vertical blue and red bands in figure 5 indicate dates when spring or neap tides occurred. Summary statistics for each analysis period are displayed in table 1. For convenience, data statistics for each measurement location are also presented in an abbreviated table embedded in the upper of the two charts for each measurement location. The lower chart displays the same seepage data on the left axis but with hydraulic gradient plotted on the right axis. Positive values indicate upward flow and negative values indicate downward flow. Values collected during drift-correction zero-flow calibration periods are not plotted in either chart. A qualitative summary describing the perceived overall quality of data collected at each measurement location is presented in table 5.

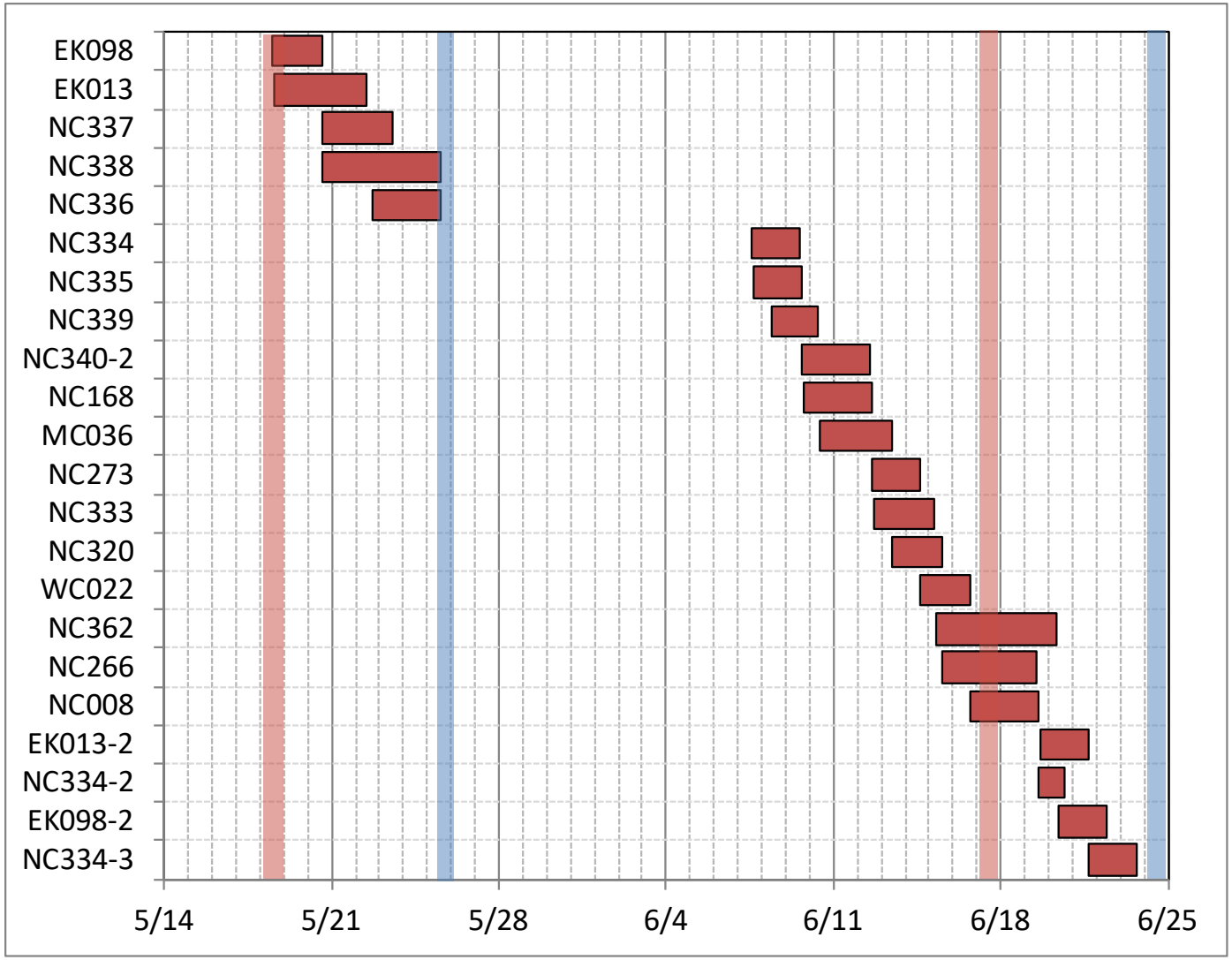

Figure 5. Duration of electromagnetic seepage meter data collection at each Newtown Creek deployment during May and June 2017 field campaigns. Locations on y-axis are also shown in figure 1. Blue vertical bands indicate spring tide; red vertical bands indicate neap tide. Perigean spring tides occurred during May and June.

Table 5. Relative quality of data collected at Newtown Creek seepage-measurement locations. [cm/d, centimeter per day; *i*, hydraulic gradient]

Location	Usability of data	Notes/discussion
EK098	Moderate	Slow seepage but with easily detectable features. Small system drift (less than 1 cm/d zero range in table 3) but zero-period standard deviation averaged greater than 2 cm/d. Data noise inexplicably increased greatly for the second half of the deployment but that did not have an effect on the time-averaged seepage value. This location was revisited because of the large increase in variance.
EK098-2	Excellent	No problems detected. Zero-range and zero-period standard deviations both were very small.
EK013	Poor	Seepage variance was small during the first 20 hours and then increased greatly after that. System drift was nearly 6 cm/d and zero-period standard deviation averaged 2.67, or 3.15 cm/d if the first 20 hours are excluded. This location was revisited because of the large variance and large range in zero values.
EK013-2	Good	No problems detected. The system performed consistently during deployment. The large early downward seepage was caused by a thunderstorm. Three of five zero-period standard deviations were less than 1 cm/d.
NC337	Poor	Electromagnetic noise was present during the entire deployment and was dealt with by filtering the noise that occurred regularly near the top of each hour. A sudden shift in data output occurred on May 22. A power inverter failed that resulted in loss of data for 18 hours. Data were very noisy after the system was restored. Seepage and *i* indicated flow in opposite directions.
NC338	Moderate/good	Seepage responded substantially to tides. Zero-value range was moderate at 2.81 cm/d and zero-period standard deviation was less than 2 cm/d during four of eight zeroing periods.
NC336	Moderate/good	Seepage was very noisy during the first 15 hours of deployment. Zero-value range was the third largest of the deployments, although five of eight zero-period standard deviations were less than 1. The large spikes observed on May 23 are similar to what was observed during documented barge passage in 2015.
NC334	Poor	Seepage pattern was strange and unrelated to tides, and seepage values were large and negative, indicating fast downward flow while *i* was always indicating upward flow. The range in zero values was the second largest of all deployments and three of five zero-value standard deviations were greater than 2.5 cm/d. For all these reasons, this location was revisited. Seepage and *i* indicated flow in opposite directions.
NC334-3	Good	Seepage varied over a relatively large range, but zero-period seepage values had a small range with standard deviations that were all less than 1 cm/d.
NC335	Excellent	Seepage was consistently slow and responsive to tides and the zero-value range was small at 0.59 cm/d. Zero-period standard deviations were all very small with four of five values well less than 0.1.
NC339	Excellent	Very clean data during the entire deployment with a substantial tidal influence. Zero-value range was small at 0.66 cm/d and zero-period standard deviations averaged 0.28 cm/d.
NC340-2	Poor/moderate	Data were fairly noisy and poorly related to tide or *i*. The range in zero-period values was the largest of all deployments at greater than 13 cm/d, although zero-period standard deviations were tolerably small, ranging from 0.31 to 2.19 cm/d.

Location	Usability of data	Notes/discussion
NC168	Excellent	Clean data, small range in zero-flow values, and small standard deviations during zero-flow periods. Seepage and *i* indicated flow in opposite directions.
MC036	Good/excellent	Clean data with two periods of greater noise that, based on their timing, likely were indicative of ebullition periods. The range in zero-flow values was less than 0.3 cm/d and zero-period standard deviations averaged 0.40 cm/d.
NC273	Poor/moderate	The first 5 hours of data were very noisy but then short-term variance became comparable to other datasets. Data were not correlated with tides or *i*, and variations were unusual, perhaps indicating the influence of biological activity. The range of zero-period averages was fairly large at 7.61 cm/d, but zero-period standard deviations were reasonably small and were all less than 1 cm/d. Seepage and *i* indicated flow in opposite directions during the second analysis period.
NC333	Good/excellent	Seepage was small and alternated between upward and downward flow in response to tides. The cause of larger noise until about 03:00 on June 13 is unknown. Both the zero-period range and the average of zero-period standard deviations were very small.
NC320	Moderate	Data were very noisy during the first 16 hours and the last 4 hours of data collection with patterns that are similar to those associated with filtering benthic animals. However, the range of zero-period values was less than 1 cm/d, as was the average of standard deviations during zero-flow periods.
WC022	Good	Data were clean with consistent variance and were correlated with both stage and *i*. The range of zero-period values was relatively large at 9.04 cm/d and two of five zero-period standard deviations were greater than 1 cm/d. Seepage and *i* indicated flow in opposite directions during the first analysis period, likely because of slow recovery of overpressuring during vertical hydraulic gradient rod installation. If analysis periods are shifted by one-half of a tidal period, both analysis periods indicate slow upward seepage.
NC362	Good	Seepage varied over a relatively narrow range most of the time and both the range in zero-period averages and zero-period standard deviations were small. However, some larger deviations in seepage were unexplained and may be due to a maneuvering barge or filtering benthic animals. Seepage and *i* indicated flow in opposite directions.
NC266	Excellent	Alternating periods of large variance and small variance are because of waves generated by boat traffic. Both range of zero-period averages and zero-period standard deviations are reasonably small.
NC008	Good	Noise was relatively small except for a period of slightly larger variance during the morning to early afternoon on June 18 that suggests a wavy period, similar to that observed at NC266. The range in zero-period values was slightly greater than 1 cm/d and zero-period standard deviations were reasonably small with three of four values less than 1 cm/d.

EK098

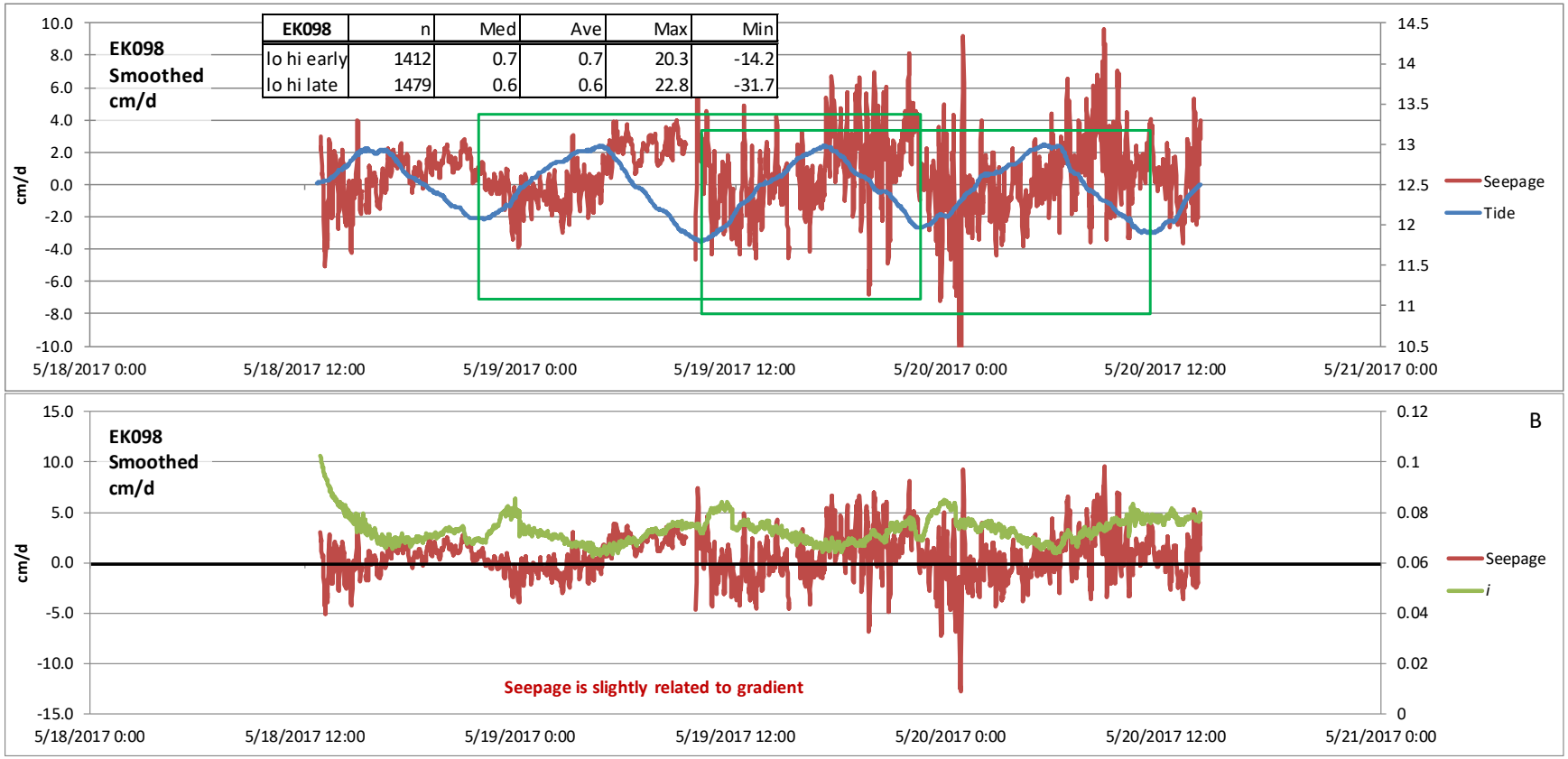

EK098	n	Med	Ave	Max	Min
lo hi early	1412	0.7	0.7	20.3	-14.2
lo hi late	1479	0.6	0.6	22.8	-31.7

Figure 6. Seepage measured each minute during deployment at EK098, in centimeters per day (cm/d). Chart A displays seepage smoothed with a 7-minute moving average, and relative tide in meters (m). The green rectangles indicate the duration of the data-analysis periods. In the inset table, "lo hi early" indicates the first instance of two complete tidal cycles beginning and ending with low tide, and "lo hi late" indicates the last two complete tidal cycles beginning and ending with low tide. Chart B displays smoothed seepage, with vertical hydraulic gradient (*i*) in m/m plotted on the right axis. (n, number of 1-minute values; Med, median of n values; Ave, average of n values; Max, maximum of n values; Min, minimum of n values)

Seepage at EK098 typically varied between −2 and 3 cm/d with a time-averaged value that was upward at less than 1 cm/d (fig. 6A). Tidally averaged values for the two periods indicated by the two green rectangles in figure 6A were 0.6 and 0.7 cm/d, respectively. Seepage was generally upward when the tide was falling and downward when the tide was rising. The transition from upward to downward seepage occurred a few hours after tidal nadir but the transition from downward to upward seepage was nearly coincident with tidal apex. The variance in measured seepage increased substantially following a zeroing period at about 9:30 on May 19. The cause of the increased variance is unknown, but it may have been caused by the presence of gas within the horizontally deployed flowmeter. The volume of gas collected in the ebullition collection chamber increased greatly following the 9:30 zeroing period on May 19 coincident with the beginning of the increased seepage variance. Whatever the cause of increased variance, it did not appear to affect the time-averaged seepage rate based on the similar time-averaged values of the two analysis periods. The largest spikes in the data occurred at 0:30 (downward) and 0:43 (upward) on May 20. Based on the time of day and the general lack of marine activity at this location, it is unlikely the spikes were caused by boat traffic.

The large upward *i* at the beginning of the measurement period (fig. 6B) was due to increased local hydraulic pressure created by sediment displacement during insertion of the VHG rod. The disturbance-induced pressure pulse appears to have dissipated by 16:30, about 3.5 hours after sensor installation. Subsequent *i* was upward during the entire measurement period, averaging 0.073±0.005. Vertical hydraulic gradient generally is inversely related to tide, but with a slight offset. Although the smallest upward *i* commonly was nearly coincident with highest stage, the largest upward *i* occurred about 1 to 1.5 hours after tidal nadir. Seepage is only slightly related to *i*, but not as one would expect if seepage were completely controlled by *i*. Hydraulic gradient was generally largest at the transition from upward to downward seepage and then decreased until 1–2 hours after seepage transitioned from downward to upward, after which *i* generally increased.

EK098-2

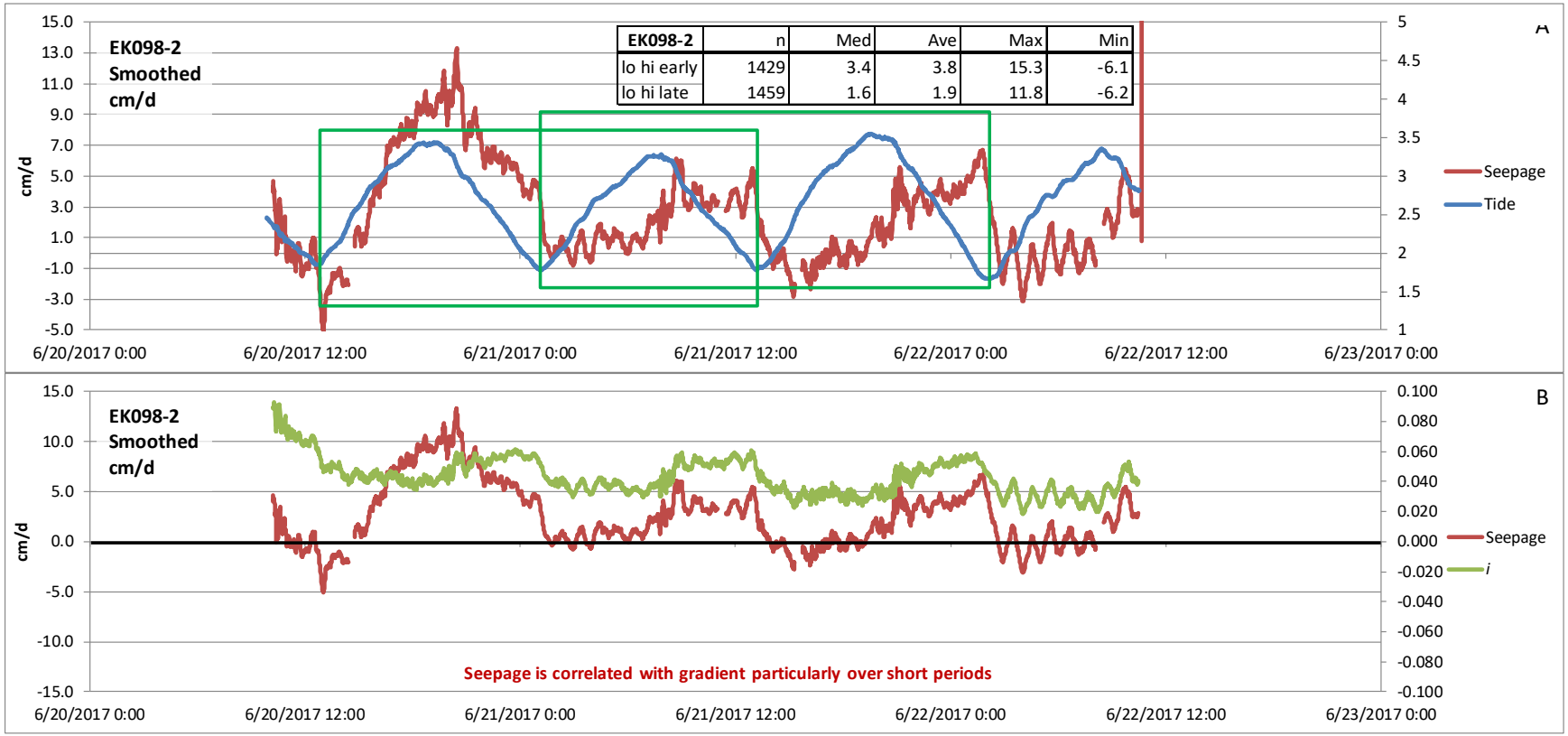

Figure 7. Seepage measured each minute during deployment at EK098-2, in centimeters per day (cm/d). Chart A displays seepage smoothed with a 7-minute moving average, and relative tide in meters (m). The green rectangles indicate the duration of the data-analysis periods. In the inset table, "lo hi early" indicates the first instance of two complete tidal cycles beginning and ending with low tide, and "lo hi late" indicates the last two complete tidal cycles beginning and ending with low tide. Chart B displays smoothed seepage, with vertical hydraulic gradient (*i*) in m/m plotted on the right axis. (n, number of 1-minute values; Med, median of n values; Ave, average of n values; Max, maximum of n values; Min, minimum of n values)

Location EK098 was revisited a month after the first visit in response to concerns regarding the unexplained increased variance during the second half of the May 18–20 deployment. Whereas seepage during the May deployment alternated between upward and downward flow in response to tides, seepage a month later was upward 76 percent of the time and average seepage was about 2 to 4 times faster than during the May deployment. Seepage during the first two of three tidal cycles averaged 3.8 cm/d and seepage during the second and third tidal cycles averaged 1.9

cm/d. The cause for substantially faster seepage between about 14:00 on June 20 and 01:00 on June 21 is unknown. It does not appear to be related to *i* hydraulic gradient, which was largely and unexpectedly inversely related to seepage during that period. Increased ebullition could also be responsible because gas trapped inside the seepage cylinder (by design) would displace water and cause greater flow out of the flowmeter. That is unlikely, however, as only 90 milliliters gas were collected during the period that spanned the fastest seepage rates.

Two other features are prominent in fig. 7A. Seepage is correlated with tide but is lagged several hours compared to the tidal cycle. Fastest seepage occurred 1.25 to 1.5 hours after tidal apex during the first two tidal cycles, but maximum seepage during the third tidal apex occurred about 6 hours after tidal apex. Upward seepage decreased rapidly coincident with tidal nadir and became downward about 1 hour after tide began to rise and remained downward for several hours before becoming upward again. The fast downward seepage shortly after midday tidal nadir on June 20 occurred during a fast-moving thunderstorm.

Seepage also was directly and strongly related to *i*, except during the large upward seepage rates that occurred during the first recorded tidal cycle (fig. 7B). The strong correlation with *i* may have actually been controlled by surface-water stage. When plotted inversely with smoothed change in surface-water stage, smoothed seepage shows a remarkable inverse correlation, with reversals in short-term seepage trends occurring within 1 to 3 minutes of reversals in change in surface-water stage (fig. 8).

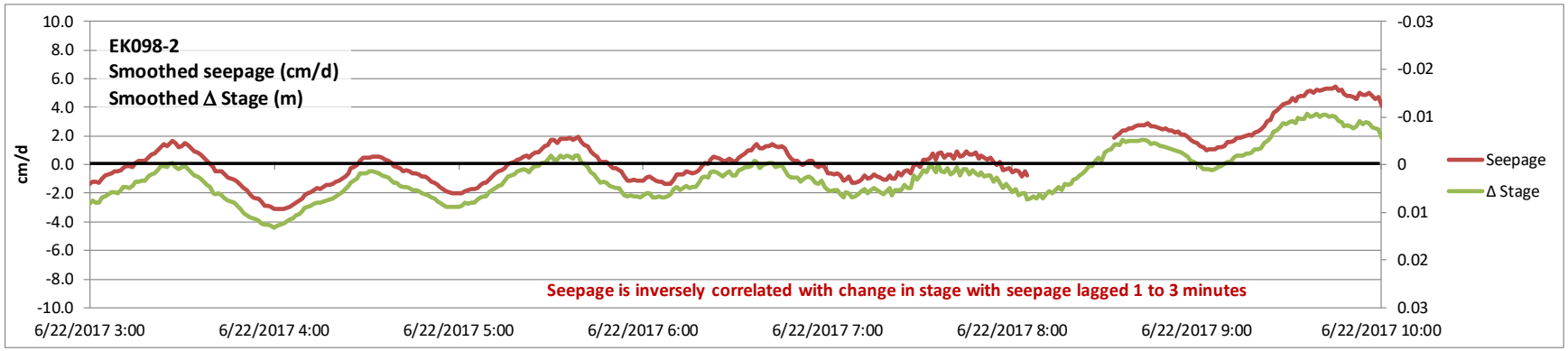

Figure 8. Seepage, in centimeters per day (cm/d), at EK098-2 measured each minute and smoothed with a 7-minute moving average, and change in stage (ΔStage), in meters (m), measured each minute and smoothed with a 7-minute moving average. Note that ΔStage is plotted inversely on the right axis.

EK013

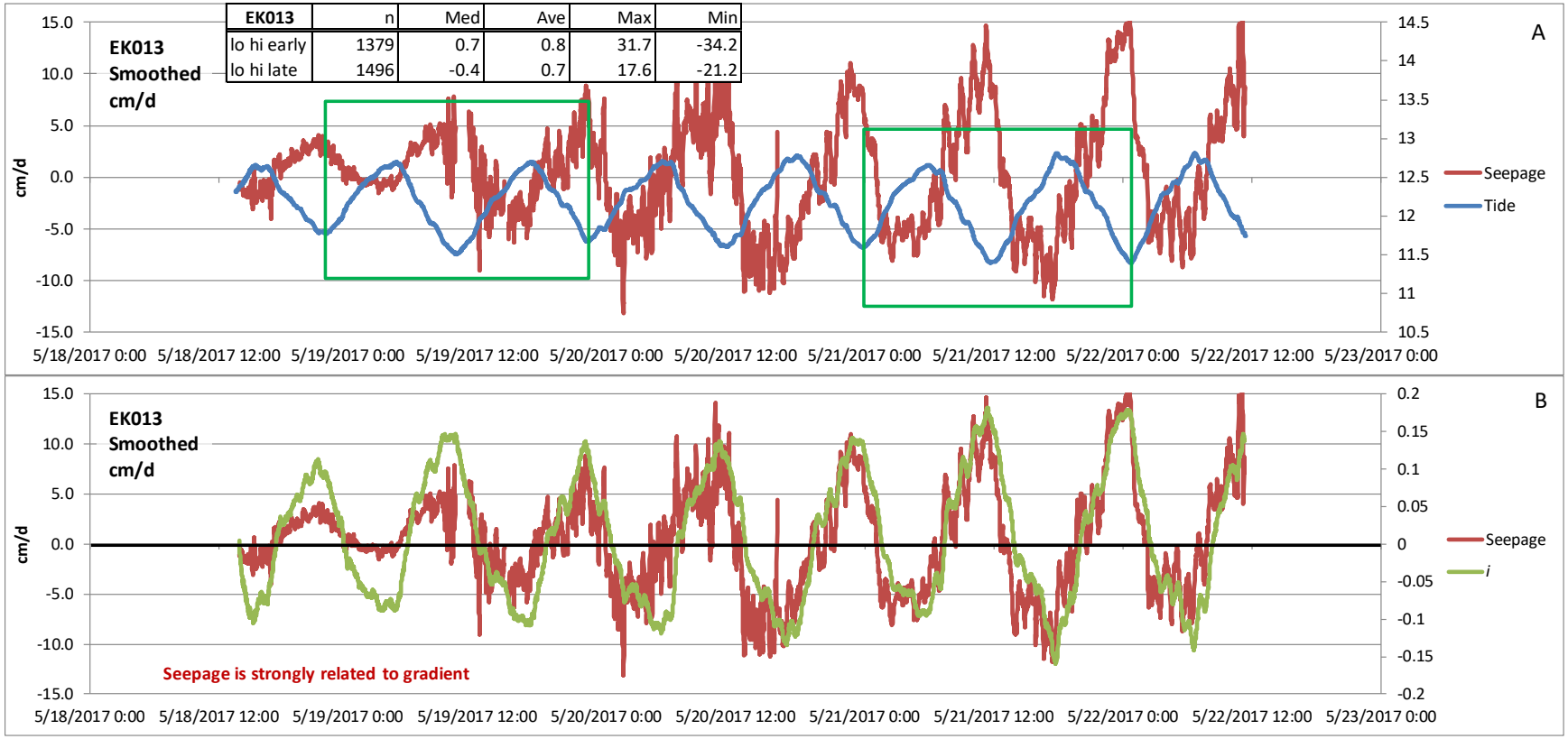

EK013	n	Med	Ave	Max	Min
lo hi early	1379	0.7	0.8	31.7	-34.2
lo hi late	1496	-0.4	0.7	17.6	-21.2

Figure 9. Seepage measured each minute during deployment at EK013, in centimeters per day (cm/d). Chart A displays seepage smoothed with a 7-minute moving average, and relative tide in meters (m). The green rectangles indicate the duration of the data-analysis periods. In the inset table, "lo hi early" indicates the first instance of two complete tidal cycles beginning and ending with low tide, and "lo hi late" indicates the last two complete tidal cycles beginning and ending with low tide. Chart B displays smoothed seepage, with vertical hydraulic gradient (*i*) in m/m plotted on the right axis. (n, number of 1-minute values; Med, median of n values; Ave, average of n values; Max, maximum of n values; Min, minimum of n values)

Seepage at EK013 varied substantially in response to tides, ranging from approximately −10 to 10 cm/d, but average seepage was upward at less than 1 cm/d (fig. 9A). Increasing variability between maximum upward seepage and maximum downward seepage did not substantially affect the time-averaged values. Average seepage during the first two tidal cycles was 0.8 cm/d and average seepage during the fifth and sixth tidal cycles was 0.7 cm/d. A third analysis period (not shown) beginning and ending with high tide that covers the last two tidal cycles included all of the largest diurnal seepage cycles at the end of the measurement period. Average seepage during that "hi-lo-hi-lo-hi" period was 0.9 cm/d. Maximum upward seepage always occurred close to tidal nadir but minimum seepage preceded tidal apex, ranging from about 45 minutes before tidal apex during the early portion of the data-collection period to 1.5–2 hours prior to apex during the latter portion of the data-collection period. Upward seepage decreased rapidly within minutes of tidal nadir.

Hydraulic gradient strongly controlled seepage at EK013 (fig. 9B). Seepage was nearly perfectly in phase with *i* and both seepage and *i* reversed during each tidal cycle, indicating upward and downward flow with every tidal cycle. The larger diurnal variability in both seepage and *i* during the last two tidal cycles was caused by greater variability in tidally driven stage change.

EK013-2

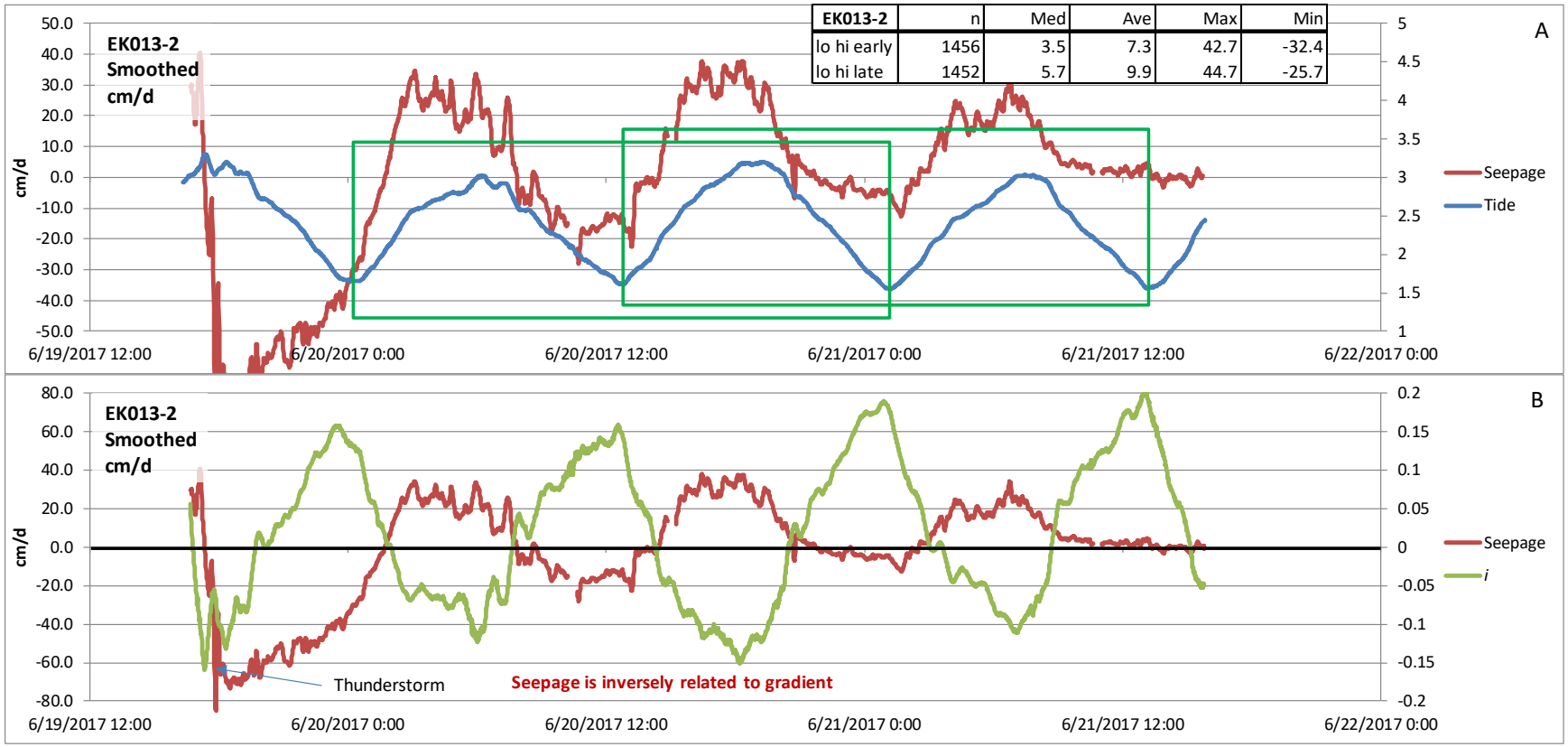

Figure 10. Seepage measured each minute during a second deployment at EK013, in centimeters per day (cm/d). Chart A displays seepage smoothed with a 7-minute moving average, and relative tide in meters (m). The green rectangles indicate the duration of the data-analysis periods. In the inset table, "lo hi early" indicates the first instance of two complete tidal cycles beginning and ending with low tide, and "lo hi late" indicates the last two complete tidal cycles beginning and ending with low tide. Chart B displays smoothed seepage, with vertical hydraulic gradient (*i*) in m/m plotted on the right axis. Blue line indicates zero seepage. (n, number of 1-minute values; Med, median of n values; Ave, average of n values; Max, maximum of n values; Min, minimum of n values)

Measured seepage at EK013 a month later during the June deployment was about an order of magnitude faster than during the May deployment. Upward seepage reached a value of about 30 to 35 cm/d and downward seepage typically reached a maximum value of −10 to −20 cm/d (fig. 10A). Time-averaged seepage was 7.3 and 9.9 cm/d during the two analysis periods. The very large downward seepage values shortly after deployment likely were in response to passage of a thunderstorm at about 17:45 on June 19, which caused an increase in the elevation and rate of

stage rise during the approach to high tide that generated exceptionally large downward hydraulic gradients. Because the first analysis period starting shortly after midnight on June 20 included a portion of the thunderstorm-influenced seepage values, a third period (not shown in fig. 10), starting with high tide at about 6:30 on June 20 and ending at high tide at about 7:45 on June 21, was analyzed. Average seepage during that period was 7.0 cm/d.

Seepage was greatly out of phase with *i*, indicating that measured seepage was in response to more than *i*. Seepage was about 3.5–4 hours lagged relative to *i*. Seepage, however, was substantially correlated with the rate of change in stage, which was determined by taking the difference between sequential stage values and then creating a 7-minute smooth to be comparable with the smoothed seepage data (fig. 11). If seepage is lagged by -3 hours, the correlation is particularly good. The substantial correlation with ΔStage may be related to trapped gas in the sediment as indicated by ebullition during deployment. Ebullition was greatly increased during the June deployment relative to the May deployment.

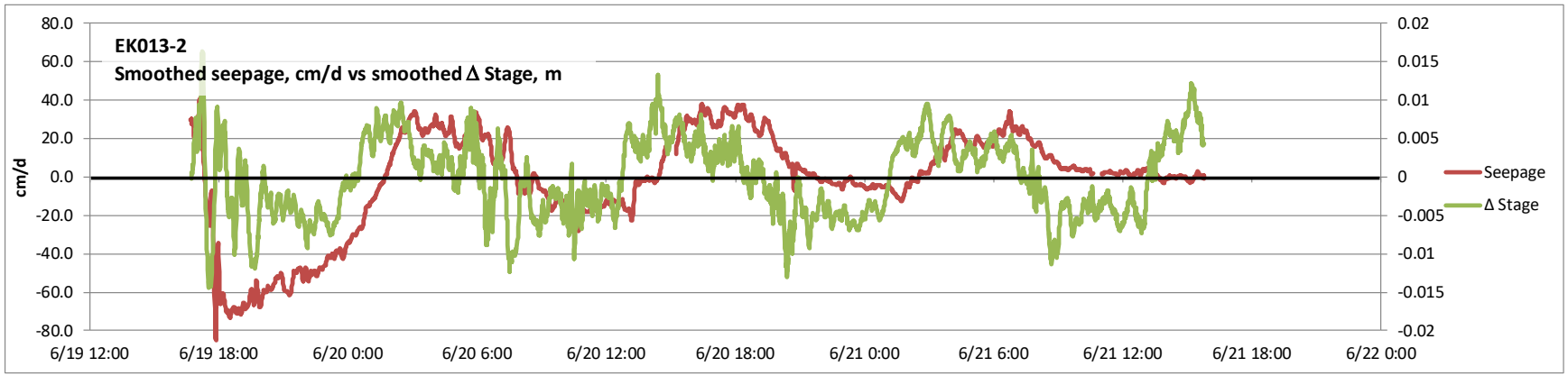

Figure 11. Seepage during a second deployment at EK013, in centimeters per day, with change in stage, in meters (m), plotted on the right axis.

NC337

Seepage recorded at NC337 exhibited a substantial and cyclical signal that was not related to the seepage itself (fig. 12). It is likely the signal was electromagnetic noise generated from an industrial operation near the bank or perhaps from an electrical cable buried in the sediment. Most of the noise occurred once every hour and extended from about 7 minutes before to about 5 minutes after the top of each hour. Therefore, the raw data were filtered to remove data from 9 minutes before to 8 minutes after the top of each hour. It is possible that additional cyclical electromagnetic noise existed, but only these largest signals were filtered. The resulting data are plotted in figure 13.

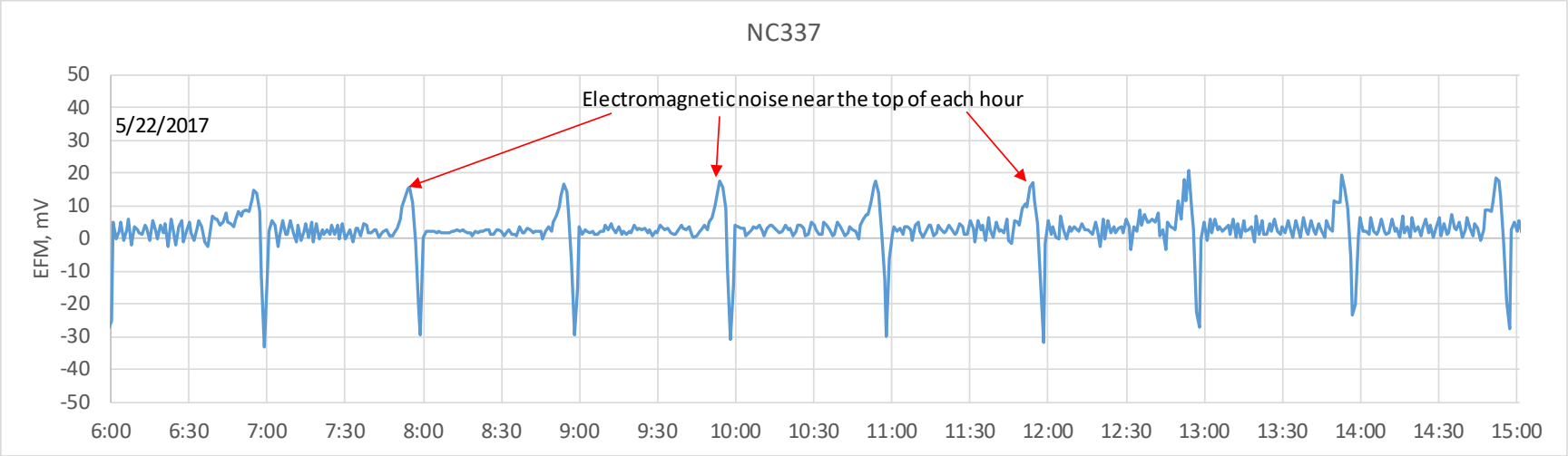

Figure 12. Raw electromagnetic seepage meter output, in millivolts, during a 9-hour period on May 22, 2017.

Seepage at NC337 was slow and downward on average. Average seepage during each of the two analysis periods was −0.3 cm/d. There was virtually no relation between seepage and tides or seepage and *i*. Permeability of sediments likely is slow at this location based on the approximately 10-hour period of equilibration following installations of both the seepage meter and the VHG rod (fig. 13B).

Downward seepage was increasing slightly until seepage suddenly decreased from about −0.5 cm/d to about −0.1 cm/d at about 03:50 on May 22. The cause for this shift is unknown. Following that shift, seepage averaged 0.0 cm/d until a power inverter failed at 15:51. Data were exceptionally noisy and clearly bad after ESM2 was replaced with ESM3 at 9:15 on May 23; output was ±100 mV. Therefore, the entire system was removed later in the day at 13:15. Because of the likely slow seepage in the center of the turning basin and the added exposure to barge and other large-watercraft traffic, this location was not revisited.

Hydraulic gradient was upward during the entire deployment but was trending downward the entire time. Average *i* was about 0.03 cm/d during the last two tidal cycles.

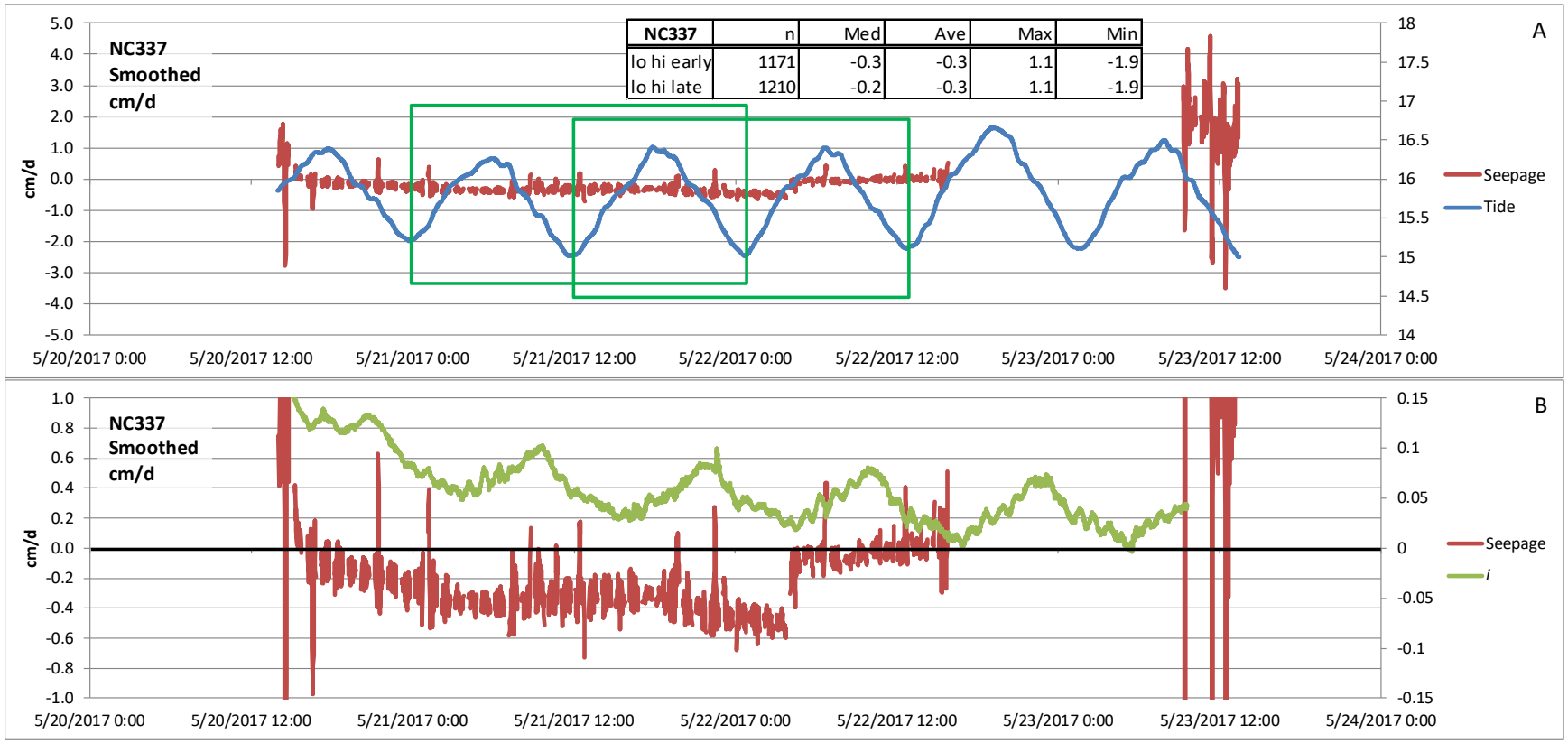

NC337	n	Med	Ave	Max	Min
lo hi early	1171	-0.3	-0.3	1.1	-1.9
lo hi late	1210	-0.2	-0.3	1.1	-1.9

Figure 13. Seepage measured each minute at NC337, in centimeters per day (cm/d). Chart A displays seepage smoothed with a 7-minute moving average, and relative tide, in meters (m). The green rectangles indicate the duration of the data-analysis periods. In the inset table, "lo hi early" indicates the first instance of two complete tidal cycles beginning and ending with low tide, and "lo hi late" indicates the next two complete tidal cycles beginning and ending with low tide. Chart B displays smoothed seepage, with vertical hydraulic gradient (*i*) in m/m plotted on the right axis. (n, number of 1-minute values; Med, median of n values; Ave, average of n values; Max, maximum of n values; Min, minimum of n values)

NC338

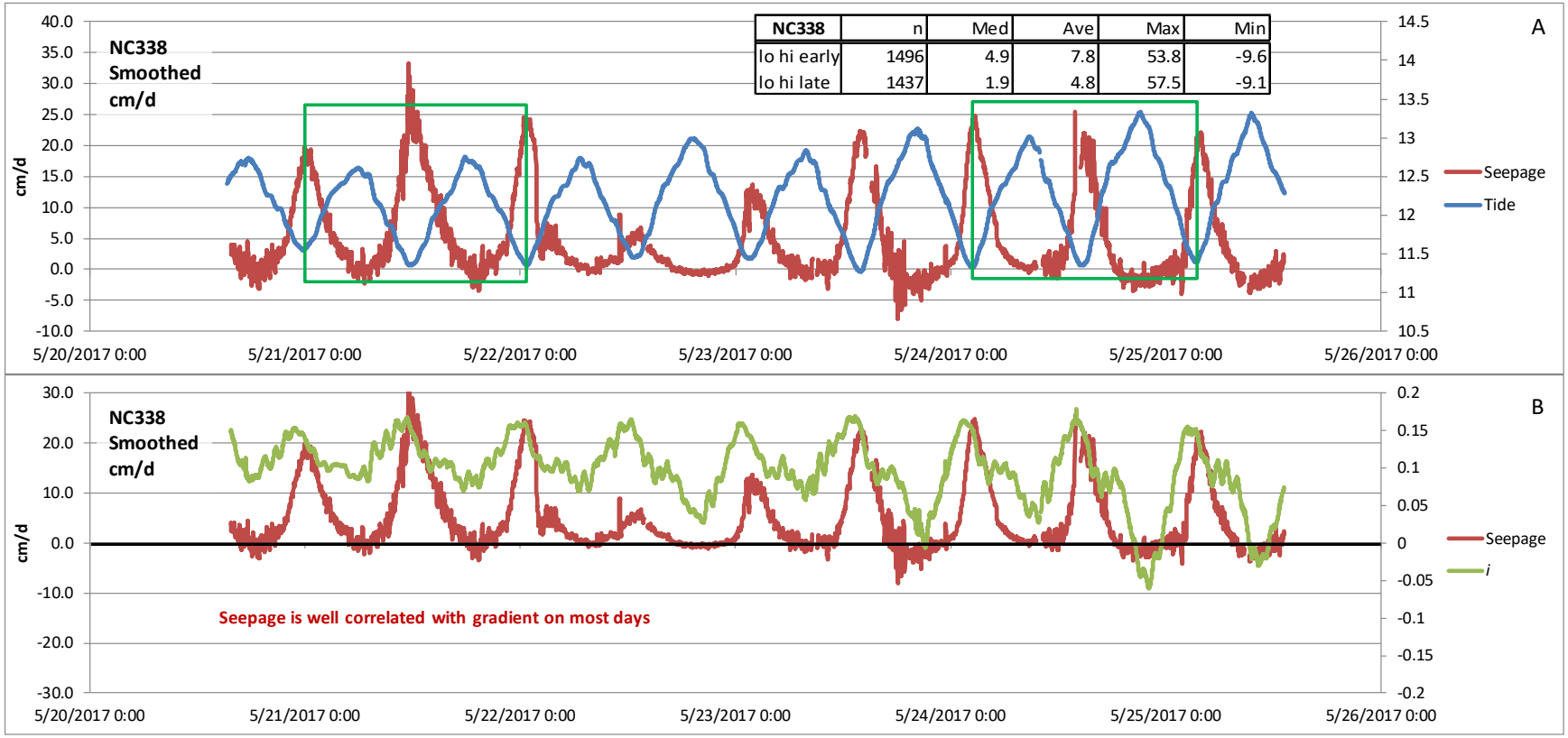

Figure 14. Seepage measured each minute at NC338, in centimeters per day (cm/d). Chart A displays seepage smoothed with a 7-minute moving average, and relative tide in meters (m). The green rectangles indicate the duration of the data-analysis periods. In the inset table, "lo hi early" indicates the first instance of two complete tidal cycles beginning and ending with low tide, and "lo hi late" indicates the last two complete tidal cycles beginning and ending with low tide. Chart B displays smoothed seepage, with vertical hydraulic gradient (*i*) in m/m plotted on the right axis. (n, number of 1-minute values; Med, median of n values; Ave, average of n values; Max, maximum of n values; Min, minimum of n values)

Seepage was highly variable and responsive to tides at NC338, ranging from nearly 35 cm/d during low tide during midday on May 21 to almost −10 cm/d during high tide during the evening of May 23 (fig. 14A). Average seepage during the two analysis periods was 7.8 and 4.8 cm/d, the second largest average seepage recorded during the 2017 deployments. However, the analysis periods, beginning and ending at low tide, occurred when seepage rates were sharply peaking. Therefore, periods that began and ended at high tide when seepage was not changing rapidly (fig. 15) also were selected for analysis. Average seepage during two of those analysis periods was little changed, at 7.4 and 4.6 cm/d. Seepage was not

nearly as fast during the two low tides shortly after noon on May 22 and at about 01:00 on May 23. If the analysis period began at the end of the "hi-lo" early period, average seepage would be only 2.4 cm/d. Standard deviations during zero-flow calibration periods were larger than at most other locations (table 3). However, given the large range in measured seepage at this location, the larger short-term measurement uncertainty did not affect period-averaged seepage rates or interpretation of the data.

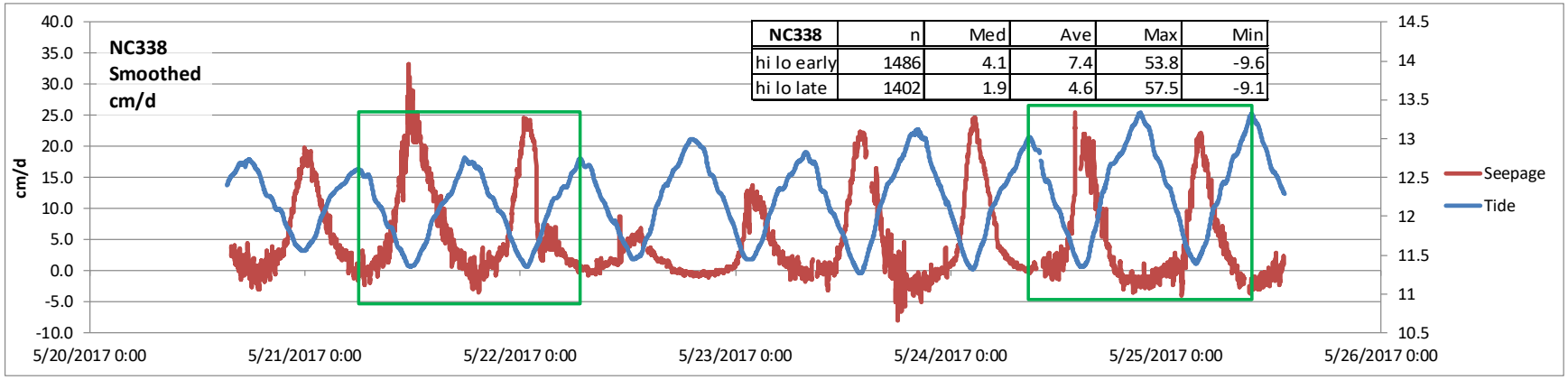

NC338	n	Med	Ave	Max	Min
hi lo early	1486	4.1	7.4	53.8	-9.6
hi lo late	1402	1.9	4.6	57.5	-9.1

Figure 15. Seepage measured each minute at NC338, in centimeters per day (cm/d), and relative tide, in meters (m), similar to figure 14. However, in this case the green rectangles indicate the duration of the data-analysis periods, "hi lo early" and "hi lo late," that begin and end with high tide rather than low tide. In the inset table, "hi lo early" indicates the first instance of two complete tidal cycles beginning and ending with high tide, and "hi lo late" indicates the last two complete tidal cycles beginning and ending with high tide. (n, number of 1-minute values; Med, median of n values; Ave, average of n values; Max, maximum of n values; Min, minimum of n values)

Maximum upward seepage rates were very sensitive to low tide, with upward seepage increasing at a rapid rate as the tide fell and then decreasing at a rapid rate as the tide rose. Large seepage rates did not occur, however, during the low tides shortly after noon and midnight on May 22. Those low tides were not as low as preceding and subsequent low tides, suggesting that the slightly higher low tide created smaller upward hydraulic gradients. However, that theory is not supported by the hydraulic gradient data. Values for *i* during those two tidal cycles were not appreciably different from those during preceding and subsequent tidal cycles (fig. 14B). It is likely that seepage was responding to hydraulic gradients over shallower intervals closer to the sediment-water interface.

Hydraulic gradient and seepage were well correlated. Maximum seepage, whether upward or downward, generally lagged maximum *i* by approximately 1 hour.

NC336

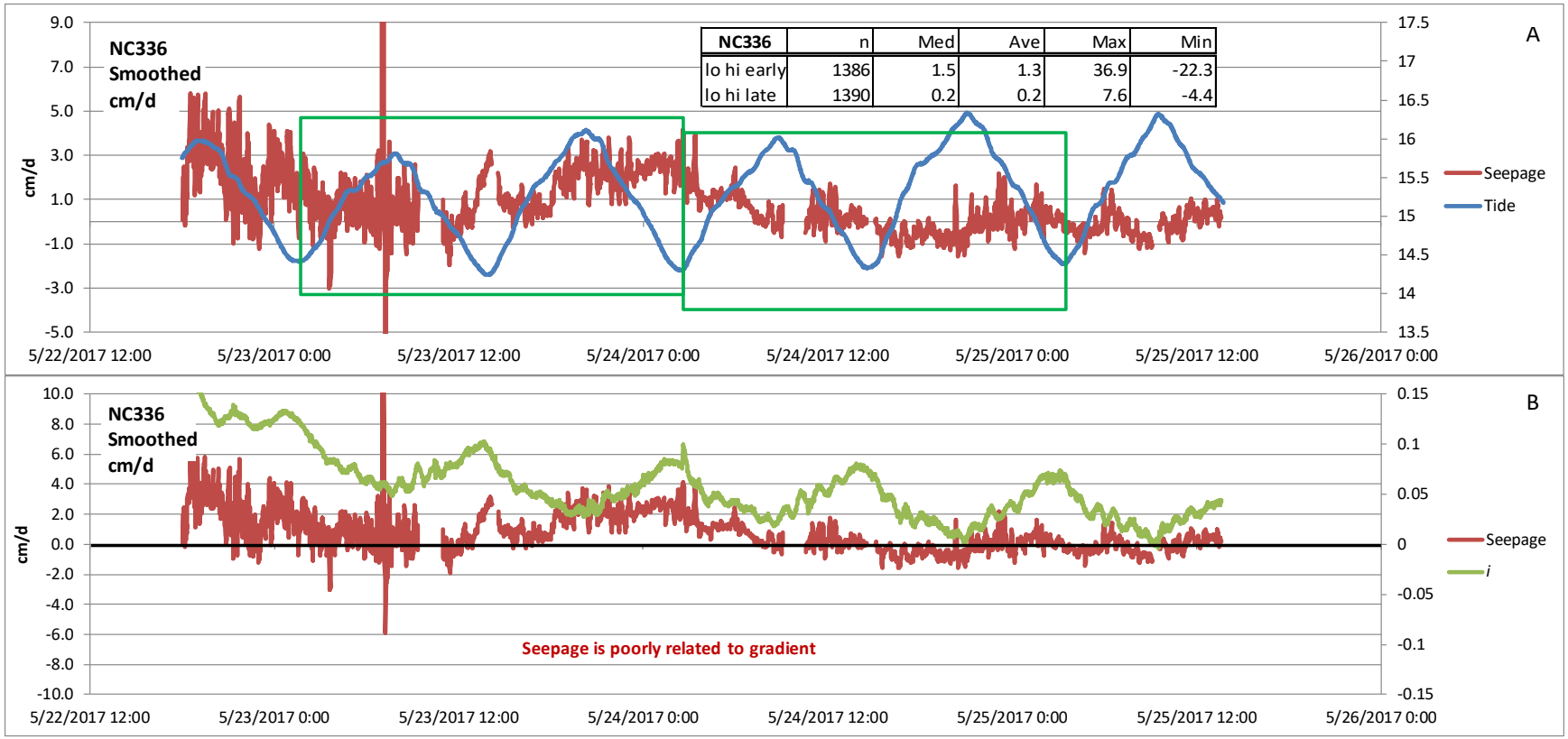

Figure 16. Seepage measured each minute at NC336, in centimeters per day (cm/d). Chart A displays seepage smoothed with a 7-minute moving average, and relative tide in meters (m). The green rectangles indicate the duration of the data-analysis periods. In the inset table, "lo hi early" indicates the first instance of two complete tidal cycles beginning and ending with low tide, and "lo hi late" indicates the last two complete tidal cycles beginning and ending with low tide. Chart B displays smoothed seepage, with vertical hydraulic gradient (*i*) in m/m plotted on the right axis. (n, number of 1-minute values; Med, median of n values; Ave, average of n values; Max, maximum of n values; Min, minimum of n values)

Measured seepage at NC336 was exceptionally noisy during the first 15 hours of deployment until a faulty data cable was replaced, after which variance decreased greatly during the rest of the deployment (fig. 16A). Average seepage was 1.3 and 0.2 cm/d, respectively, during the early and late analysis periods. To test the extent to which the larger early-period seepage rates and the large early-period variance may have increased the

early period value of 1.3 cm/d, additional periods beginning and ending with high tide and essentially one-half tidal cycle later than the periods shown in fig. 16A, were also analyzed. The averages of those two periods were 1.4 and −0.1 cm/d, respectively, indicating that the additional noise prior to 11:00 on May 23 had little effect on the time-averaged value. The cause of the large spikes in seepage, both upward at 36.9 cm/d and downward at −22.3 cm/d, are unknown. However, given the location (turning basin) and the time of day (07:00), the spikes may have been due to tug boat or barge traffic (fig. 17). Also, the magnitude and duration of the upward and downward spikes is remarkably similar to patterns in seepage recorded in 2015 during barge passage at NC271 (Rosenberry, 2016, p. 56).

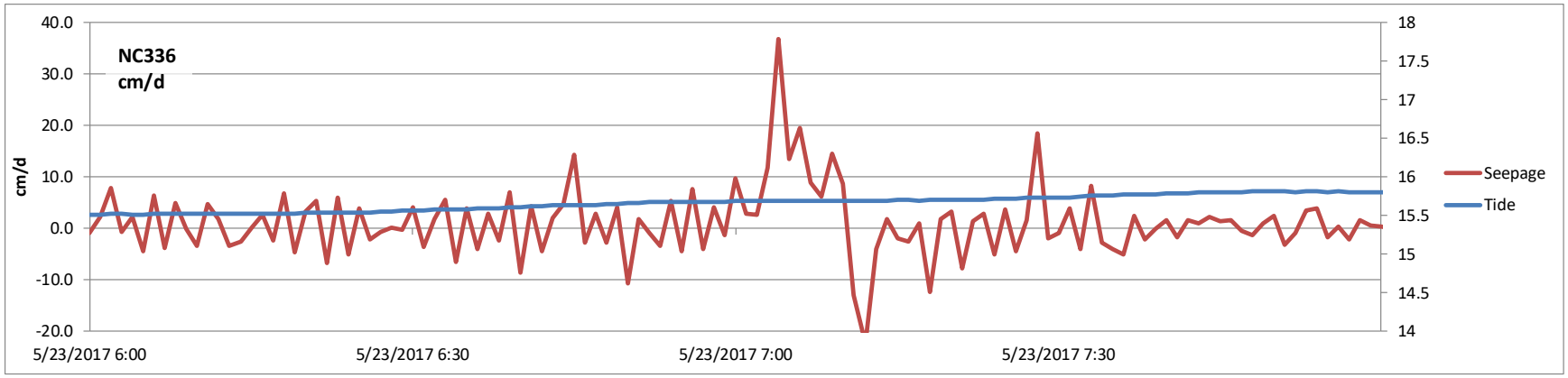

Figure 17. Seepage at NC336 prior to, during, and following large upward and downward seepage spikes on May 23, in centimeters per day (cm/d). Relative tide is in meters (m). Data are 1-minute averages of measurements made with 5-second resolution.

Seepage was poorly related to *i* (fig. 16B), tide, and change in stage. Although seepage was essentially zero during the morning of May 23 and from about noon to noon on May 24–25, *i* was nearly always positive, briefly decreasing to zero at 20:55 on May 24 and at 09:05 on May 25.

NC334

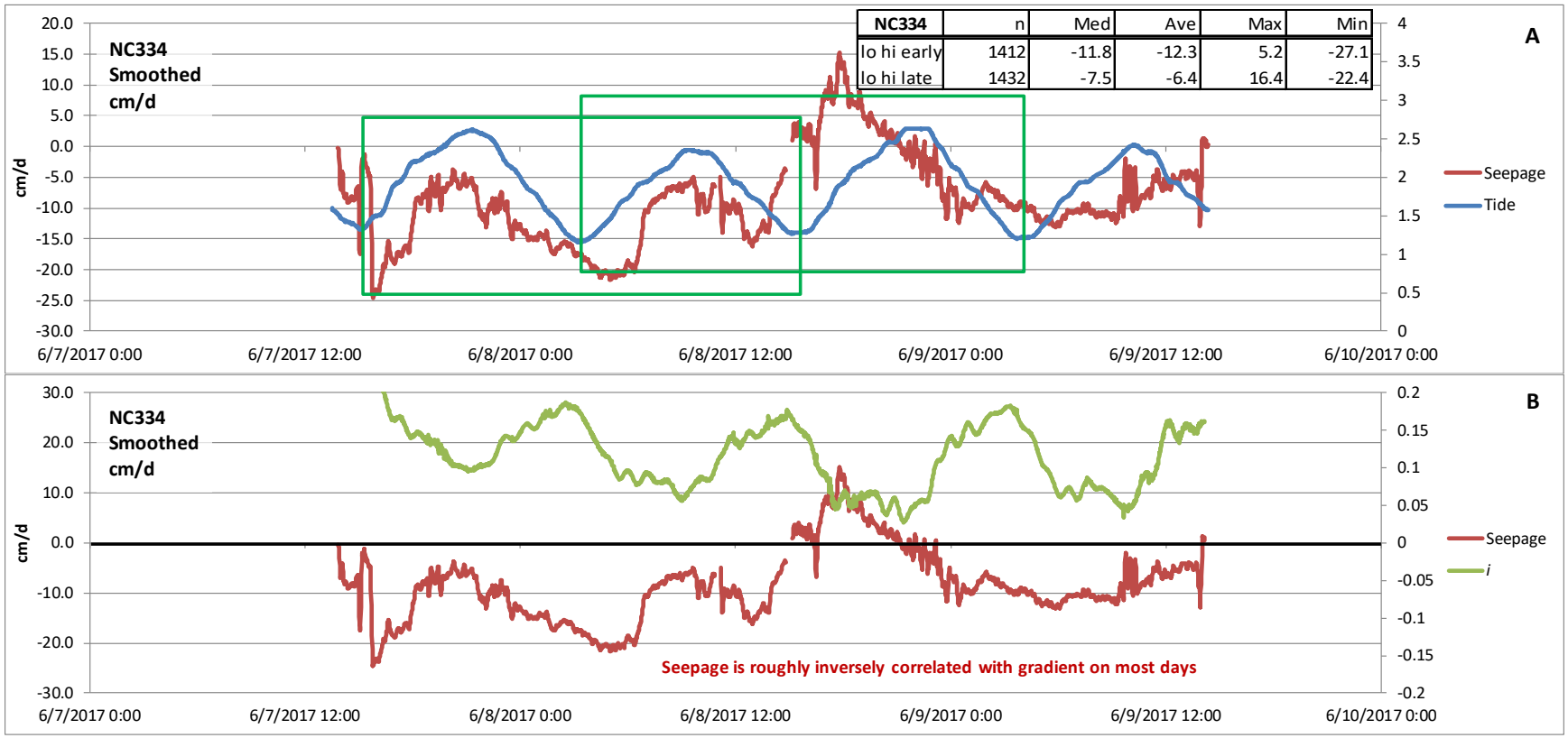

Figure 18. Seepage measured each minute at NC334, in centimeters per day (cm/d). Chart A displays seepage smoothed with a 7-minute moving average, and relative tide in meters (m). The green rectangles indicate the duration of the data-analysis periods. In the inset table, "lo hi early" indicates the first instance of two complete tidal cycles beginning and ending with low tide, and "lo hi late" indicates the last two complete tidal cycles beginning and ending with low tide. Chart B displays smoothed seepage, with vertical hydraulic gradient (*i*) in m/m plotted on the right axis. (n, number of 1-minute values; Med, median of n values; Ave, average of n values; Max, maximum of n values; Min, minimum of n values)

Seepage at NC334 was very unusual and difficult to explain. Seepage was strongly downward during most of the deployment period, averaging −12.3 and −6.4 cm/d during the two analysis periods (fig. 18A). During most of the first two tidal cycles, seepage responded to tide opposite of what one would expect if it were driven by *i*, that is, increasing with increasing tide and decreasing with decreasing tide. Beginning at about 13:00 on June 8, however, that pattern dissolved and there was no discernible relation between seepage and tide thereafter. Furthermore, variance during zeroing periods was large and the range of zero-output values was much larger than nearly all deployments.

Seepage also was approximately inversely related to *i*, but not consistently (fig. 18B). For these reasons, seepage data were suspect and the location was revisited two weeks later.

The second deployment at NC334 produced similarly suspect data that are not shown. Upon system removal, a shrimp was discovered inside the rubber boot attached to the flowmeter (fig. 19). Based on previous experience, it is likely that the shrimp and perhaps other organisms were creating seepage as they filtered water in proximity of the electromagnetic flowmeter. However, the third deployment seems to have been unaffected by filtering organisms.

Figure 19. Shrimp removed from the neoprene boot to which the electromagnetic flowmeter was attached at NC334-2.

NC334-3

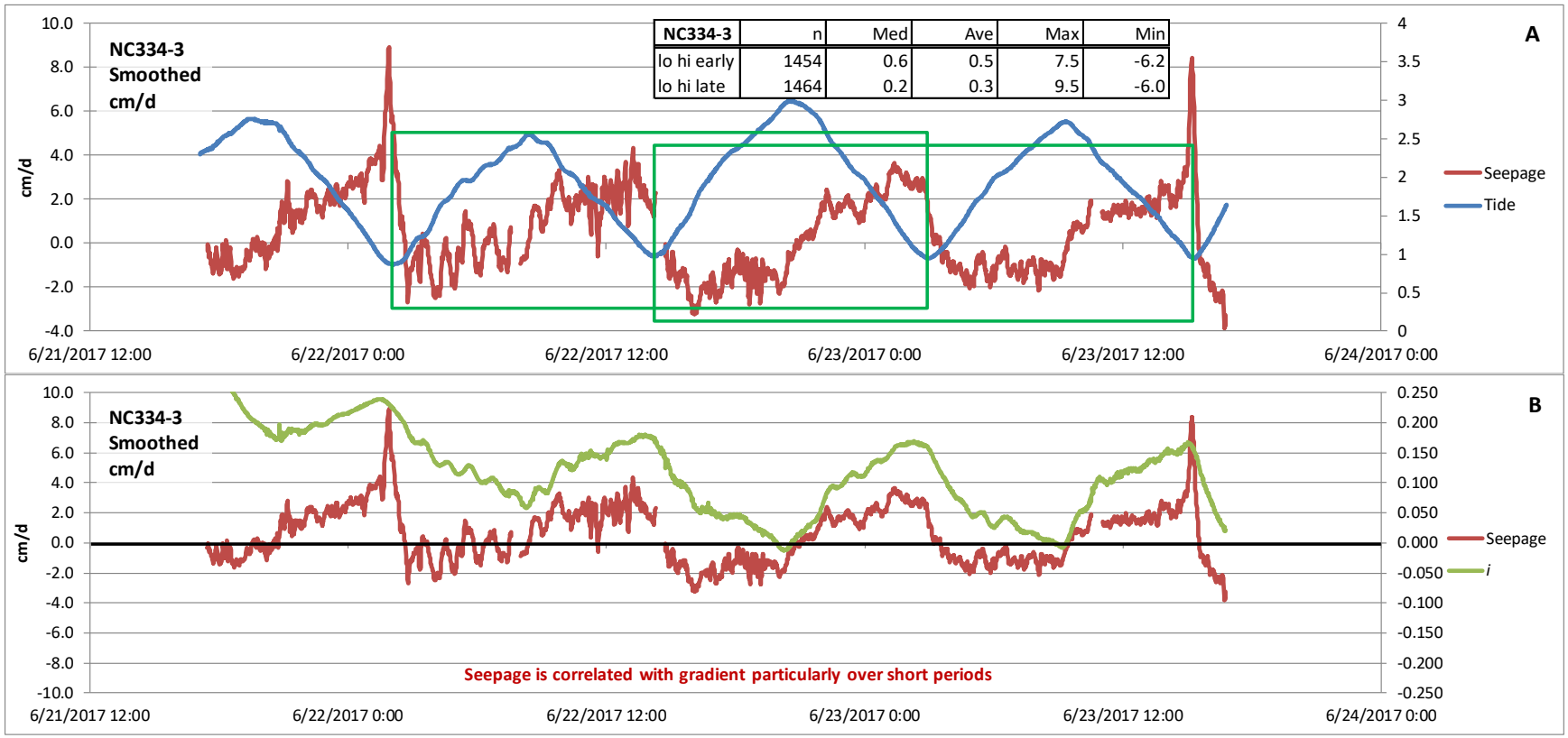

NC334-3	n	Med	Ave	Max	Min
lo hi early	1454	0.6	0.5	7.5	-6.2
lo hi late	1464	0.2	0.3	9.5	-6.0

Figure 20. Seepage measured each minute during a third deployment at NC334, in centimeters per day (cm/d). Chart A displays seepage smoothed with a 7-minute moving average, and relative tide, in meters (m). The green rectangles indicate the duration of the data-analysis periods. In the inset table, "lo hi early" indicates the first instance of two complete tidal cycles beginning and ending with low tide, and "lo hi late" indicates the last two complete tidal cycles beginning and ending with low tide. Chart B displays smoothed seepage, with vertical hydraulic gradient (*i*) in m/m plotted on the right axis. (n, number of 1-minute values; Med, median of n values; Ave, average of n values; Max, maximum of n values; Min, minimum of n values)

Seepage at NC334 during the third deployment varied substantially in response to tide. Upward seepage increased with decreasing tide until tidal nadir, at which point seepage decreased rapidly, becoming downward about 1 hour after the tide began to rise (fig. 20A). Seepage remained downward until high tide, after which it transitioned to upward seepage once again. Upward seepage exceeded 8 cm/d during low tide and downward seepage typically exceeded −3 cm/d at tidal apex. Seepage averaged over two tidal cycles was 0.3–0.5 cm/d. Because both analysis periods included brief durations of very fast seepage, another analysis period beginning with high tide, but excluding the periods of fastest upward seepage, was selected. Average seepage during this third analysis period was 0.3 cm/d, indicating the fast upward seepage values for the two "lo-hi" analysis periods had little effect on the average values.

Seepage was moderately correlated with *i* (fig. 20B) but with several exceptions. Seepage increased as *i* increased in response to falling tide, but seepage decreased much more rapidly following tidal apex and became downward while *i* remained positive, indicating the potential for upward flow. Upward *i* gradually decreased during the deployment period, but became downward during only two brief periods, at about 20:15 on June 22 and about 09:05 on June 23. Seepage also was correlated with change in stage nearly as well as with *i*.

NC335

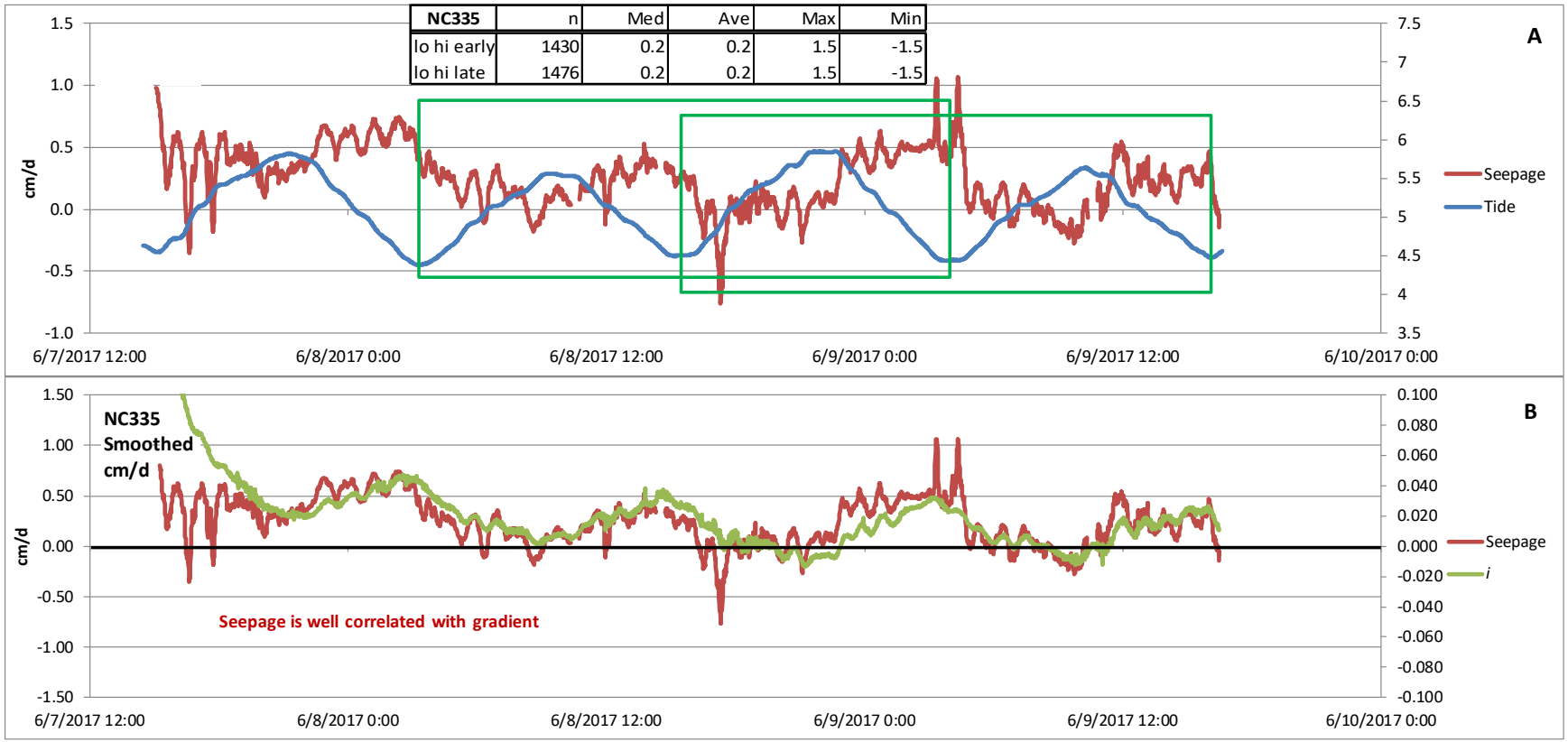

Figure 21. Seepage measured each minute at NC335, in centimeters per day (cm/d). Chart A displays seepage smoothed with a 7-minute moving average, and relative tide in meters (m). The green rectangles indicate the duration of the data-analysis periods. In the inset table, "lo hi early" indicates the first instance of two complete tidal cycles beginning and ending with low tide, and "lo hi late" indicates the last two complete tidal cycles beginning and ending with low tide. Chart B displays smoothed seepage, with vertical hydraulic gradient (*i*) in m/m plotted on the right axis. (n, number of 1-minute values; Med, median of n values; Ave, average of n values; Max, maximum of n values; Min, minimum of n values)

Seepage at NC335 varied over a relatively narrow range and was nearly always within −1 and 1 cm/d (fig. 21A). Period-average seepage values were slightly upward and were both 0.2 cm/d. Seepage responded slightly to tide, commonly increasing during falling tide and decreasing during rising tide. The cause of spikes at 17:20 on June 8 and at 03:20 and 04:20 on June 9 is unknown but all three deviations were small compared to spikes at most other measurement locations.

Seepage was very well correlated with *i* (fig. 21B). Reversals in seepage trends preceded reversals in *i* by about 15 minutes. This likely is the result of seepage also being well correlated with change in stage, which precedes patterns in both *i* and stage (fig. 22).

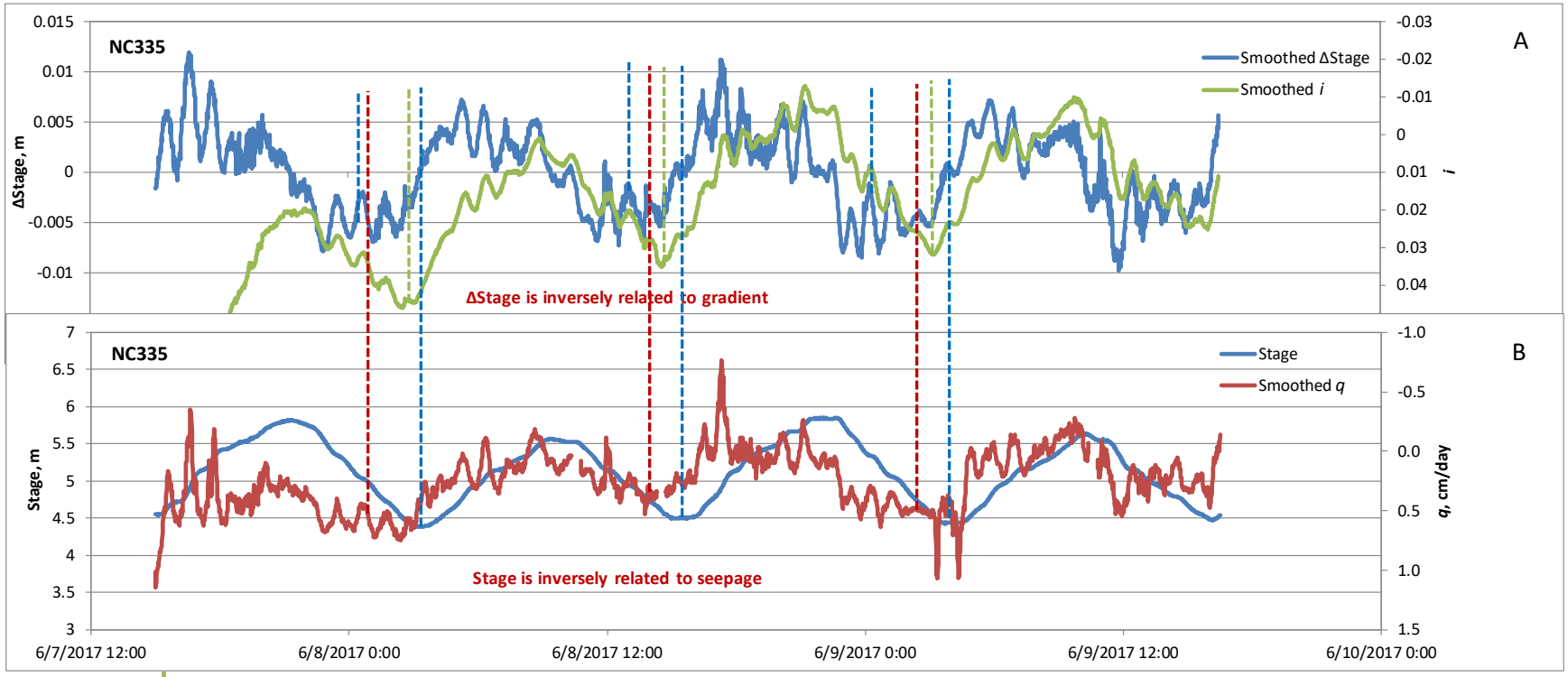

Figure 22. Smoothed (7-minute average) change in stage (ΔStage) in meters (m), smoothed (7-minute average) vertical hydraulic gradient (*i*), in m/m, and smoothed (7-minute average) seepage (*q*), in cm/d, at NC335 compared to relative stage, in m. Chart A shows ΔStage with *i* plotted on the right axis. Chart B shows unsmoothed relative stage with seepage plotted on the right axis. Vertical lines indicate the timing of nadirs in plots of the four types of data. The right axes are plotted inversely.

NC339

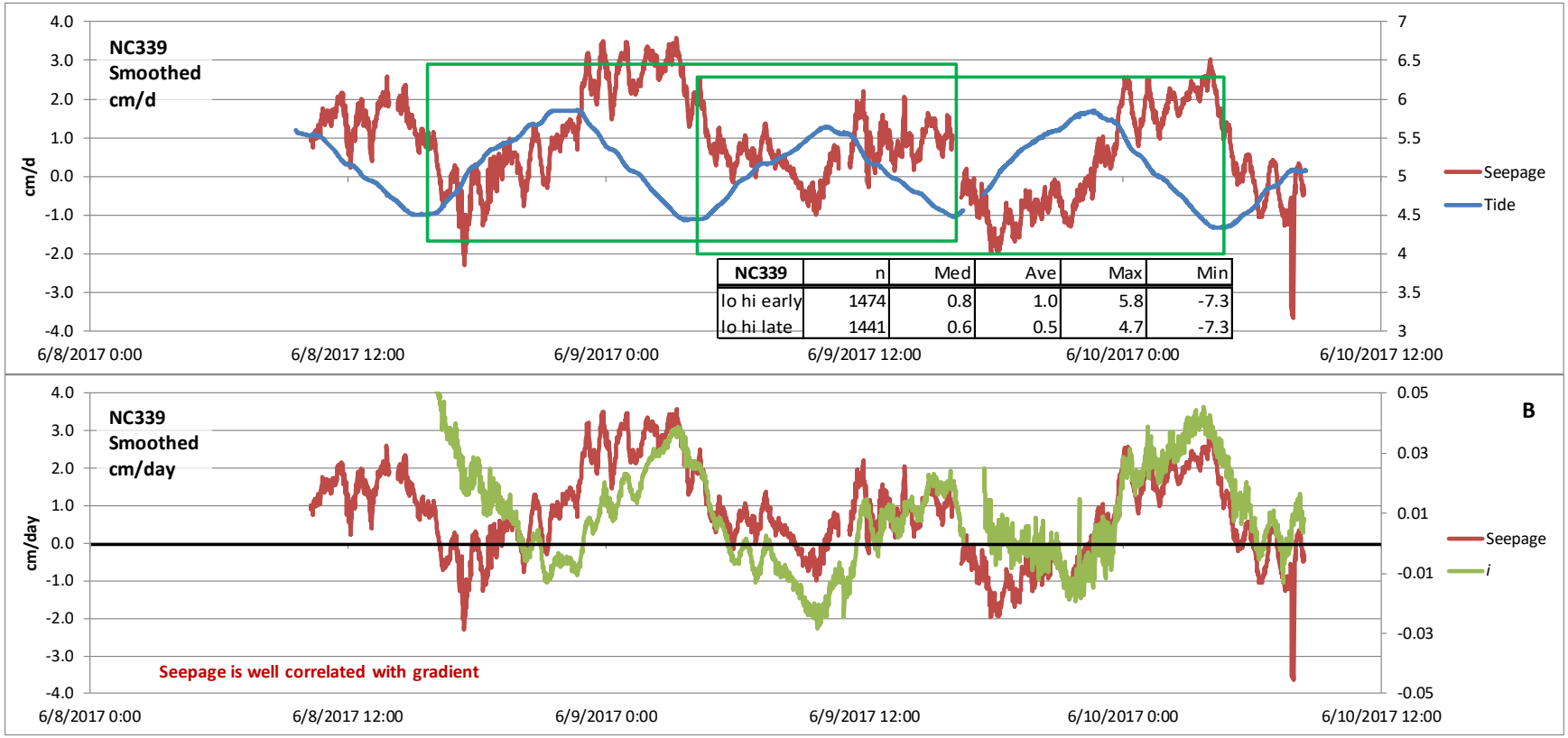

Figure 23. Seepage measured each minute at NC339, in centimeters per day (cm/d). Chart A displays seepage smoothed with a 7-minute moving average, and relative tide, in meters (m). The green rectangles indicate the duration of the data-analysis periods. In the inset table, "lo hi early" indicates the first instance of two complete tidal cycles beginning and ending with low tide, and "lo hi late" indicates the last two complete tidal cycles beginning and ending with low tide. Chart B displays smoothed seepage, with vertical hydraulic gradient (*i*) in m/m plotted on the right axis. (n, number of 1-minute values; Med, median of n values; Ave, average of n values; Max, maximum of n values; Min, minimum of n values)

Seepage at NC339 was related to tides but with an approximately 3-hour delay. Seepage ranged between about −2 and 3.5 cm/d with time-average values of 1.0 and 0.5 cm/d (fig. 23A). The cause of the 4-hour period of large upward seepage between about 23:00 and 03:00 on June 8–9 is

unknown. However, the large downward spike at 7:52–7:54 on June 10 almost certainly was caused by passage of the dive boat on the way to service NC340.

Seepage was strongly correlated with *i* but with variable offsets (fig. 23B). As at several other locations, peaks and valleys in the seepage plot preceded those for *i*. However, the temporal offset was not consistent and peaks and valleys in the seepage plot preceded peaks and valleys in *i* by 0 to 2.5 hours, depending on the tidal cycle.

NC340-2

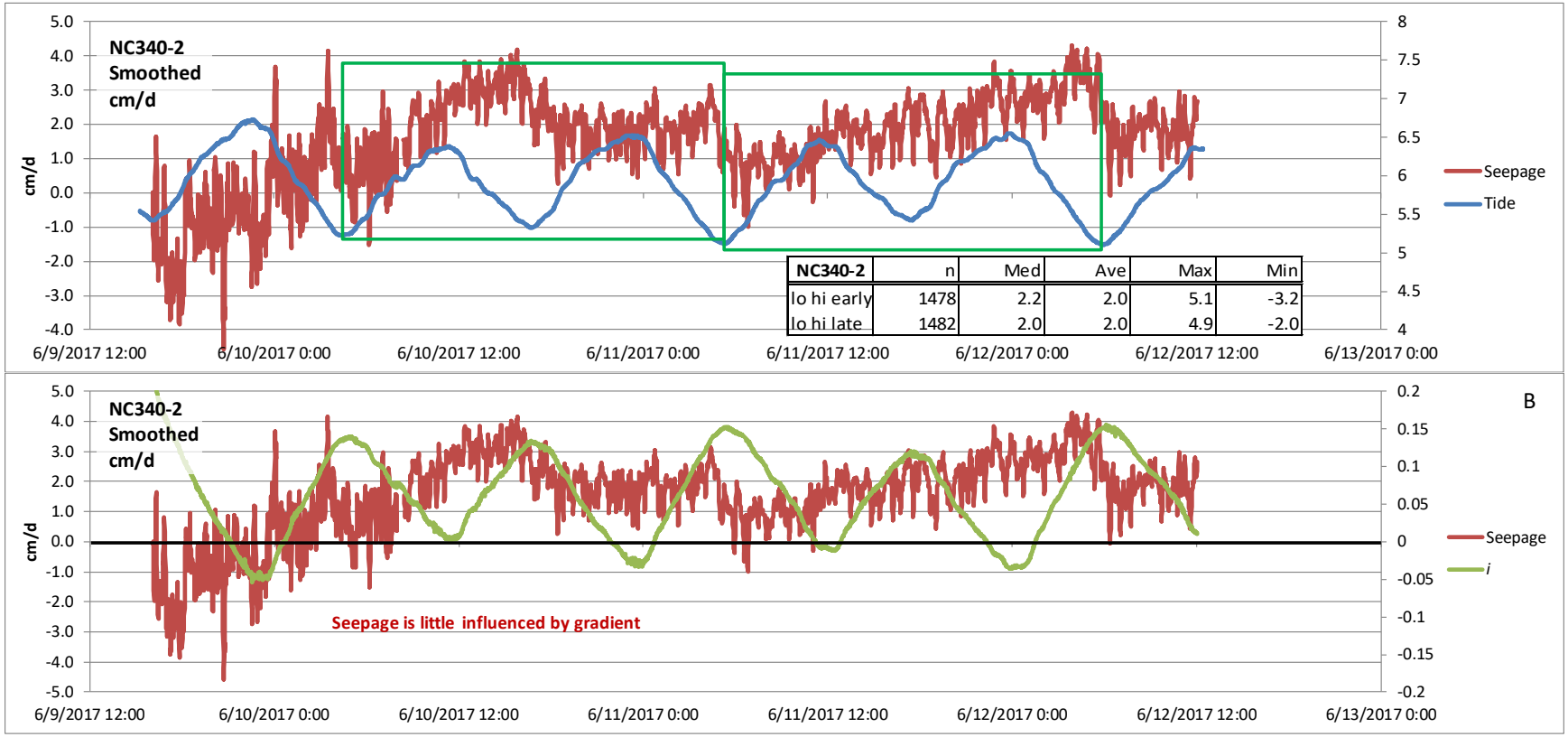

Figure 24. Seepage measured each minute during a second deployment at NC340, in centimeters per day (cm/d). Chart A displays seepage smoothed with a 7-minute moving average, and relative tide in meters (m). The green rectangles indicate the duration of the data-analysis periods. In the inset table, "lo hi early" indicates the first instance of two complete tidal cycles beginning and ending with low tide, and "lo hi late" indicates the last two complete tidal cycles beginning and ending with low tide. Chart B displays smoothed seepage, with vertical hydraulic gradient (*i*) in m/m plotted on the right axis. (n, number of 1-minute values; Med, median of n values; Ave, average of n values; Max, maximum of n values; Min, minimum of n values)

Data were unacceptably noisy during the entire deployment at NC340 in May, likely due to a defective data cable. Therefore, data were not processed and the location was revisited in June. During this second deployment at NC340, seepage was downward and relatively noisy during the first 8 hours of the data-collection period, but then upward seepage existed during nearly the entire remainder of the data-collection period (fig. 24A). Noise decreased substantially after a zero-flow calibration period on June 10 at 8:15. The two data-analysis periods were both during the

stable upward-seepage portion of the data record that varied little with tide. Seepage typically ranged between 0 and 3.5 cm/d and averaged 2.0 cm/d during both periods. The only noticeable and repeating tidal influence was a gradual decrease in seepage beginning at tidal nadir and continuing for about the next 6 hours, followed by steady to slowly increasing seepage. This reduction in seepage did not occur during the higher-than-normal low tide during the late afternoon of June 11.

Hydraulic gradient was upward most of the time with short periods of downward gradient centered on high tide during four of five high-tide periods (fig. 24B). Seepage and *i* were not correlated.

NC168

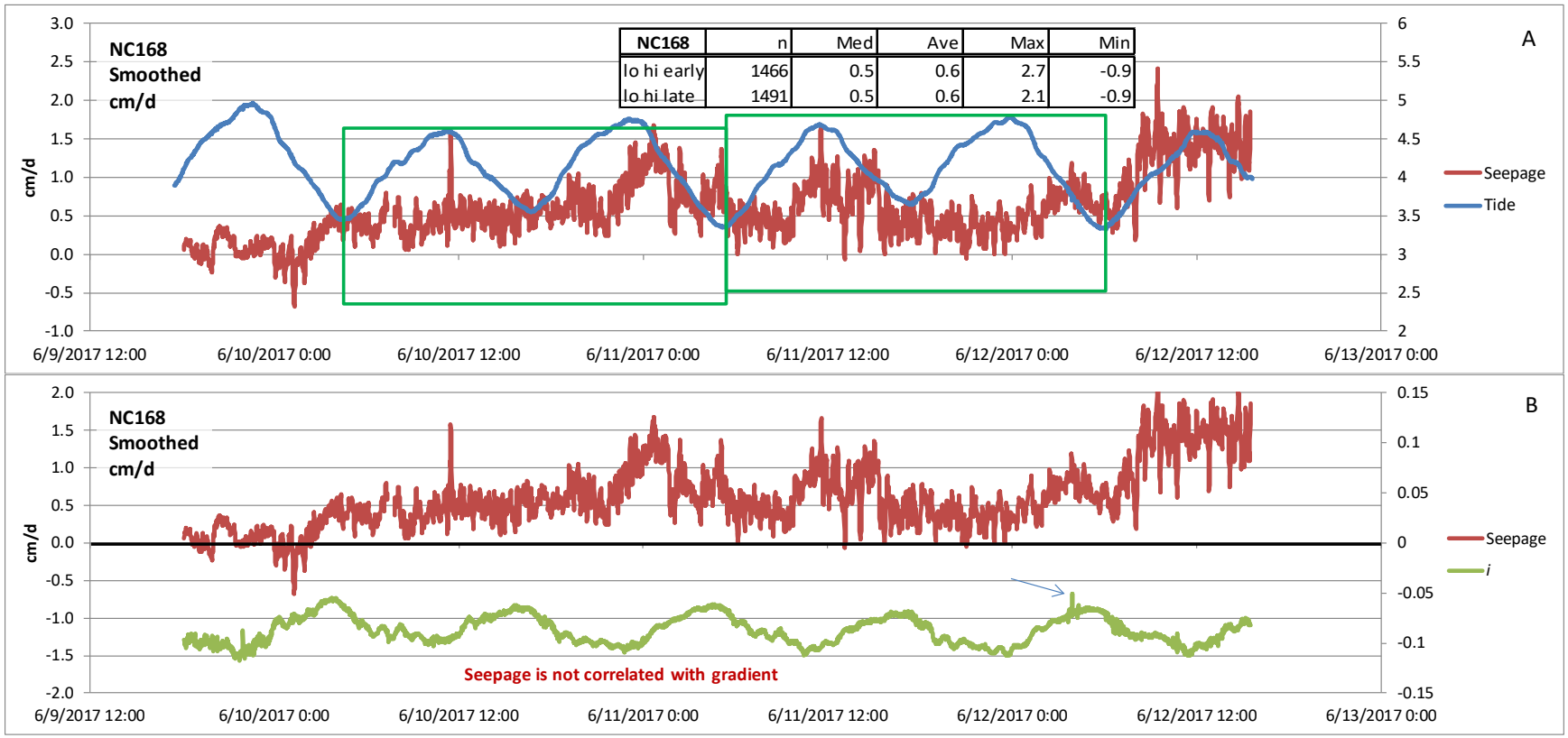

NC168	n	Med	Ave	Max	Min
lo hi early	1466	0.5	0.6	2.7	-0.9
lo hi late	1491	0.5	0.6	2.1	-0.9

Figure 25. Seepage measured each minute at NC168, in centimeters per day (cm/d). Chart A displays seepage smoothed with a 7-minute moving average, and relative tide in meters (m). The green rectangles indicate the duration of the data-analysis periods. In the inset table, "lo hi early" indicates the first instance of two complete tidal cycles beginning and ending with low tide, and "lo hi late" indicates the last two complete tidal cycles beginning and ending with low tide. Chart B displays smoothed seepage, with vertical hydraulic gradient (*i*) in m/m plotted on the right axis. (n, number of 1-minute values; Med, median of n values; Ave, average of n values; Max, maximum of n values; Min, minimum of n values)

Similar to the data recorded at NC340, seepage at NC168 during June 9 was zero to slightly downward until about midnight, and then it transitioned to upward flow, ranging between about 0.5 and 1.5 cm/d and averaging 0.6 cm/d during both analysis periods (fig. 25). Seepage increased again following the last low tide of the period and averaged about 1.5 cm/d until the end of data collection. There was no relation between seepage and tide.

No relation exists between seepage and *i* either. Hydraulic gradient was downward during the entire data-collection record whereas seepage was upward during most of the period. This discrepancy is difficult to explain, although it has been observed elsewhere. For example, downward seepage was recorded at several locations in the Puget Sound area in Washington where hydraulic gradients indicated that groundwater should have been discharging (Simonds and others, 2008). Seepage and vertical hydraulic gradient also have been shown to indicate flow in the opposite direction in fluvial settings affected by surface-water currents (Rosenberry and Pitlick, 2009). Biological activity also could be the cause; organisms can create seepage rates of 5 cm/d or more (for example, Cable and others, 2006; Meysman and others, 2006). However, if filtering animals did create time-averaged upward seepage, it likely was a different organism than the shrimp that was observed at NC334. No strange pattern in the data exists at NC168, nor were there any large spikes in recorded seepage. Ebullition also likely is not a factor as very little gas was collected at this location.

MC036

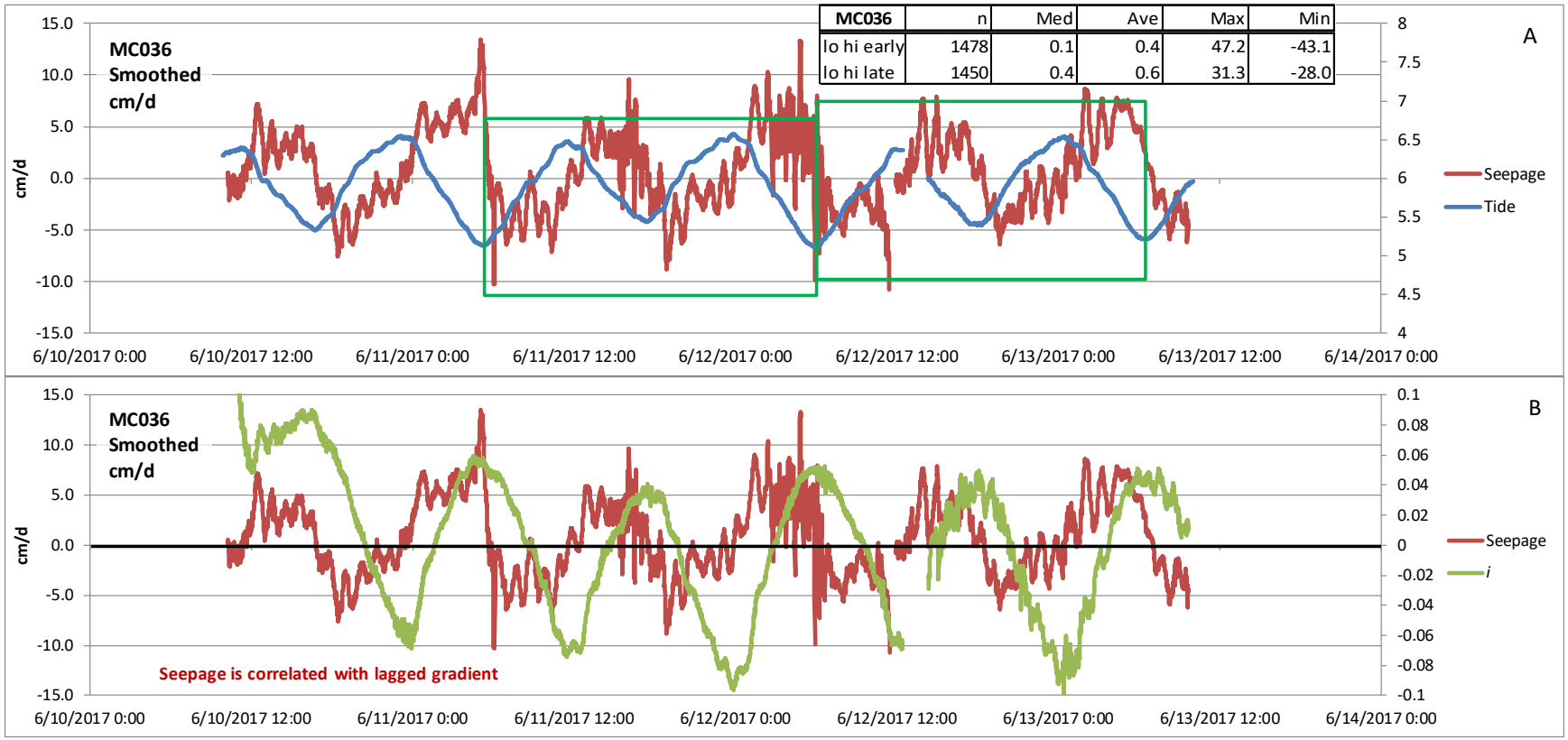

MC036	n	Med	Ave	Max	Min
lo hi early	1478	0.1	0.4	47.2	-43.1
lo hi late	1450	0.4	0.6	31.3	-28.0

Figure 26. Seepage measured each minute at MC036, in centimeters per day (cm/d). Chart A displays seepage smoothed with a 7-minute moving average, and relative tide, in meters (m). The green rectangles indicate the duration of the data-analysis periods. In the inset table, "lo hi early" indicates the second instance of two complete tidal cycles beginning and ending with low tide, and "lo hi late" indicates the last two complete tidal cycles beginning and ending with low tide. Chart B displays smoothed seepage, with vertical hydraulic gradient (*i*) in m/m plotted on the right axis. (n, number of 1-minute values; Med, median of n values; Ave, average of n values; Max, maximum of n values; Min, minimum of n values)

Seepage at MC036 was strongly influenced by tide, changing from upward to downward as stage fell and rose, but with a substantial offset (fig. 26A). Maximum upward and downward seepage ranged between about −11 and 13 cm/d and period-average values were 0.4 and 0.6 cm/d, indicating a small net upward seepage rate. The first analysis period was shifted to begin at the second low tide of the deployment because of the

slow stabilization of head at the deeper pressure transducer in the VHG rod. Because seepage during the early portion of the deployment also was faster, it is possible that hydraulic conductivity was particularly small and stabilization of seepage following deployment was particularly slow.

Hydraulic gradient was strongly inversely related to tide and, therefore, reversals in *i* also were not coincident with reversals in seepage (fig. 26B). The upper pressure transducer in the VHG rod failed shortly after deployment. Therefore, data were filled in from the upper transducers at NC340-2 for the early part of deployment and from NC168 during the latter part of deployment. The gap in the data record was a period when no other VHG rod was in operation. Increased noise in *i* starting at 14:30 on June 12 was due to greater wave heights at NC168 than at NC340.

The ebullition data indicate that more gas was produced at MC036 than at any of the other locations. Gas generation and the presence of large amounts of gas trapped in the sediment may be responsible for the unusual seepage pattern during the 3-day deployment. Although seepage increased steadily until tidal apex, after which it often declined sharply, more commonly maximum upward seepage occurred 1 hour before low tide and maximum downward seepage occurred 5 or more hours before high tide.

Measured seepage appears to be influenced by *i* and also tide and change in stage (fig. 27). As demonstrated for NC335 (fig. 22), the timing of nadirs can indicate the relative influence of various factors on measured seepage. A seepage apex close to or coincident with tidal nadir indicates that seepage is primarily influenced by *i*, assuming that the *i* apex also is nearly coincident with tidal nadir. In fig. 27, seepage apex instead is nearly coincident with the nadir of change in stage, which commonly occurred between 2 and 3.5 hours before low tide at MC036. Given the strong inverse correlation between seepage and change in stage, this indicates that change in stage also can greatly affect measured seepage. This effect is pursued more thoroughly in the “Discussion” section.

Very large amounts of gas were released during deployment at MC036. During the first ebullition measurement period, discussed in greater detail in the “Ebullition Results” section, the capacity to trap and quantify gas was exceeded. Increased noise in measured seepage during a falling tide in the afternoon of June 11 and again in the early morning of June 12 likely was caused by ebullition displacing water that exited the ESM through the flowmeter. Assuming the single good measurement at MC036 is representative, ebullition was equivalent to 0.3 cm/d when ebullition volume was divided by the area of the seepage cylinder. If adjusted for the effect of ebullition, the average seepage rates of 0.4 and 0.6 cm/d during the two analysis periods would be reduced to 0.1 and 0.3 cm/d.

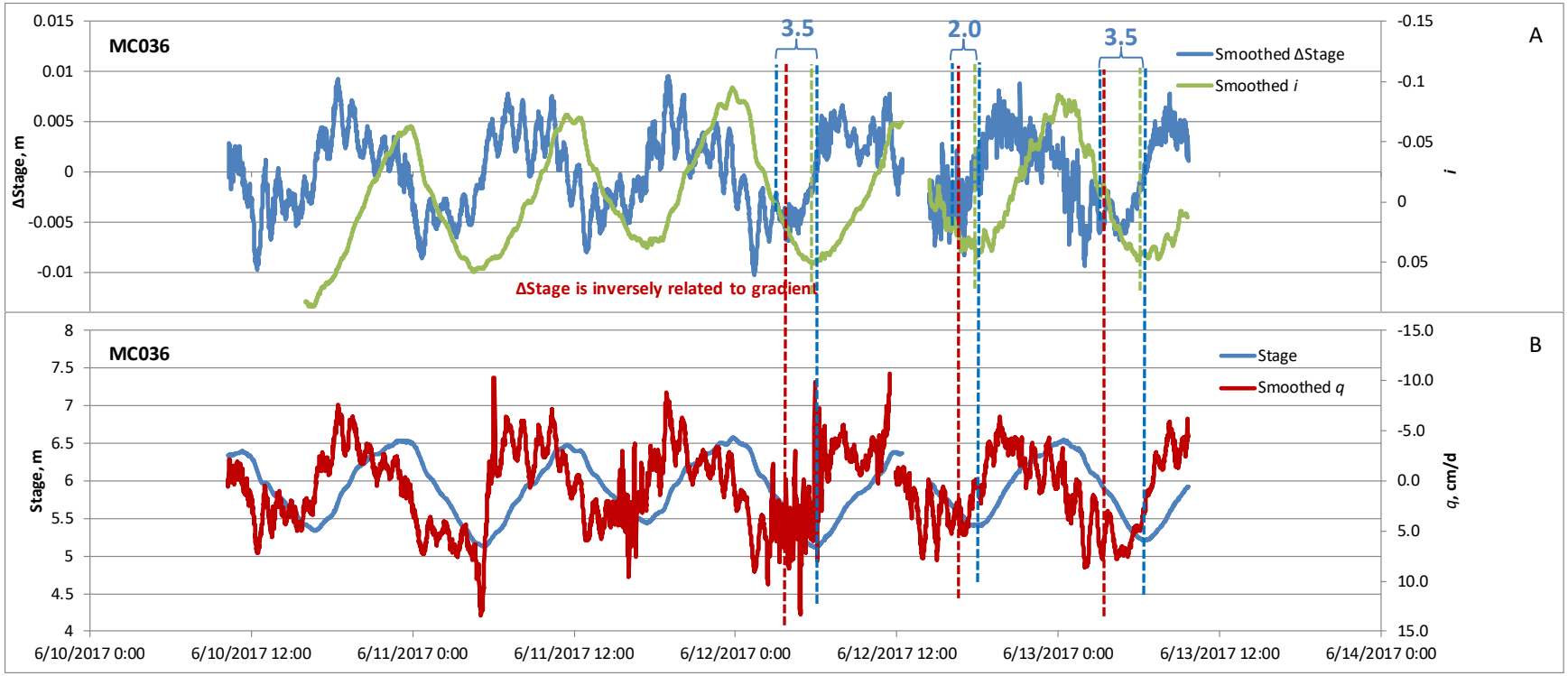

Figure 27. Smoothed (7-minute average) change in stage (ΔStage) in meters (m), smoothed (7-minute average) vertical hydraulic gradient (*i*), in m/m, and smoothed (7-minute average) seepage (*q*), in cm/d, at MC036 compared to relative stage, in m. Chart A shows ΔStage with *i* plotted on the right axis. Chart B shows unsmoothed relative stage with seepage plotted on the right axis. Vertical lines indicate the timing of nadirs in plots of the four types of data. Values in blue are differences in timing of the nadirs of smoothed ΔStage and Stage. The right axes are plotted inversely.

This page intentionally left blank

NC273

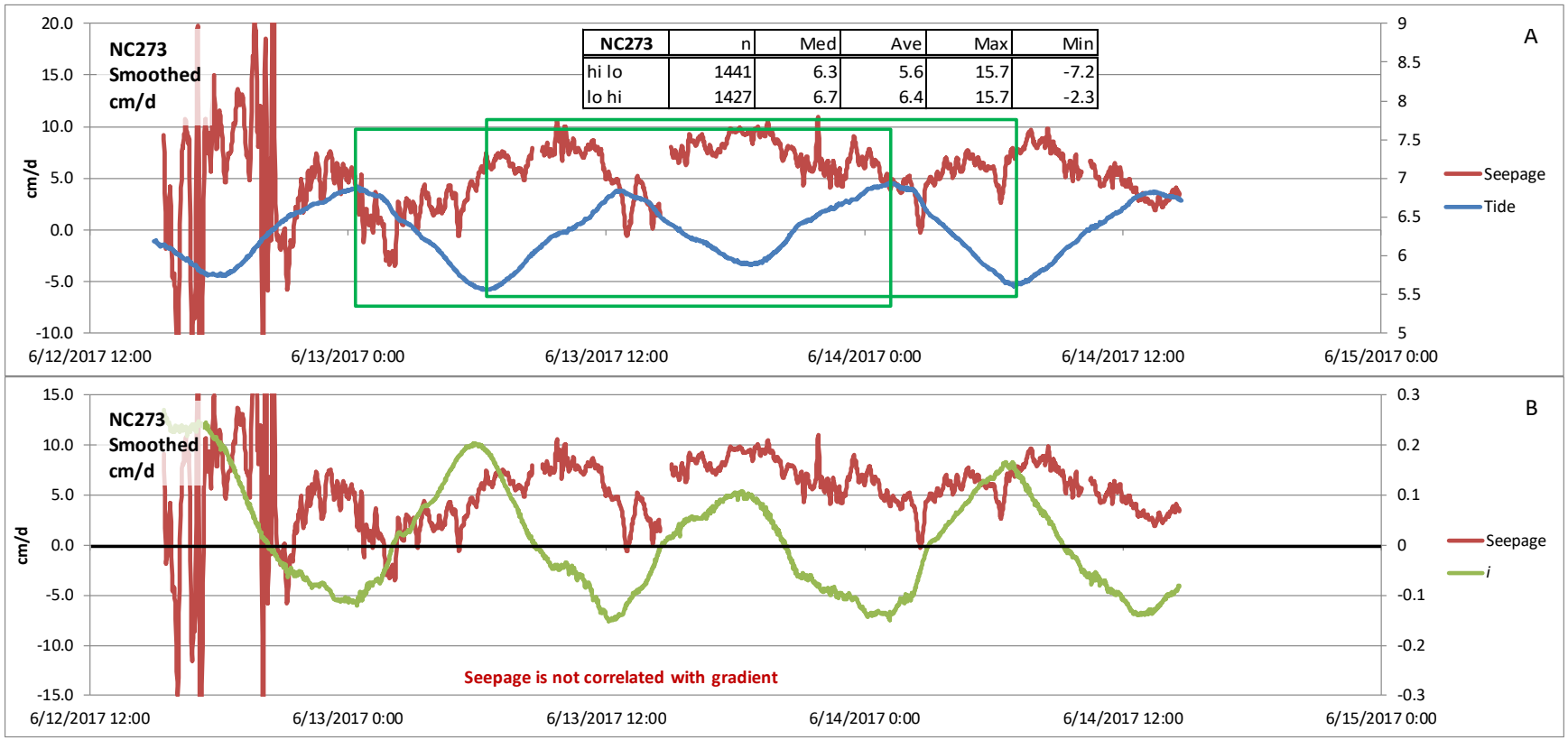

NC273	n	Med	Ave	Max	Min
hi lo	1441	6.3	5.6	15.7	-7.2
lo hi	1427	6.7	6.4	15.7	-2.3

Figure 28. Seepage measured each minute at NC273, in centimeters per day (cm/d). Chart A displays seepage smoothed with a 7-minute moving average, and relative tide in meters (m). The green rectangles indicate the duration of the data-analysis periods. In the inset table, "hi lo" indicates the first instance of two complete tidal cycles beginning and ending with high tide, and "lo hi" indicates the last two complete tidal cycles beginning and ending with low tide. Chart B displays smoothed seepage, with vertical hydraulic gradient (*i*) in m/m plotted on the right axis. (n, number of 1-minute values; Med, median of n values; Ave, average of n values; Max, maximum of n values; Min, minimum of n values)

Seepage at NC273 was not correlated with tide or with hydraulic gradient. The large amount of noise during the first 5 hours of deployment is perplexing, but it suddenly ended at 20:20 and variance after that time was typical of the instrument (fig. 28A). Because of a concern that the large noise would bias an averaging period, the first analysis period began and ended with high tide instead of the standard method of beginning and ending with low tide. However, the second analysis period did begin and end with low tide. Seepage during the two analysis periods averaged 5.6

and 6.4 cm/d. If the second analysis period was shifted one-half tidal cycle and began and ended with high tide, average seepage during that period would be 6.2 cm/d.

Although seepage during deployment was almost always upward, *i* indicated regular reversals between upward and downward flow (fig. 28B), suggesting that seepage should be both upward and downward. Because of the unusual seepage pattern that was unrelated to any of the other measured physical parameters, it is possible that these data were influenced by biological activity.

NC333

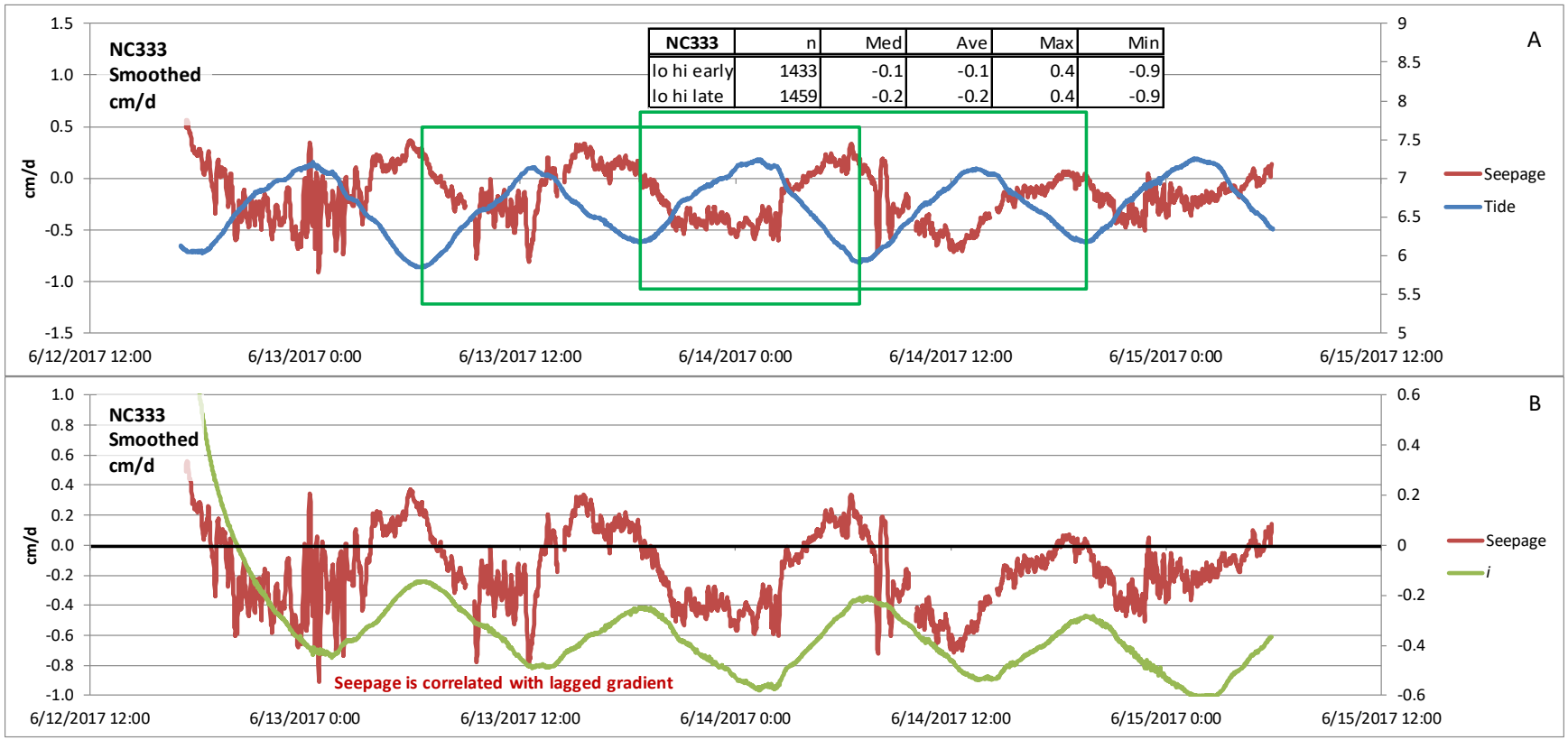

Figure 29. Seepage measured each minute at NC333, in centimeters per day (cm/d). Chart A displays seepage smoothed with a 7-minute moving average, and relative tide in meters (m). The green rectangles indicate the duration of the data-analysis periods. In the inset table, "lo hi early" indicates the first instance of two complete tidal cycles beginning and ending with low tide, and "lo hi late" indicates the last two complete tidal cycles beginning and ending with low tide. Chart B displays smoothed seepage, with vertical hydraulic gradient (*i*) in m/m plotted on the right axis. (n, number of 1-minute values; Med, median of n values; Ave, average of n values; Max, maximum of n values; Min, minimum of n values)

Seepage was well correlated with tides at NC333, but with an offset of 1–2 hours (fig. 29). Seepage was mostly downward with periods of upward seepage starting 1 to 3 hours after high tide and lasting 4 to 5 hours. Seepage ranged from to −0.7 to 0.3 cm/d and averaged −0.1 and −0.2 cm/d during the two analysis periods.

Seepage was also correlated with *i*, particularly if seepage is lagged 1 hour. Although *i* was always negative, upward seepage occurred during the smallest downward gradients.

NC320

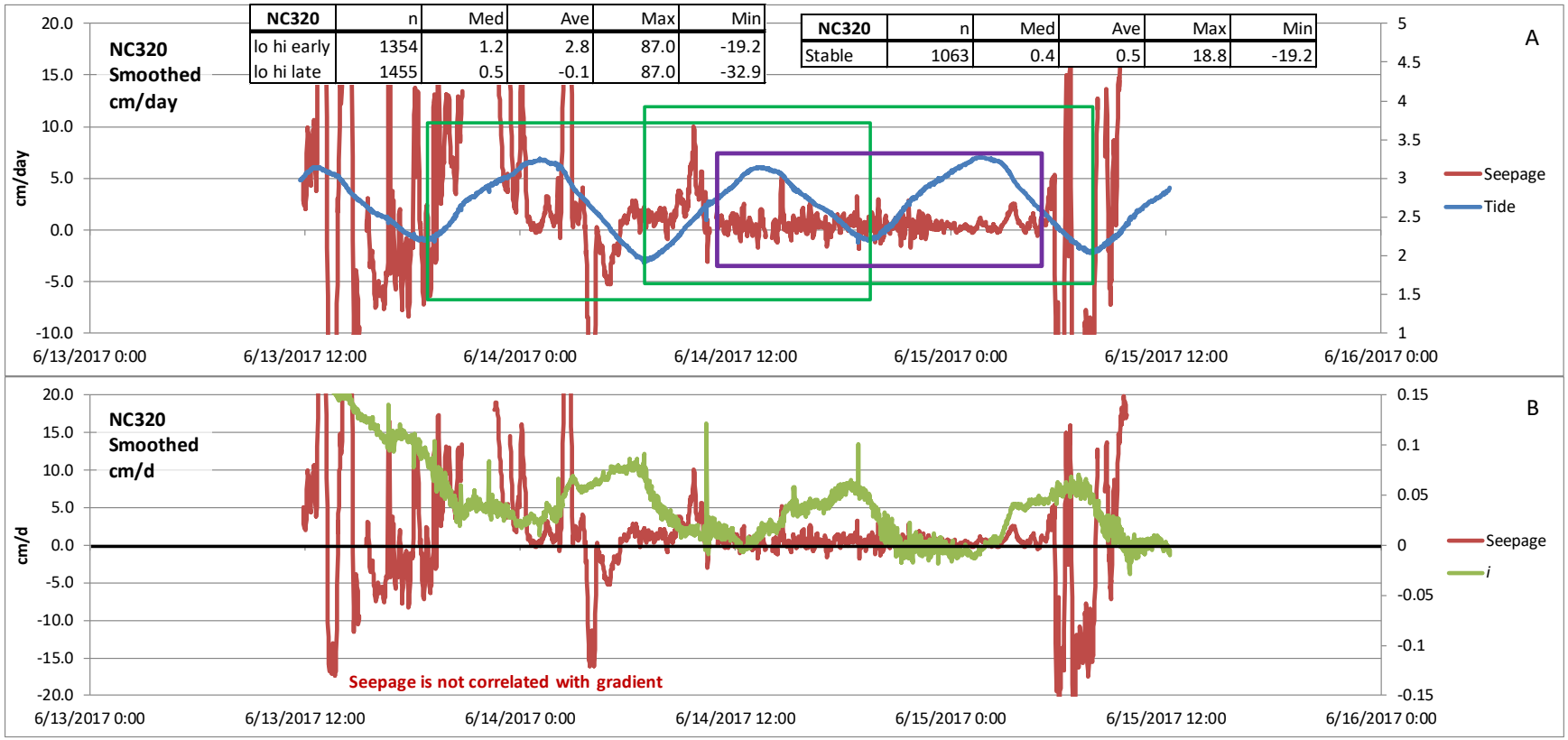

Figure 30. Seepage measured each minute at NC320, in centimeters per day (cm/d). Chart A displays seepage smoothed with a 7-minute moving average, and relative tide in meters (m). The green rectangles indicate the duration of the data-analysis periods and the purple rectangle indicates an additional analysis period during particularly stable data. In the inset table, "lo hi early" indicates the first instance of two complete tidal cycles beginning and ending with low tide, "lo hi late" indicates the last two complete tidal cycles beginning and ending with low tide, and "Stable" indicates the period within the purple rectangle. Chart B displays smoothed seepage, with vertical hydraulic gradient (*i*) in m/m plotted on the right axis. (n, number of 1-minute values; Med, median of n values; Ave, average of n values; Max, maximum of n values; Min, minimum of n values)

Measured seepage at NC320 was strange and difficult to interpret because of very large variability both early and late in the data-collection period, with relatively stable and small upward seepage in between (fig. 30A). It is unlikely that the ESM was defective because variance during zero-flow periods, as well as variability of average zero-output values, was small (table 3). The large range of seepage values during the first 16 hours and the last 4 hours is similar to data collected at NC334 where it is likely that a filtering shrimp was creating measurable seepage. The two analysis

periods indicated an average seepage value of 2.8 and −0.1 cm/d. Because nearly the entire first half of the first period included exceptionally noisy seepage data, and the second period also had noisy data during the latter portion, the period in the purple rectangle (fig. 30A) likely is most representative of undisturbed seepage. Data from this period are those presented in figure 1 and table 1. Seepage averaged 0.5 cm/d during this nearly 18-hour period (purple rectangle in fig. 30A) beginning at about 11:15 on June 14.

Hydraulic gradient was upward during most of the data-collection period (fig. 30B) and tended to increase shortly after high tide until just prior to low tide, at which point it began to decrease. It is unlikely that the large upward spike in *i* at 10:23 on June 14 was due to our boat traffic or to disturbance by the diver who was conducting a zero-flow measurement at NC273 at the time. The spike in gradient was caused by a decrease in stage of 0.17 m at 10:23. This is atypical of barge passage, which generally creates an increase in stage for a few minutes as the barge approaches and then a decrease in stage as the barge moves away from the measurement location.

WC022

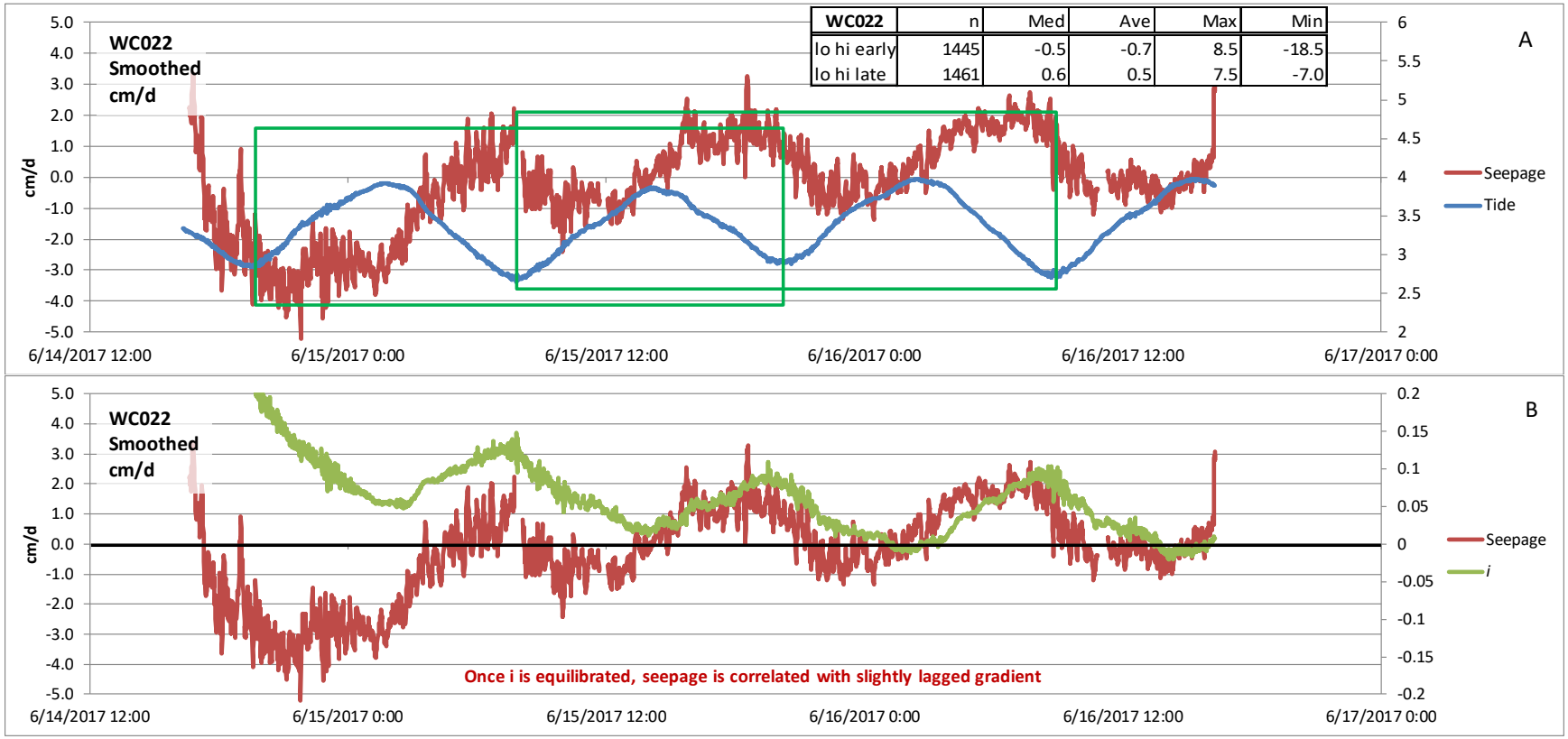

WC022	n	Med	Ave	Max	Min
lo hi early	1445	-0.5	-0.7	8.5	-18.5
lo hi late	1461	0.6	0.5	7.5	-7.0

Figure 31. Seepage measured each minute at WC022, in centimeters per day (cm/d). Chart A displays seepage smoothed with a 7-minute moving average, and relative tide, in meters (m). The green rectangles indicate the duration of the data-analysis periods. In the inset table, "lo hi early" indicates the first instance of two complete tidal cycles beginning and ending with low tide, and "lo hi late" indicates the last two complete tidal cycles beginning and ending with low tide. Chart B displays smoothed seepage, with vertical hydraulic gradient (*i*) in m/m plotted on the right axis. (n, number of 1-minute values; Med, median of n values; Ave, average of n values; Max, maximum of n values; Min, minimum of n values)

Seepage at WC022 responded inversely to tides with alternating upward and downward seepage but with a nadir and apex in the pattern that preceded high and low tide by about 1–3 hours. Seepage was downward during the first 12 hours with a maximum downward seepage of about −4 cm/d, but then alternated between maximum upward and downward seepage rates of about 1.5 and −1.0 cm/d, respectively (fig. 31A). Average seepage during the two analysis periods was −0.7 and 0.5 cm/d. The substantial discrepancy in the two values was due to the first analysis period

including much of the larger rate of downward seepage during the early part of deployment. If the two analysis periods were shifted later in time by one-half tidal cycle and with periods beginning and ending with high tide, average values would be 0.0 and 0.6 cm/d.

Hydraulic gradient took a particularly long time (24 hours, table 1) to equilibrate after installation of the VHG rod, indicating that hydraulic conductivity may be particularly small at WC022. Because of the slow stabilization, it may be that measured *i* was not indicative of steady-state conditions until 24 hours after installation. From that point onward, *i* was usually positive with brief periods of negative values coincident with or slightly preceding high tide (fig 30B). Seepage was well correlated with *i*, particularly so when *i* was offset by −1 hour.

NC362

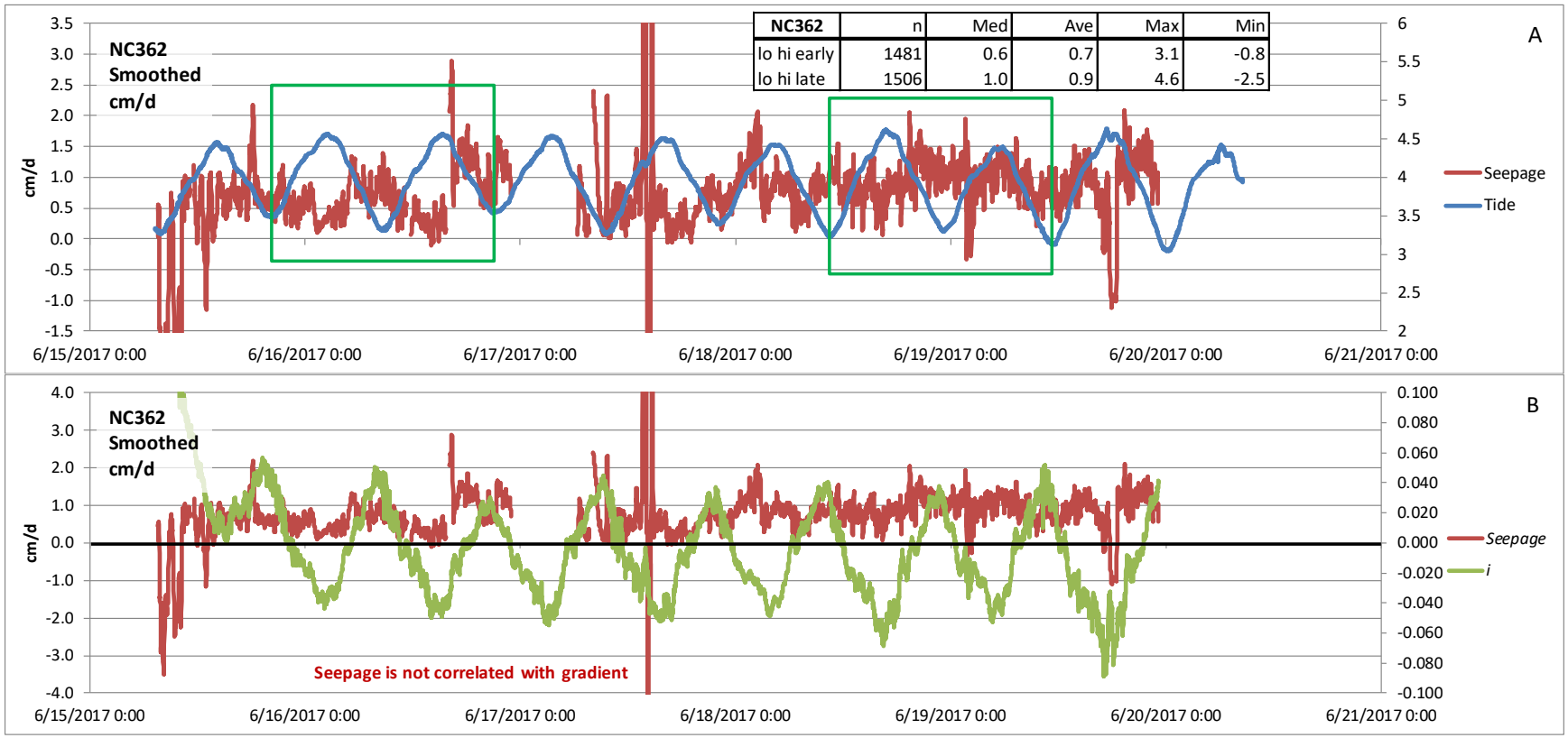

Figure 32. Seepage measured each minute at NC362, in centimeters per day (cm/d). Chart A displays seepage smoothed with a 7-minute moving average, and relative tide in meters (m). The green rectangles indicate the duration of the data-analysis periods. In the inset table, "lo hi early" indicates the first instance of two complete tidal cycles beginning and ending with low tide, and "lo hi late" indicates the next to last two complete tidal cycles beginning and ending with low tide. Chart B displays smoothed seepage, with vertical hydraulic gradient (*i*) in m/m plotted on the right axis. (n, number of 1-minute values; Med, median of n values; Ave, average of n values; Max, maximum of n values; Min, minimum of n values)

Seepage was not well correlated with either tide or *i*. Seepage typically ranged between 0 and 1.5 cm/d and averaged 0.7 and 0.9 cm/d during the two analysis periods (fig. 32A). Large deviations in seepage between 13:30 and 15:00 on June 17 may have been due to barge traffic, although the pattern of the deviations is not indicative of a simple passage of a large watercraft (fig. 33). The prolonged duration (nearly 1.5 hours) of the perturbations to more typical seepage rates suggests a different process, perhaps a maneuvering watercraft or filtering animals. When viewed as a whole, the seepage record at NC362 presents numerous deviations from what might be expected based on measurements at other locations,

perhaps indicative of episodic biological activity at this location. However, the reversal of seepage that occurred during the afternoon of June 19 was caused by a thunderstorm. The storm caused the rate of stage rise toward high tide to increase, which resulted in excessively large downward hydraulic gradients and caused seepage to become downward for about 1 hour.

Hydraulic gradients indicated the potential for tidally driven, alternating upward and downward seepage (fig. 32B). After a relatively rapid stabilization of gradient following VHG-rod insertion, the average gradient was −0.009.

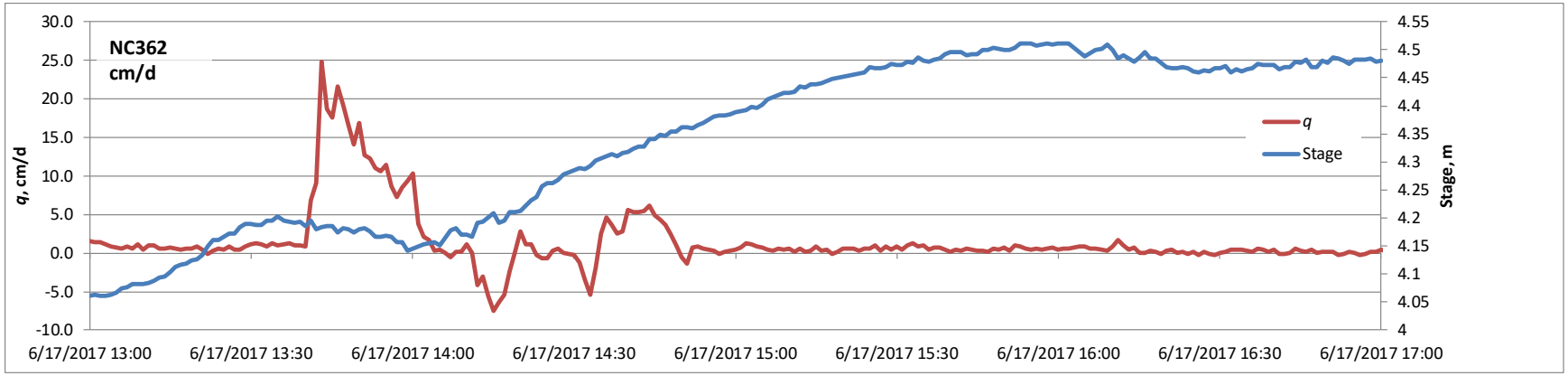

Figure 33. Seepage at NC362 prior to, during, and following the large upward and downward seepage spikes on June 17, in centimeters per day (cm/d). Stage is in meters (m). Data are 1-minute averages of measurements made with 5-second resolution.

NC266

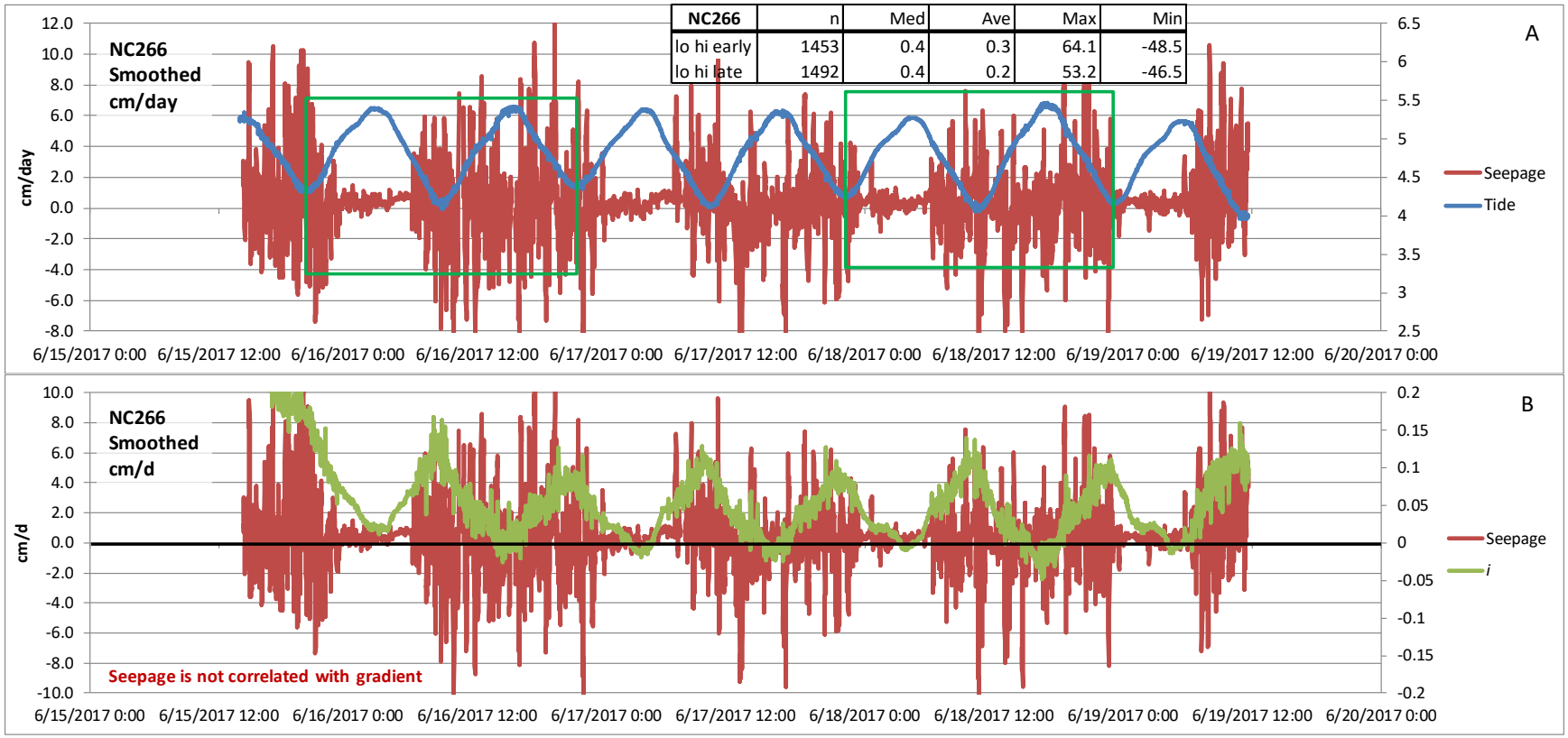

Figure 34. Seepage measured each minute at NC266, in centimeters per day (cm/d). Chart A shows seepage smoothed with a 7-minute moving average, and relative tide in meters (m). The green rectangles indicate the duration of the data-analysis periods. In the inset table, "lo hi early" indicates the first instance of two complete tidal cycles beginning and ending with low tide, and "lo hi late" indicates the last two complete tidal cycles beginning and ending with low tide. Chart B shows smoothed seepage, with vertical hydraulic gradient (*i*) in m/m plotted on the right axis. (n, number of 1-minute values; Med, median of n values; Ave, average of n values; Max, maximum of n values; Min, minimum of n values)

Seepage at NC266 was slightly related to tide. When high tide occurred during nighttime, seepage usually began a trend of increasing slightly shortly after high tide. That pattern likely was present when high tide occurred during the day, but it was impossible to determine this due to the greater daytime noise in the seepage data. Any other relations between seepage and tide, or seepage and *i*, were washed out by the vastly larger influence of waves generated by boat traffic on the East River (fig. 34A). Between about 06:00 and 23:00, seepage commonly varied by ±8 cm/d. Between 23:00 and 06:00, seepage commonly varied between −0.5 and 1 cm/d. Average seepage during the two analysis periods was 0.3 and 0.2

cm/d. Hydraulic gradient was upward 88 percent of the time with brief periods of downward *i* shortly preceding and following high tide (fig. 34B). Increased noise in *i* during daytime hours was due to the surface-water stage being influenced by waves from boat traffic on the East River.

Substantial gas was released to the seepage meter during two of the four collection periods. Low tide was substantially higher during the two periods when no gas was collected. The substantial release of gas suggests that seepage and ΔStage may be inversely related, as observed previously at EK098 (fig. 8) and MC036 (fig. 27). In a general sense, this is true. Seepage indeed was more variable during periods when change in stage was greater, based on nonsmoothed, 1-minute seepage and ΔStage data (fig 35A). However, correlation between seepage and ΔStage on a minute scale was not as good as at other locations where gas was collected during measurements. Some of the minute-to-minute changes in stage were well matched by changes in seepage, but others were not (fig. 35B).

Figure 35. Seepage in centimeters per day (cm/d) and change in stage (ΔStage), in meters (m), at NC266. Chart A shows the 1-minute values of seepage and ΔStage on June 15–16, 2017. Chart B shows the 1-minute values of seepage and ΔStage on June 16, 2017, from 06:00 to 08:00. The right axes are plotted inversely.

NC008

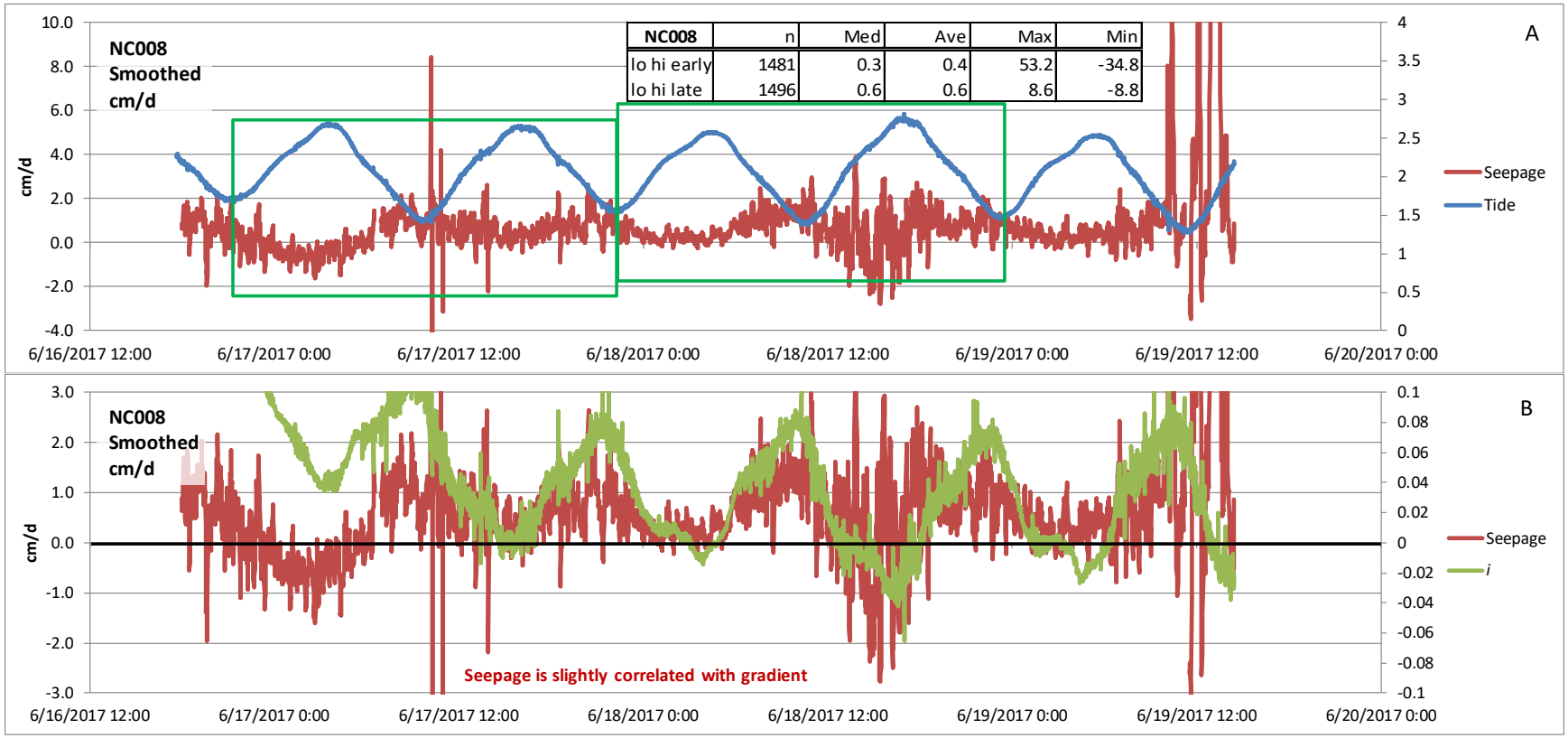

Figure 36. Seepage measured each minute at NC008, in centimeters per day (cm/d). Chart A displays seepage smoothed with a 7-minute moving average, and relative tide in meters (m). The green rectangles indicate the duration of the data-analysis periods. In the inset table, "lo hi early" indicates the first instance of two complete tidal cycles beginning and ending with low tide, and "lo hi late" indicates the next to last two complete tidal cycles beginning and ending with low tide. The last low-tide period was not included in the analysis because of the greatly increased noise in the seepage data at the end of the period of record. Chart B displays smoothed seepage, with vertical hydraulic gradient (*i*) in m/m plotted on the right axis. (n, number of 1-minute values; Med, median of n values; Ave, average of n values; Max, maximum of n values; Min, minimum of n values)

Seepage at NC008 was slightly related with tide. With the approach and passage of high tide, seepage generally decreased and then increased, or decreased until it because downward before transitioning back to upward seepage (fig. 36A). Seepage commonly varied over a fairly narrow range of -2 to 2 cm/d. Average seepage during the two analysis periods was 0.4 and 0.6 cm/d. The two spikes in seepage between 10:00 and 11:00 on June 17 likely were due to passage of a barge on two separate occasions. As mentioned earlier in the description for NC336, the seepage patterns (fig. 37) are remarkably similar to patterns observed and documented during passage of a barge during the 2015 data collection (Rosenberry, 2016, p. 56).

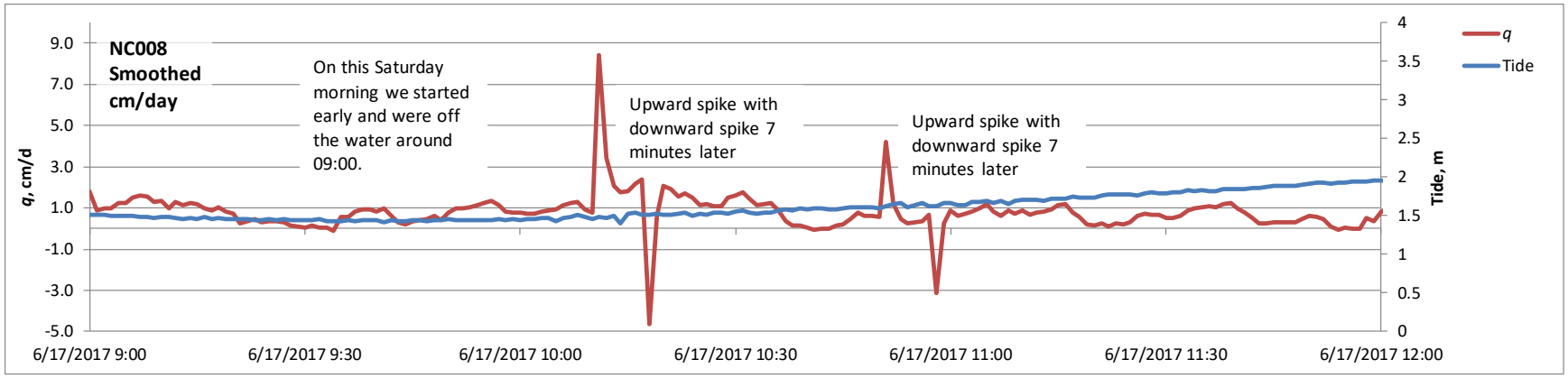

Figure 37. Seepage at NC008 in centimeters per day (cm/d) prior to, during, and following two sets of large upward and downward seepage spikes during the morning of June 17. Relative tide is in meters (m). Data are 1-minute averages of measurements made with 5-second resolution.

On first observation, the noisy seepage data beginning about 10:00 on June 19 appears to have been due to ebullition given that low tide was particularly low and a substantial volume of gas was collected prior to the zero-flow period that began at 11:10. However, ebullition likely is not the cause because the noise continued after the zero-flow period (no gas was collected after 11:33) and well past low tide. Based on the pattern of the noise (fig. 38), it is more likely biological activity was the cause.

Hydraulic gradient was mostly upward with short periods of downward gradients, the centroids of which preceded high tide by about 1 hour (fig. 36B). The largest downward gradients, as well as the largest downward seepage rates, occurred just before the highest high tide of the data-collection period. Reversals in seepage trends occurred about 1 hour before reversals in trends in *i*.

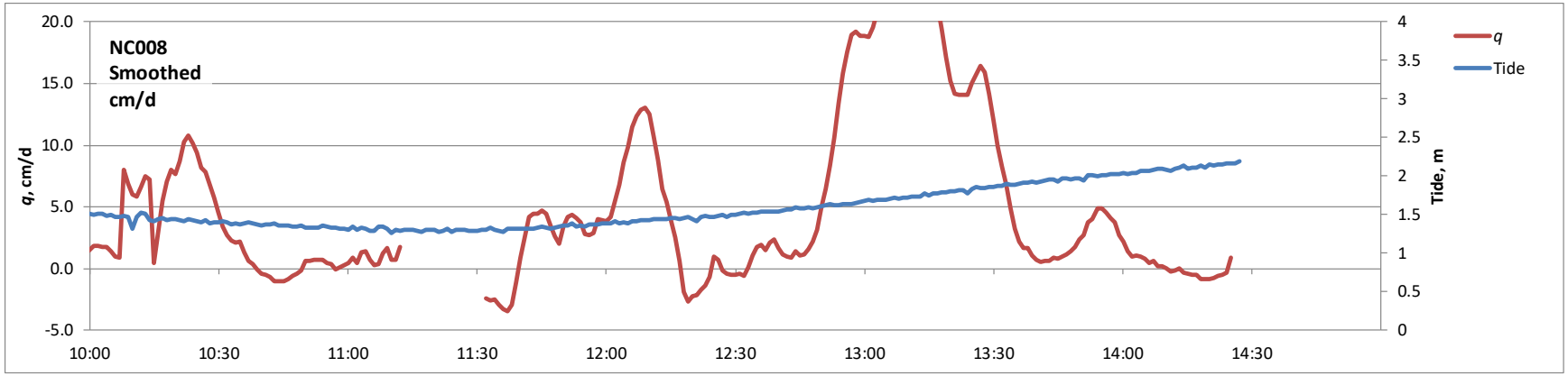

Figure 38. 1-minute values of seepage at NC008 in centimeters per day (cm/d), and relative tide in meters (m) on June 19 during a period of larger-than-normal variability in seepage.

Ebullition Results

Gas was released at 17 of 23 seepage-measurement deployments at Newtown Creek (table 6). At 6 of these 17 deployments, gas was released only during low or particularly low tides. Substantial gas was released during all or almost all measurements at the remaining eleven deployments. At three locations, no or very little gas was released during the deployment in May or early June, but when the locations were revisited several weeks later, substantial gas was released. At EK013, average ebullition increased from 136 to 792 milliliters per day (ml/d) from May to June, a nearly six-fold increase, and the 136 ml/d average value was based on gas released during only one of three periods. At EK098, gas release increased from 499 to 638 ml/d from May to June, and at NC334 gas release increased from 0 during early June to 845 ml/d 2 weeks later. This indicates that gas generation likely was temperature dependent. Average sediment temperatures at 1.5-m depth were 12.4–15.4 °C in May or early June and 13.0–15.6 °C in late June. However, average temperatures at the sediment-water interface increased from 17.7–17.9 °C in May or early June to 20.5–22.2 °C in late June, a 3–4°C increase. As the bed sediments warmed, processes that generate gas likely started or accelerated.

Largest ebullition rates occurred at EK013, EK098, and NC334 during late-June deployments, and at MC036. The largest average ebullition was recorded during a second deployment at NC334, but because measured seepage was influenced by filtering shrimp, the data were not processed. Average ebullition during that second deployment at NC334 was 2,579 ml/d. A close second, however, was measured at MC036 where two measurement periods averaged 2,188 ml/d (table 6). This value likely was even larger because the gas-collection chamber during the first ebullition-measurement period was full and gas likely escaped through the flowmeter.

Ebullition also creates a bias in measured seepage because it displaces water inside the seepage cylinder that then exits through the flowmeter. For most locations, this effect was very small and could be ignored. For all deployments where ebullition occurred, the effect created an average

increase of 0.06 cm/d. Only at five locations was ebullition large enough to substantially influence the average measured seepage rates. Ebullition averaged 0.3 cm/d at NC334-2 (where seepage was not determined due to biological activity); 0.3 cm/d at MC036; and 0.1 cm/d at EK013-2, EK098-2, and NC334-3. All of these deployments were in June. Seepage averages were reduced where adjustments for ebullition were 0.1 cm/d or greater and ebullition-adjusted values are presented in figure 39.

Table 6. Gas released (ebullition) during deployment at seepage measurement locations at Newtown Creek, New York. [Dates are given in M/DD/YYYY format; time is given in HH:MM format on a 24-hour clock. ml, milliliter; min, minute; d, day; cm/d, centimeter per day. Yellow highlights indicate the gas-collection chamber was full; total gas released likely was greater than 3,090 ml. Missing values indicate the top valve was opened but gas (if any was released) was not collected.]

Location	Start date and time	Stop date and time	Mid date and time	Vol. collected (ml)	Elapsed time (minutes)	Vol/time (ml/min)	Vol/time (ml/d)	Dist./time (cm/d)	Location average, cm/d
EK098	5/18/2017 11:56	5/19/2017 9:17	5/18/2017 22:36	10	1,281	0.008	11	0.001	
EK098	5/19/2017 9:37	5/19/2017 15:02	5/19/2017 12:19	425	325	1.308	1883	0.211	
EK098	5/19/2017 15:22	5/20/2017 10:01	5/20/2017 0:41	55	1,119	0.049	71	0.008	
EK098	5/20/2017 10:19	5/20/2017 14:00	5/20/2017 12:09	5	221	0.023	33	0.004	0.06
EK013	5/18/2017 13:50	5/19/2017 10:02	5/18/2017 23:56	0	1,212	0	0	0	
EK013	5/19/2017 10:18	5/19/2017 14:35	5/19/2017 12:26		257				
EK013	5/19/2017 14:52	5/20/2017 9:35	5/20/2017 0:13	0	1,123	0	0	0	
EK013	5/20/2017 9:51	5/22/2017 11:21	5/21/2017 10:36	840	2,970	0.283	407	0.046	0.02
NC340	5/18/2017 11:30	5/18/2017 15:49	5/18/2017 13:39	0	259	0	0	0	
NC340	5/19/2017 11:20	5/19/2017 14:04	5/19/2017 12:42		164				
NC340	5/19/2017 14:21	5/20/2017 8:56	5/19/2017 23:38	10	1,115	0.009	13	0.001	
NC340	5/20/2017 9:13	5/20/2017 12:37	5/20/2017 10:55	5	204	0.025	35	0.004	0.00
NC336	5/22/2017 15:05	5/23/2017 9:25	5/23/2017 0:15	0	1,100	0	0	0	
NC336	5/23/2017 10:53	5/23/2017 14:13	5/23/2017 12:33	5	200	0.025	36	0.004	
NC336	5/23/2017 14:29	5/24/2017 9:09	5/23/2017 23:49	70	1,120	0.063	90	0.010	
NC336	5/24/2017 9:27	5/24/2017 14:36	5/24/2017 12:01	40	309	0.129	186	0.021	
NC336	5/24/2017 14:54	5/25/2017 9:11	5/25/2017 0:02	20	1,097	0.018	26	0.003	
NC336	5/25/2017 9:27	5/25/2017 13:40	5/25/2017 11:33	5	253	0.020	28	0.003	0.01
NC337	5/20/2017 16:00	5/22/2017 14:18	5/21/2017 15:09	0	2,778	0	0	0	
NC337	5/22/2017 14:35	5/23/2017 10:16	5/23/2017 0:25		1,181				
NC337	5/23/2017 10:33	5/23/2017 13:28	5/23/2017 12:00	0	175	0	0	0	0
NC338	5/20/2017 15:34	5/22/2017 13:51	5/21/2017 14:42		2,777				
NC338	5/22/2017 14:07	5/23/2017 8:47	5/22/2017 23:27	0	1,120	0	0	0	
NC338	5/23/2017 9:03	5/23/2017 14:39	5/23/2017 11:51	0	336	0	0	0	
NC338	5/23/2017 14:55	5/24/2017 9:35	5/24/2017 0:15	0	1,120	0	0	0	

Location	Start date and time	Stop date and time	Mid date and time	Vol. collected (ml)	Elapsed time (minutes)	Vol/time (ml/min)	Vol/time (ml/d)	Dist./time (cm/d)	Location average, cm/d
NC338	5/24/2017 9:51	5/24/2017 13:58	5/24/2017 11:54	0	247	0	0	0	
NC338	5/24/2017 14:19	5/25/2017 8:45	5/24/2017 23:32	0	1,106	0	0	0	
NC338	5/25/2017 9:06	5/25/2017 13:11	5/25/2017 11:08	0	245	0	0	0	0
NC334	6/7/2017 13:47	6/8/2017 10:50	6/8/2017 0:18	0	1,263	0	0	0	
NC334	6/8/2017 11:06	6/8/2017 14:52	6/8/2017 12:59	0	226	0	0	0	
NC334	6/8/17 15:07	6/9/2017 9:56	6/9/2017 0:31	0	1,129	0	0	0	
NC334	6/9/17 10:14	6/9/2017 14:10	6/9/2017 12:12	0	236	0	0	0	0
NC335	6/7/2017 14:54	6/8/2017 10:23	6/8/2017 0:38	5	1,169	0.004	6	0.001	
NC335	6/8/2017 10:41	6/8/2017 14:23	6/8/2017 12:32	5	222	0.023	32	0.004	
NC335	6/8/2017 14:39	6/9/2017 10:25	6/9/2017 0:32	0	1,186	0	0	0	
NC335	6/9/2017 10:43	6/9/2017 16:33	6/9/2017 13:38	5	350	0.014	21	0.002	0.00
NC339	6/8/2017 10:10	6/8/2017 13:58	6/8/2017 12:04	0	228	0	0	0	
NC339	6/8/2017 14:14	6/9/2017 10:50	6/9/2017 0:32	0	1,236	0	0	0	
NC339	6/9/2017 11:12	6/9/2017 16:09	6/9/2017 13:40	0	297	0	0	0	
NC339	6/9/2017 16:25	6/10/2017 8:29	6/10/2017 0:27	0	964	0	0	0	0
NC168	6/9/2017 18:01	6/10/2017 7:28	6/10/2017 0:44	0	807	0	0	0	
NC168	6/10/2017 7:46	6/12/2017 15:36	6/11/2017 11:41	5	3,350	0.001	2	0.000	0.00
NC340-2	6/9/2017 16:01	6/10/2017 8:03	6/10/2017 0:02	10	962	0.010	15	0.002	
NC340-2	6/10/2017 8:19	6/12/2017 12:05	6/11/2017 10:12	10	3,106	0.003	5	0.001	0.00
MC036	6/10/2017 10:11	6/12/2017 11:23	6/11/2017 10:47	3,090	2,952	1.047	1507	0.169	
MC036	6/12/2017 11:45	6/13/2017 9:40	6/12/2017 22:42	2,620	1,315	1.992	2869	0.321	0.32
NC273	6/12/2017 15:21	6/13/2017 8:37	6/12/2017 23:59	0	1,036	0	0	0	
NC273	6/13/2017 8:57	6/13/2017 14:36	6/13/2017 11:46	0	339	0	0	0	
NC273	6/13/2017 14:52	6/14/2017 10:08	6/14/2017 0:30	0	1,156	0	0	0	
NC273	6/14/2017 10:25	6/14/2017 14:44	6/14/2017 12:34	0	259	0	0	0	0
NC333	6/12/2017 17:17	6/13/2017 9:00	6/13/2017 1:08	0	943	0	0	0	
NC333	6/13/2017 9:23	6/13/2017 14:07	6/13/2017 11:45	10	284	0.035	51	0.005	
NC333	6/13/2017 14:24	6/14/2017 9:42	6/14/2017 0:03	0	1,158	0	0	0	
NC333	6/14/2017 9:58	6/14/2017 14:14	6/14/2017 12:06	0	256	0	0	0	0.00
NC320	6/13/2017 11:45	6/13/2017 15:04	6/13/2017 13:24	20	199	0.101	145	0.016	
NC320	6/13/2017 15:22	6/14/2017 10:35	6/14/2017 0:58	5	1,153	0.004	6	0.001	
NC320	6/14/2017 10:52	6/14/2017 13:44	6/14/2017 12:18	0	172	0	0	0	
NC320	6/14/2017 13:59	6/15/2017 8:15	6/14/2017 23:07	0	1,096	0	0	0	
NC320	6/15/2017 8:31	6/15/2017 12:15	6/15/2017 10:23	15	224	0.067	96	0.011	0.01

Location	Start date and time	Stop date and time	Mid date and time	Vol. collected (ml)	Elapsed time (minutes)	Vol/time (ml/min)	Vol/time (ml/d)	Dist./time (cm/d)	Location average, cm/d
WC022	6/14/2017 16:33	6/15/2017 7:45	6/15/2017 0:09	5	912	0.005	8	0.001	
WC022	6/15/2017 8:04	6/15/2017 11:44	6/15/2017 9:54	5	220	0.023	33	0.004	
WC022	6/15/2017 12:00	6/16/2017 10:50	6/15/2017 23:25	0	1,370	0	0	0	
WC022	6/16/2017 11:12	6/16/2017 16:20	6/16/2017 13:46	0	308	0	0	0	0.00
NC266	6/15/2017 14:10	6/16/2017 10:22	6/16/2017 0:16	190	1,212	0.157	226	0.025	
NC266	6/16/2017 10:37	6/16/2017 15:15	6/16/2017 12:56	0	278	0	0	0	
NC266	6/16/2017 15:30	6/17/2017 6:58	6/16/2017 23:14	0	928	0	0	0	
NC266	6/17/2017 7:13	6/19/2017 11:36	6/18/2017 9:24	590	3,143	0.188	270	0.030	0.01
NC362	6/15/2017 7:31	6/15/2017 11:15	6/15/2017 9:23	0	224	0	0	0	
NC362	6/15/2017 11:31	6/16/2017 11:25	6/15/2017 23:28	0	1,434	0	0	0	
NC362	6/16/2017 11:42	6/16/2017 15:46	6/16/2017 13:44	0	244	0	0	0	
NC362	6/16/2017 16:01	6/17/2017 7:45	6/16/2017 23:53	0	944	0	0	0	
NC362	6/17/2017 8:00	6/20/2017 8:31	6/18/2017 20:15	0	4,351	0	0	0	0
NC008	6/16/2017 17:53	6/17/2017 6:35	6/17/2017 0:14	0	762	0	0	0	
NC008	6/17/2017 6:51	6/19/2017 11:10	6/18/2017 9:00	230	3,139	0.073	106	0.011	
NC008	6/19/2017 11:28	6/19/2017 14:28	6/19/2017 12:58	30	180	0.167	240	0.026	0.01
NC334-2	6/19/2017 14:06	6/20/2017 11:00	6/20/2017 0:33	420	1,254	0.335	482	0.054	
NC334-2	6/20/2017 11:19	6/20/2017 13:53	6/20/2017 12:36	500	154	3.247	4675	0.523	0.29
EK013-2	6/19/2017 16:34	6/20/2017 10:17	6/20/2017 1:25	20	1,063	0.019	27	0.003	
EK013-2	6/20/2017 10:33	6/20/2017 14:55	6/20/2017 12:44	200	262	0.763	1099	0.119	
EK013-2	6/20/2017 15:10	6/21/2017 10:40	6/21/2017 0:55	255	1,170	0.218	314	0.034	
EK013-2	6/21/2017 10:56	6/21/2017 15:48	6/21/2017 13:22	350	292	1.199	1726	0.186	0.09
EK098-2	6/20/2017 10:07	6/20/2017 14:27	6/20/2017 12:17	40	260	0.154	222	0.024	
EK098-2	6/20/2017 14:42	6/21/2017 11:06	6/21/2017 0:54	90	1,224	0.074	106	0.011	
EK098-2	6/21/2017 11:22	6/21/2017 15:22	6/21/2017 13:22	250	240	1.042	1500	0.162	
EK098-2	6/21/2017 15:38	6/22/2017 8:11	6/21/2017 23:54	940	993	0.947	1363	0.147	
EK098-2	6/22/2017 8:27	6/22/2017 10:31	6/22/2017 9:29	0	124	0	0	0	0.07
NC334-3	6/21/2017 17:22	6/22/2017 7:39	6/22/2017 0:30	570	857	0.665	958	0.103	
NC334-3	6/22/2017 7:55	6/22/2017 14:20	6/22/2017 11:07	65	385	0.169	243	0.026	
NC334-3	6/22/2017 14:37	6/23/2017 10:41	6/23/2017 0:39	10	1,204	0.008	12	0.001	
NC334-3	6/23/2017 10:56	6/23/2017 16:48	6/23/2017 13:52	530	352	1.506	2168	0.234	0.09

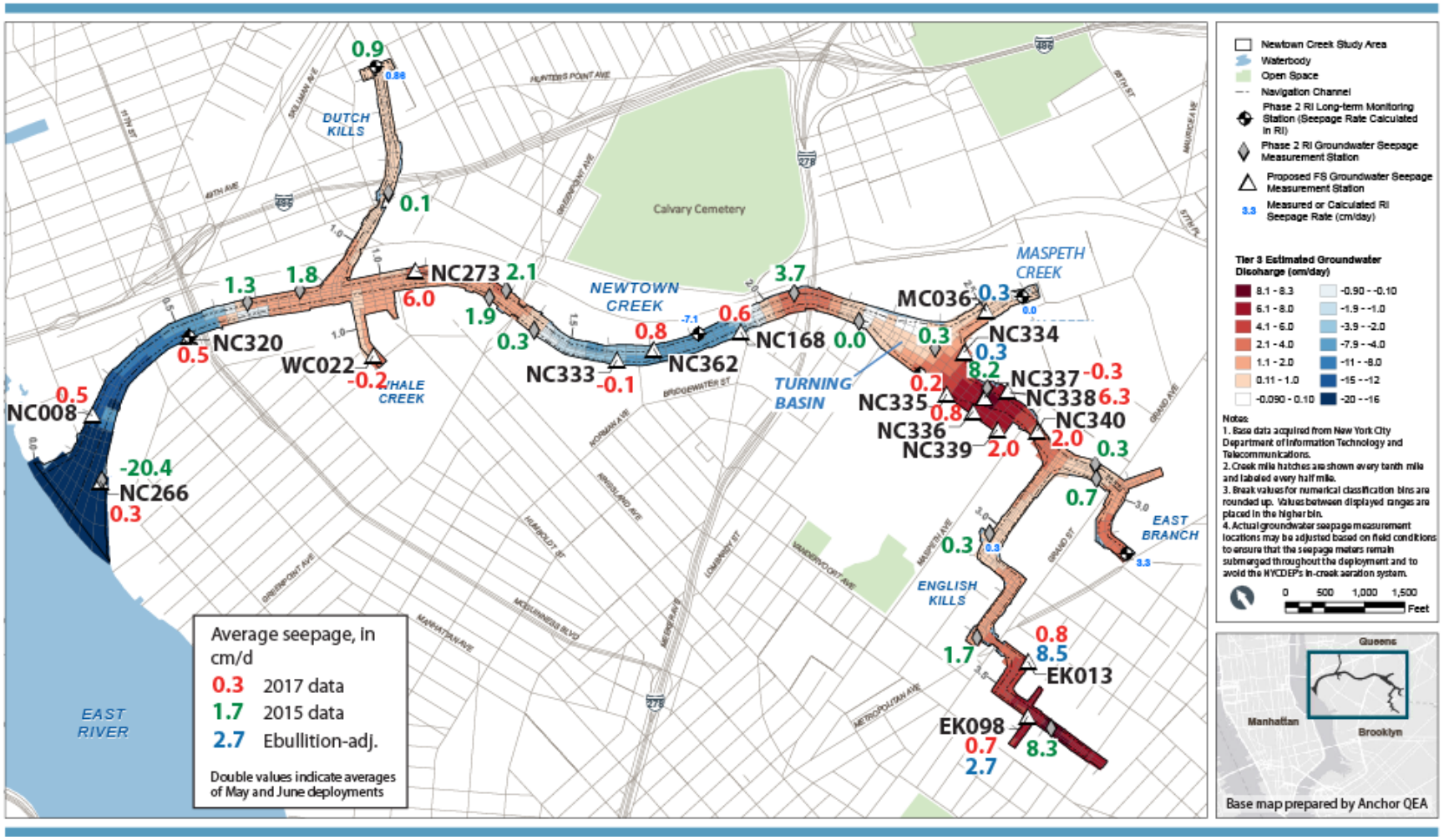

Figure 39. Seepage-measurement locations at Newtown Creek, New York, showing 2017 average seepage rates with values in blue indicating locations (MC036, NC334, EK013, EK098) where values were adjusted to remove the effects of ebullition. Values in blue are adjusted average seepage rates during 2017 sensor deployments. Values in red are unadjusted average seepage rates during 2017 sensor deployments. Values in green are average seepage during 2015 sensor deployments (Rosenberry, 2016). Positive values indicate upward flow and negative values indicate downward flow. (cm/d, centimeter per day RI, remedial investigation; NYCDEP, New York City Department of Environmental Protection)

Discussion

Relations Between Seepage and Vertical Hydraulic Gradient

Seepage at several locations flowed in the opposite direction of what would be expected based on vertical hydraulic gradients. At NC337, after the effects of electromagnetic noise were removed, period-average seepage values indicated slow downward seepage but the relatively large *i* indicated upward flow. Given the questionable seepage results, which were likely due to a defective data cable, the small downward seepage values are suspect. Seepage data collected during the first deployment at NC334 also are suspect because of the pattern displayed (fig. 18) and because a shrimp was discovered inside the rubber boot attached to the flowmeter during a subsequent deployment. As mentioned earlier, several types of animals that live in and on the sediment are known to create flow that can easily be measured and interpreted as seepage. This biological effect may also have affected seepage at times during deployments at NC320, NC362, and possibly NC273. At NC273, NC168, and NC362, upward seepage at locations where *i* indicated downward flow may be related to currents. The hydraulic effects of flowing surface water on seepage measurements have been shown for fluvial settings (for example, Rosenberry, 2008) and all three of these locations are in relatively narrow portions of the main channel in Newtown Creek where tidally generated currents may be strongest. Flow in opposite directions also was indicated at WC022 during the early portion of the deployment. That condition resulted from a period of downward seepage during the first half-day of deployment that occurred while an upward hydraulic gradient was artificially large due to sediment overpressuring following VHG-rod installation. The period of downward seepage ended after 12 hours and the subsequent analysis period indicated both upward seepage and upward *i*.

Seepage at NC337, NC168, NC362, and NC320 did not respond to tides or vertical hydraulic gradients. With one exception, seepage was slow at all four of these locations, all of which are in the Newtown Creek main channel. The one exception was at NC320 during the early analysis period that indicated upward seepage at 2.8 cm/d (fig. 30). However, those data were very noisy and may have been affected by filtering benthic animals. The later of two analysis periods indicated slight downward seepage at −0.1 cm/d.

Seepage showed a very weak correlation with *i* at NC266 and NC008. However, both of these locations were exposed to waves generated by boat traffic on the East River and the waves created short-term large spikes in seepage that overwhelmed other signals that may have been larger than observed.

Weak correlations between seepage and *i* also were observed at NC340, NC336, and NC273. Correlations were evident during only a portion of the deployments at NC336 and NC273 and the only feature that warrants a correlation with *i* at NC340 is the sharp decline in upward seepage that occurred just prior to four of the five high tides.

Much stronger correlations between seepage and *i*, however, can be observed at EK098, EK013, NC339, NC338, NC335, and NC334-3, which are all located beyond the turning basin. By far the best correlation occurred at EK013 during the first deployment in May (fig. 9B). Although the

ESM performed poorly during installation, seepage rates were so large and tidally driven that there is no question that seepage was wholly driven by *i*. Similar conclusions can be reached for the other locations in this "strongly correlated" list, with a couple of interesting exceptions. Seepage at EK098 showed very little correlation with *i* during the May deployment (fig. 6B) but there was good correlation during the June deployment (fig. 7B). The most perplexing exception occurred at EK013 during the second deployment in June, where there was an excellent correlation between seepage and *i*, but it was an inverse correlation, the opposite of what one would expect. Resolving this conundrum led to the hypothesis that seepage measured at Newtown Creek is a combination of gradient-driven flow and displacement of water contained inside the seepage cylinder as the sediment bed rises and falls in response to expansion and compression of gas trapped in the sediment as the tide falls and rises. This theory is elucidated in the following paragraphs.

Moving-Bed Hypothesis

Gas trapped within the sediment will expand as the tide falls and hydrostatic pressure is reduced. Alternately, gas volume will be reduced as the tide rises and hydrostatic pressure is increased. If sediment permeability is relatively low, such that ebullition is limited and only a small percentage of gas is released to the water column, expansion and compression of the remaining trapped gas will cause the sediment surface to rise and fall. A rising bed during a falling tide will displace water contained within a seepage cylinder that is anchored to deeper, competent sediment and cause the water to exit the seepage meter through the electromagnetic (EM) flowmeter, which would be interpreted as upward seepage. As the sediment lowers in response to rising tide, water will flow into the seepage meter, which would be interpreted as downward seepage. This process will occur in concert with and generally in the same direction as gradient-driven seepage. If the volume of trapped gas is sufficiently large, moving-bed flow through the EM flowmeter could overwhelm seepage driven by hydraulic gradients. If the bed is moving in response to stage, then change in stage should be strongly inversely related to seepage. This is definitely the case at MC036, the location where the greatest volume of gas was recorded (fig. 40). This is an exceptional example; data were not this well inversely correlated at most other locations. It is possible that the larger changes in seepage that began around 03:00 on June 12, right about at low tide, may be the result of ebullition (fig. 40B).

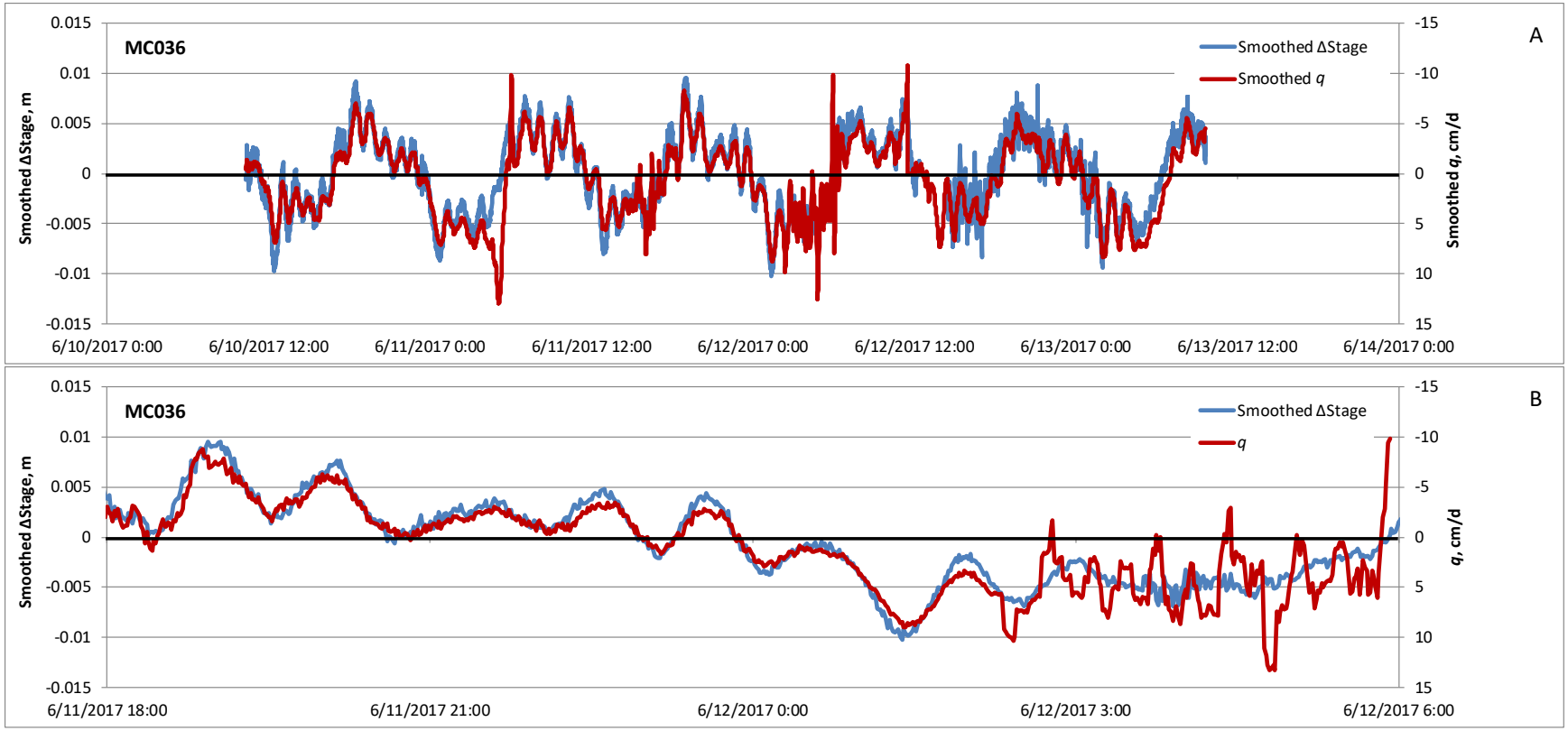

Figure 40. Smoothed (7-minute average) change in stage (ΔStage) in meters (m), and smoothed (7-minute average) or un-smoothed seepage (*q*) in centimeters per day (cm/d) at MC036. Note that seepage is plotted on an inverse axis, demonstrating the inverse relation between ΔStage and *q*. Chart A shows smoothed data plotted over the entire period of deployment. Chart B shows smoothed ΔStage and unsmoothed seepage plotted over a 12-hour period.

However, if the sediment is relatively permeable, the opposite may occur. With a relatively permeable bed, conditions become more complex, resulting in a net response that could be the opposite of a gradient-driven response, as was recorded at EK013 during the second deployment. Where sediments are more permeable, generated gas has a smaller chance of being trapped; the gas is more likely to be released as it is generated, leading to less gas storage. As tide begins to fall, any gas contained in the sediment begins to expand, becoming more buoyant. Combined with a reducing downward gradient, or increasing upward gradient, bubbles begin to be released. The sediment volume formerly occupied by gas is reduced, which allows the sediment bed to compress, resulting in a lowering of the sediment-water interface, inducing flow into the seepage meter

through the EM flowmeter that is interpreted as downward seepage. This process would partially offset an increasing upward hydraulic gradient that would lead to upward seepage. Any gas released from the sediment would rise into the seepage cylinder, displace water, and also partially offset water flowing into the meter in response to a lowering bed. This process would continue as stage decreases until either the gas contained in the sediment is exhausted or the increasingly large upward hydraulic gradient causes upward seepage to dominate, making the measured seepage plateau prior to low tide. As the tide reverses and begins to rise, the size of bubbles remaining in the sediment, or added to the sediment as gas-generating processes continue, begins to decrease, upward gradient-driven seepage begins to decrease, and conduits for rapid advection close up. This traps gas in the sediment. Continued increase in stage creates smaller upward gradients that then become downward. But with conduits closed, little downward advection occurs as bubble accumulation causes the sediment bed to rise, displacing water in the seepage cylinder and causing net upward seepage to be recorded by the flowmeter. At some point prior to high tide, the downward hydraulic gradient gets large enough to induce some downward flow into the sediment, offsetting sediment-bed rise, and causing a plateau in measured upward seepage. This process is enhanced if the sediment is more permeable during upward flow than it is during downward flow, as has been documented in the literature (Rosenberry and Pitlick, 2009).

This hypothesis implies that seepage responds to both hydraulic gradient and change in stage. There are several ways to test this. First, low-permeability sediment containing trapped gas would create flow interpreted as seepage that would be in phase with tides, whereas gas trapped and (or) released in higher-permeability sediment would create a process causing net seepage to be somewhat out of phase with tides. The phase shifts relative to tide shown in figures 22 and 27 can be determined for all locations. If seepage responded solely to *i*, the phase shift for seepage relative to tide should be the same as the phase shift for *i* relative to tide. The red dashed line in figure 22 would be coincident with the green dashed line that indicates *i* nadir. If seepage responded solely to ΔStage, the phase shift for seepage would be the same as the phase shift for ΔStage and the red dashed line in fig. 22 would be coincident with the blue dashed line indicating the nadir of ΔStage. A "*q* ratio" was created that indicates the relative phase shift for seepage compared to the boundaries represented by *i* and ΔStage with a value of 0 indicating complete influence of *i* and a value of 1 indicating complete influence of ΔStage (table 7). Analyses were not made for locations that were not responsive to tides or for NC266 or NC008 because the wave-induced noise made interpretations impossible at those locations.

Based on the *q*-ratio analysis, seepage at NC338 and EK013 was controlled to the greatest extent by *i*, whereas seepage at EK013 during the second deployment was controlled to the greatest extent by ΔStage (table 7). A negative *q* ratio occurred at NC338 because seepage was completely in phase with tide whereas *i* was lagged by -1 hour (fig. 14), perhaps indicating that seepage was controlled by hydraulic conditions closer to the sediment-water interface rather than the gradient integrated over a 1.5-m sediment interval. Additionally, equilibration time following VHG-rod installation was the shortest of all locations at both EK013 and NC338 (1 hour, table 1) supporting the hypothesis that sediments were particularly permeable at these two locations. Seepage at locations EK098-2, WC022, and MC036 were controlled approximately equally by both *i* and ΔStage. Seepage was mostly controlled by *i* at NC334-3 and NC335 and seepage was controlled mostly by ΔStage at EK098. Determination of phase shift was somewhat subjective and the *q*-ratio value sometimes was substantially influenced by changes in interpretation of the phase shift

of 30 minutes. Therefore, multiple linear regression using *i* and ΔStage as independent variables and seepage as the dependent variable also was employed to indicate the relative influence of *i* and ΔStage on measured *q*. In this case, analyses were made at all locations (table 7).

Table 7. Results of phase-shift analysis to determine the relative influence of vertical hydraulic gradient (*i*) and change in stage (ΔStage) on smoothed seepage (*q*), and results of multiple linear regression of seepage as the dependent variable and ΔStage and *i* as independent variables. All t-score values were significant at the 0.001 probability unless an asterisk is present. Seepage at locations with gray text had little to no response to tides. [*q* lag, phase shift in hours between plots for seepage and tide; *i* lag, phase shift in hours between plots for *i* and tide; ΔStage lag, phase shift in hours between plots for ΔStage and tide; *q* ratio, relative indication of the effect of *i* (0) or ΔStage (1) on *q*; MLR, multiple linear regression; Adj. R^2, coefficient of determination indicating the multiple linear regression model goodness of fit, adjusted for the number of independent variables; n, number of observations; Model F, overall fit of regression model; t score ΔStage, an indication of the relative degree to which ΔStage affects modeled *q*; t score *i*, an indication of the relative degree to which *i* affects modeled *q*. Negative t-score values indicate an inverse relation between the independent variable and *q*.]

Location	*q* lag, hours	*i* lag, hours	ΔStage lag, hours	*q* ratio	MLR Model Adj. R^2	n	Model F	t score ΔStage	t score *i*
EK098	−2.5	0.0	−3.5	0.71	0.32	2,640	613	−34.1	*1.12
EK098-2	−2.0	−1.0	−3.0	0.50	0.49	2,568	1,259	−14.3	17.7
EK013	−0.75	−0.5	−2.5	0.13	0.80	5,439	10,699	−60.6	98.3
EK013-2	−4.0	−0.5	−4.0	1.00	0.69	2,384	2,638	−6.1	−68.5
NC337					0.004	1,391	3	*0.62	*−2.63
NC338	0	−1.0	−2.5	−0.67	0.40	6,828	2,303	31.4	62.2
NC336					0.20	3,416	430	−9.6	24.7
NC334					0.17	2,428	253	−5.6	−20.2
NC334-3	−1.25	−0.5	−3.0	0.30	0.80	2,546	5,045	−61	37.9
NC335	−1.5	−1.0	−3.0	0.25	0.80	2,655	5,348	−53.4	56.2
NC339	−0.75	−0.75	−1.75	0.00	0.69	2,024	2,267	−36.7	24.9
NC340-2					0.10	3,639	196	−19.8	4.1
NC168					0.02	4,130	47	−8.8	−7.9
MC036	−2.0	−0.5	−3.75	0.46	0.81	3,797	8,344	−128.6	21.1
NC273					0.16	2,419	227	19.7	4.5
NC333	−1.0	0.0	−2.5	0.40	0.55	3,137	1,937	−45.9	46.3
NC320					0.04	2,286	50	9.9	*2.85
WC022	−2.3	−2.0	−2.5	0.50	0.44	2,164	861	−27	6.4
NC362					0.01	5,729	36	−7.5	*0.53
NC266					0.02	5,073	66	−9.3	3.7
NC008					0.02	3,463	32	7.9	4.9

Not surprisingly, regression statistics indicated weak relations between seepage and *i* or ΔStage at the locations shown in gray (table 7). As with the *q*-ratio analysis, the strongest relation between seepage and *i* based on t scores occurred at EK013 during the first deployment, followed in descending order by NC338, NC335, and NC333. As indicated earlier, multiple-regression analysis also indicates a strong inverse relation between seepage and *i* at EK013 during the June deployment. By far, the location with the strongest influence of ΔStage on seepage was at MC036. The second-strongest relation between seepage and ΔStage occurred at EK013 during the first deployment with a t score less than half as large as at MC036. That likely is due to the much stronger relation with *i* at EK013. The next strongest influences of ΔStage on seepage occurred at NC335, NC333, and NC339.

Regression-based indications of the relative influences of *i* and ΔStage did not always compare well with lag-based seepage ratios. For example, *q*-ratio results indicated the greatest likelihood of sediment-bed movement at EK013-2 and EK098. Although regression results did indicate a strong inverse relation between seepage and *i* at EK013-2, the t score for EK098 indicated the sixth strongest relation with ΔStage. Similarly, the location with the strongest relation between seepage and ΔStage based on regression analysis was MC036, followed by EK013 and NC333. Based on *q*-ratio analysis, MC036 was slightly more influenced by *i* than ΔStage, EK013 was much more influenced by *i* than ΔStage (which also is what the regression model indicated), and NC333 also was influenced to a greater extent by *i* than by ΔStage. There clearly is multicollinearity in the regression model and also subjectivity in the *q*-ratio values.

A final attempt was made to determine the relative influence of *i* and ΔStage on seepage at the various locations. One additional indicator was added, that being R^2 values of simple linear regressions between seepage and ΔStage and seepage and *i*. Considering only those locations where seepage clearly responded to tide, locations were ranked based on indicators of the strength of the response of seepage to both *i* and ΔStage (multiple-regression R^2), three indicators of the response of seepage to ΔStage, three indicators of the response of seepage to *i*. and a ranking of the volume of ebullition released at these locations (table 8). Seepage was most strongly correlated with both ΔStage and *i* at MC036, EK013, NC334-3, and NC335. Seepage was most strongly related with ΔStage at MC036, NC334-3, NC335, and EK098. Seepage was most strongly related with *i* at EK013, NC335, NC338, and NC339.

Table 8. Rankings of seepage measurement locations based on various indicators of the strength of relation between seepage (*q*) and: Both change in stage (ΔStage) and vertical hydraulic gradient (*i*) (column 2), three indicators of the strength of relation between seepage and ΔStage (columns 3–5) and their collective rank (column 6), three indicators of the strength of relation between seepage and *i* (columns 7–9) and their collective rank (column 10), and relative volumes of ebullition (column 11). [MLR, multiple linear regression; Adj. R^2, coefficient of determination indicating the multiple linear regression model goodness of fit, adjusted for the number of independent variables]

Ranking	MLR Adj. R^2	t score ΔStage	Δstage lag, hours	R^2 *q* versus ΔStage	Collective Δstage rank	t score *i*	*i* lag, hours	R^2 *q* versus *i*	Collective *i* rank	Ebullition rank
1	MC036	MC036	EK013-2	MC036	MC036	EK013	WC022	EK013-2	EK013	MC036
2	EK013	NC334-3	MC036	NC334-3	NC334-3	NC338	EK098-2	EK013	NC335	NC334-3
3	NC334-3	EK013	EK098	NC339	NC335	NC335	NC335	NC335	NC338	EK013-2
4	NC335	NC335	EK098-2	NC335	EK098	NC333	NC338	NC334-3	NC339	EK098-2
5	EK013-2	NC333	NC334-3	EK098-2	EK013	NC334-3	NC339	NC338	NC334-3	EK098
6	NC339	NC339	NC335	EK098	EK098-2	NC339	EK013	NC339	EK098-2	EK013
7	NC333	EK098	EK013	WC022	EK013-2	MC036	EK013-2	EK098-2	WC022	NC335
8	EK098-2	WC022	NC338	EK013	NC339	EK098-2	NC334-3	WC022	EK013-2	NC333
9	WC022	EK098-2	NC333	NC333	NC333	WC022	MC036	NC333	NC333	WC022
10	NC338	EK013-2	WC022	EK013-2	WC022	EK098	EK098	MC036	MC036	NC338
11	EK098	NC338	NC339	NC338	NC338	EK013-2	NC333	EK098	EK098	NC339

Local measurements of *i* and ebullition provided substantial insights related to processes that control seepage at Newtown Creek. Seepage as measured with the ESM appears to be in response to a combination of *i* and a moving sediment bed. The latter process was prevalent beyond the turning basin and in Maspeth Creek (fig. 1). A moving sediment bed may also have been a factor near the mouth of Newtown Creek based on measurement of ebullition there. A moderately strong inverse relation between seepage and ΔStage (fig. 35B) indicates this is likely.

The moving-bed hypothesis could be tested in future deployments of an automated seepage meter. An underwater camera could be mounted inside a deployed ESM or a submersible accelerometer could be place on the sediment bed inside an ESM during deployment.

References Cited

Anchor QEA, LLC, 2015, Phase 2 Field Sampling and Analysis Plan – Volume 2, Addendum No. 2, Remedial Investigation/Feasibility Study, Newtown Creek, Attachment 1, SOP NC-34 – Seepage Measurement, February, 2015, 10 p.

Cable, J.E., Martin, J.B., and Jaeger, J., 2006, Exonerating Bernoulli? On evaluating the physical and biological processes affecting marine seepage meter measurements: Limnology and Oceanography: Methods, v. 4, p. 172–183.

Clesceri, L.S., Greenberg, A.E., and Eaton, A.D., eds., 1999, Standard methods for the examination of water and wastewater (20th ed.): American Public Health Association, Washington DC, 1325 p.

Hunters Point (8517673), 2017, https://tidesandcurrents.noaa.gov/noaatideannual.html?id=8517673: NOAA Tides and Currents.

Martin, J.B., Cable, J.E., Jaeger, J., Hartl, K., and Smith, C.G., 2006, Thermal and chemical evidence for rapid water exchange across the sediment–water interface by bioirrigation in the Indian River Lagoon, Florida: Limnology and Oceanography, v. 51, p. 1332–1341.

McCutcheon, S.C., Martin, J.L, and Barnwell, T.O., Jr., 1993, Water quality, *in* Maidment, D.R. (ed.), Handbook of hydrology, New York, McGraw-Hill, 1424 p.

Meysman, F.J.R., Galaktionov, O.S., Gribsholt, B., and Middelburg, J.J., 2006, Bioirrigation in permeable sediments – Advective pore-water transport induced by burrow ventilation: Limnology and Oceanography, v. 51, p. 142–156.

National Oceanic and Atmospheric Administration, 2017, Annual prediction tide tables for Hunters Point, Newton Creek, NY (8517673): National Oceanic and Atmospheric Administration, Hunters Point (8517673), 2017,https://tidesandcurrents.noaa.gov/noaatideannual.html?id=8517673.

Rosenberry, D.O., 2008, A seepage meter designed for use in flowing water: Journal of Hydrology, v. 359, p. 118–130.

Rosenberry, D.O., 2016, Seepage Measured at 17 Locations in Newtown Creek, New York: U.S. Geological Survey Administrative Report, 59 p.

Rosenberry, D.O., and Morin, R.H., 2004, Use of an electromagnetic seepage meter to investigate temporal variability in lake seepage: Ground Water, v. 42, p. 68–77.

Rosenberry, D.O., and Pitlick, J., 2009, Effects of sediment transport and seepage direction on hydraulic properties at the sediment-water interface of hyporheic settings: Journal of Hydrology, v. 373, p. 377–391.

Simonds, F.W., Swarzenski, P.W., Rosenberry, D.O., Reich, C.D., and Paulson, A.J., 2008, Estimates of nutrient loading by ground-water discharge into the Lynch Cove area of Hood Canal, Washington: U.S. Geological Survey Scientific Investigations Report 2008–5078, 54 p.

Swarzenski, P.W., Charette, M., and Langevin, C., 2004, An autonomous, electromagnetic seepage meter to study coastal groundwater/surface-water exchange: U.S. Geological Survey Open-File Report 2004–1369, 4 p.

Waldrop, W.R., and Swarzenski, P.W., 2006, A new tool for quantifying flux rates between surface water and ground water, *in* Singh, V.P., and Xu, Y.J., eds., Coastal hydrology and processes: Highlands Ranch, Colo., Water Resources Publications, LLC, p. 305–312.